POLITECNICO DI TORINO

Master of science program in Energy and Nuclear Engineering

Master thesis

Definition and simulation of control settings for a Power-to-power application for Turin airport

Supervisor

Professor Massimo Santarelli
Ing. Marta Gandiglio
Ing. Paolo Marocco
Ing. Audisio Davide

Candidate

Alessandro Montaldo

A.Y. 2021/22

Table of contents

List of figures

List of tables

List of symbols

η_{elec}	electrolyzer efficiency
$P_{in_{elec}}$	electrolyzer input power, electricity
$P_{out_{elec}}$	electrolyzer output power, hydrogen
$P_{elec_{nom}}$	electrolyzer nominal power, referred to the input
$\%_{load\,elec}$	electrolyzer power input percentage
η_{ee}	fuel cell electric efficiency
η_{th}	fuel cell thermal efficiency
$\%_{out_{cell}}$	working percentage of the cell
$P_{in_{cell}}$	fuel cell input power, either methane, hydrogen, or a mixture
$P_{out\,ee_{cell}}$	fuel cell electric output power
$P_{out\,th_{cell}}$	fuel cell thermal output power
$P_{nom_{cell}}$	fuel cell nominal electric power, referred to output
$P_{nom_{th-cell}}$	fuel cell nominal thermal power, referred to output
ΔP	power difference
P_{RES}	power produced by the PV panels
P_{load}	power load to be fulfilled
SOC	state of charge of the battery
SOC_{max}	maximum allowed SOC
SOC_{min}	minimum allowed SOC
SOC_i SOC	at the i-th instant
Cap	battery capacity expressed in kWh
$C_{rate_{charge}}$	charging rate of the battery
$C_{rate_{discharge}}$	discharging rate of the battery
P_{charge}	battery charging power
P_{elec}	power used by the electrolyzer
$P_{grid_{out}}$	power released to the grid
Δt	time interval expressed in hours, assumed equal to fifteen minutes
LOH	level of hydrogen within the tank, expressed as a mass ratio
LOH_i	LOH at the i-th instant
LOH_{max}	maximum allowed LOH

LOH_{min}	minimum allowed LOH
$LOH_{min_{blend}}$	minimum LOH that guarantees the possibility of making correct blending
LHV_{H_2}	lower heating value of the hydrogen, mass basis
$m_{H_2 max}$	maximum hydrogen mass that can be stored in the tank
p	pressure expressed in Pa
ρ_{H_2}	hydrogen density expressed in kg/m^3
R	global gas constant
T	temperature expressed in Kelvin
$\%_{min_{elec}}$	minimum allowed working point of the electrolyzer
$P_{out_{eff-elec}}$	effective output power of the electrolyzer, power of produced hydrogen
P_{FC}	fuel cell electric output power
$P_{FC_{th}}$	fuel cell thermal output power
P_{disch}	discharging power of the battery
N_{cell}	number of installed cells
$P_{grid_{in}}$	input power from the grid
$blend_n$	the actual blending mixing in input to the n-th cell.
$\dot{m}_{H_2}$	hydrogen mass flow rate
$\dot{n}_{H_2}$	hydrogen molar flow rate
$\dot{n}_{tot}$	total mixture molar flow rate
$P_{in_{eff}}$	actual chemical power entering in the fuel cells
$load_{gua_{FC}}$	guaranteed working point of the fuel cells
P_{extra}	power output of the fuel cells not used to cover the load.
$P_{elec_{blend}}$	required power output from the electrolyzer to obtain $LOH_{min_{blend}}$
$P_{elec_{in_{blend}}}$	required power input to obtain $P_{elec_{blend}}$
$P_{elec_{it}}$	electrolyzer power used in the iteration of the fuel cell loop.
$\dot{m}_{H_2 pipe}$	pipe mass flow rate
$\Delta_{LOH_{max}}$	maximum allowed LOH rise in the storage during a single iteration.
LOH_{target}	minimum required LOH within the storage tank.

1. Abstract

This master thesis focuses on the possibility of the application of a Power-to-power solution, with the peculiar characteristic of using Solid Oxide fuel cells with the possibility of working both with methane and hydrogen in input, to ensure the balance of a small grid composed by a set of PV panels, a battery, and the possibility to rely on the grid. The prototype is developed in the framework of the TULIPS project in the Turin airport.

This thesis analyses the different solutions in terms of energy storage that are now available on the market, going in detail for the solution chosen. A more detailed description of the case study analyzed is provided considering the different technologies adopted and characterizing the supplied loads.

The model used for the simulations is described in a detailed way analyzing the different features implemented. The results are presented in form of sensitivity analysis driven by the variation of some specific parameters and determining how they affect the performances of the system.

The obtained results determine the higher impact of the fuel cells size on the storage ability to satisfy the load and the importance of the chosen blending percentage for the fuel cells, while the choice of the control logic is less impacting on the overall performances.

2. Introduction

The world is moving toward a green energy transition, with a rising level of penetration of the Renewable Energy Sources, RES, especially wind and solar. In the five years between 2015 and 2020 Europe have shown a new installed capacity of renewables of $\sim 180\ GW$ and the projections for the following five years supposed to have this value almost doubled accounting for $\sim 300\ GW$. In this supposed increase of installation, the main share will be on behalf of solar photovoltaic, $\sim 60\%$, and wind technologies $\sim 30\%$. IEA projections shows that this increase is not enough to meet the net zero emission target for 2050, as a consequence can be supposed an even higher rise in this trend [1].

Within this perspective it is crucial to determine the effects that this high level of RES penetration can have on the electricity distribution grid; the main problems brought by renewables are related to their high variability that can generate fluctuations in the grid [2-4]. The rising level of unbalances and fluctuations can be faced, according to Wang et al. [3], with two possible solutions: smoothing the electricity transmission by means of controlling methods or using some energy storage technologies that can be inserted in the energy mix. This second solution is the one proposed by Barelli et al [2] for the Italian case in which the presence of higher quantities of renewables brought to the progressive phase out from the thermoelectric plants relegated to a load following role. The possible coupling with storage technologies can make them work with a higher constancy and at the same time can increase a lot the grid reliability.

According to [4] there are several possible additional benefits that can be achieved with a higher penetration of energy storage technologies in the grid:

- Helping the meeting of electricity peak demands that are one of the most critical moments for the grid.
- Providing a time varying energy management, allowing the decoupling between production and consumption that is the main target to reach a higher energy flexibility of the grid.
- Improving the power quality and as a consequence its reliability
- Supporting the realization of smart grids

Many other positive aspects can be helped by the progressive penetration of energy storage technologies within the grid, for example it is useful in order to reduce the dependency from fossil fuel technologies, reducing in this way the amount of CO_2 emissions associated with the grid electricity [5].

The principal type of energy storage technologies that have been studied and analyzed for the integration in the grid are the ones with the higher level of technological maturity such as the Compressed Air Energy Storage $CAES$, studied by De Boer et al. [6] and Ghalelou et al [7] in order to improve the renewable energy dispatching, it has also been analyzed by Lund et al [8] within an energy system characterized by high level of fluctuations caused by the presence of RES, the obtained results showed that this is a possible solution to limit this negative effect.

The $CAES$ technology is based on the idea of exploiting the excess of energy production during peaks in order to compress the air and store it either in natural storages as empty caverns underground or in some vessels. The energy is stored in form of compressed air that can be exploited when the production is not able to meet the demand and so the cost of electricity can be higher. The exploitation of the air is composed by two steps: a first heating required to increase the power density and then the heated compressed air is used to run a turbine and obtain back electricity [4,5].

This kind of technology is the second in terms of market penetration when considering the bulk energy storage, [5], and is characterized by an average efficiency of $\sim 70\%$ and by the requirement of natural gas to heat up the air before the injection in the turbines, the latter element makes this technology not so appetible in a green energy perspective.

The most diffused technology for the energy storage in large quantities is the Pumped Hydro energy Storage, PHS. In this case the idea is to exploit the excesses during the production in order to pump the water to an upper reservoir to store it in form of potential power. This power is then converted back in electricity making it flow through a turbine. [4,5]

This kind of technology accounts for the major share of energy system installed power, according to Luo et al. [4], the share covered in 2012 was above 99% contributing for $\sim 3\%$ to the total power generation. This technology is characterized by strong geographical constraints since it requires to have two physical reservoirs in a suitable position, as a consequence cannot be applied everywhere and a large part of the most efficient sites are already exploited [4,5].

There had been several studies about the possible integrations of this kind of technologies within grids or to check their application to guarantee the grid quality, Ma et al. [9,10] have analyzed the possibility of integrating a PHS technology with renewables in order to allow continuous and safe off-grid operation; obtaining that the application of such a technology can provide very good results.

In the work of Ma et al. [9] there is a coupled use between the PHS technology and some rechargeable batteries that can be used in order to provide electricity in a short time. The electrochemical batteries are one of the older technologies when considering the energy storage [5] and stores the electricity as chemical energy with the possibility of retrieving it back within short time and with a high efficiency. The two main types of rechargeable batteries are the lead-acid batteries, characterized by a low capital cost but also by the requirement of a thermal management and low cycling time, and the lithium-ion batteries, characterized by a very high efficiency, $\sim 97\%$ [4], but with a higher cost and high degradation caused by a high depth of discharge [4,5].

Have been performed several studies on the possible applications of these technologies, Wang et al. [11] have addressed the possibilities related to the implementation of a system comprehensive of PV panels together with some batteries. The presence of a balancing element as the batteries can improve a lot the performances of the panels reducing their variability in the production.

There are also other technologies that can be used to perform energy storage as the mechanical flywheels, that stores the energy in form of rotational kinetic energy accelerating a rotating mass when there is the excess of electricity and exploiting the inertia to produce electricity when needed [5], or the superconductor energy storage that stores the energy as static charge at the interface between the two electrodes surface and the electrolyte put between them [4]. They are suitable only for small capacity storage but are one of the faster technologies to be discharged, indeed Aly et al. [12] developed a control strategy to reduce the wind turbines fluctuation applying supercapacitors for the reactive power compensation.

Together with all these possible technologies the hydrogen energy storage can play an important role especially considering the possibility for a long-term energy storage. As underlined by Escamilla et al. [13] only the $CAES$ and PHS are technologies that can be applied for a large-scale energy storage while the other applications can be suitable only for a grid balancing at small scale. The main problems related to these technologies, makes them unfeasible for a worldwide diffusion; the alternative represented by the chemical storage, especially hydrogen, appears as a consequence more and more appetible.

One of the main positive aspects about hydrogen, is that it is an energy carrier that not only can be adopted to convert it back in electricity but is also possible to use for other purposes such as drive transport vehicles or use it in the industrial sector [13,14]. Another positive aspect of this type of energy storage is the possibility related to the production of hydrogen in situ since it is possible to produce H_2 whenever it is needed. Additionally, there is a great evolution in the large-scale electrolyzers that allow a massive production of hydrogen starting from water and using electricity coming from RES [13].

This work will be focused on the possible applications of the so-called Power-to-Power, $P2P$, energy storage that is the conversion from electricity to a chemical medium, allowing the storage for longer time due to the easier handling with respect to electricity, and back to electricity; in this specific case the analyzed chemical product will be the hydrogen.

During the excess of electricity production, this energy is converted in chemical power producing hydrogen by means of an electrolyzer. At this point the hydrogen is stored, in different possible ways, and when needed it is used to drive either a gas turbine or a fuel cells stack, the analyzed case study considers the latter possibility. With this series of elements, it is possible to decouple the production and the consumption, the hydrogen storage indeed has a low self-discharge rate and ones we have the hydrogen it is an inert unless we use it. More in detail it is necessaire to consider that this kind of energy storage shows the best performances, in terms of trade-off between discharge time and storage efficiency, for a term-period in the order of days to months [13,16].

There are different solutions that can be adopted for the hydrogen storage, the main diffused and mature technologies are:

- Compressed hydrogen: this is the most used alternative among the possible technologies for the hydrogen storage, the hydrogen is compressed at high pressure and then stored within cylindrical vessels. This procedure consumes some energy, $13 - 18\%$ of the Lower Heating Value, LHV of the stored hydrogen and requires a lot of available space since the hydrogen density is not increased so much and at the same time it is not convenient to reach too high pressures due to possible safety issues.
- Liquified hydrogen: this storage alternative reaches a higher density with respect to the compressed solution but also requires a higher energy cost, up to 40% of the hydrogen LHV, in order to reach the required low temperatures. Indeed, it is necessaire to reach the temperature of $-253°C$ to make the hydrogen liquid, at this point it can be stored but suffers of self-discharge due to the boiling of hydrogen caused by the heat exchange with the vessel walls.
- Metal hydrates: in this storage solution the hydrogen molecule is stored thanks to the reaction with some metal atoms that generates the metal hydrates. This is the solution with the highest storage capacity and with the most favorable conditions in terms of safety, on the other hand it requires to refer to the sorption/desorption kinetic and is characterized by a high temperature release of the hydrogen [15].

According to [16] all the already implemented demonstration plants for the P2P technology are obtained using a compressed hydrogen storage. In this report, Marocco et al. present the applications related to the REMOTE project in which have been analyzed and addressed the techno-economic feasibility of a solution comprehensive of a P2P system coupled with a battery storage. In Figure 1 is shown the basic layout of these sites.

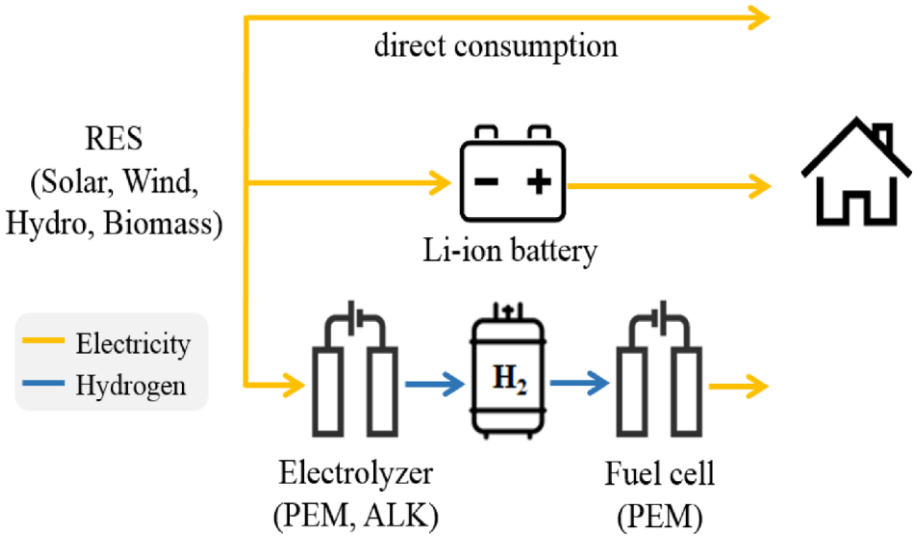

Figure 1. P2P layout analyzed in REMOTE demo plants [16].

The studied applications in this context are four: the first one in Ginostra, Italy, where the system is composed by a PV panel plant of 170 kW, a Li-ion battery with a nominal capacity of 600 kWh and the $P2P$ system composed by a alkaline electrolyzer with nominal power 50 kW, a Proton Exchange Membrane, PEM, fuel cell stack of 50 kW and a compressed hydrogen storage with a total capacity of 21,6 m^3. This system is used to cover the whole village demand that is around 172 MWh per year, but with a high seasonality, characterized by a higher load in summer, and the possibility of directly using the PV production is only equal to one third of the total PV production, as a consequence the energy storage system is necessaire to reach a good reliability of the energy provision.

The second analyzed site is in Agkistro, Greece, where the hybrid battery-$P2P$ system is coupled with a local hydro power plant of nominal power equal to 0.9 MW, and due to the more constant power supply produced by the hydro-plant the storage sizes are smaller with respect to the Ginostra ones: the Li-ion battery has a capacity of 92 kWh and the alkaline electrolyzer a nominal power of 25 kW, the PEM fuel cell stack 50 kW while the hydrogen tank a total volume of 12 m^3. In this case the storage solution is more used as a backup system for critical moments, i.e., to cover possible faults in the hydro power plant.

The third demo-plant of the REMOTE project is the Ambornetti one, Italy, where the aim is to analyze the possible applications for such a solution in a complete off-grid application. In this case the installed renewables are of two different natures, a PV plant of 75 kW and a biomass-fed CHP plant of 49 kW; this production is then coupled with a series of Li-ion batteries for a total capacity of 92 kWh, a alkaline electrolyzer of 18 kW, 85 kW of air-fed fuel cells and a hydrogen storage of 6 m^3. Also in this case, as for the Akgistro one, the renewables are characterized by a quite constant power production, guaranteed by the presence of biomass CHP plant, and as a consequence the storage system is used only to cover the demands during the periods in which the CHP plant is under manutention.

The last site is the one of Froan islands, Norway, where the storage system is coupled with a wind farm composed by three turbines of 225 kW each and by a PV plant of 250 kW. The storage system is the second one for what concerns the Li-ion battery size, equal to 110 kWh, and the biggest in terms of installed PEM fuel cells, reaching 100 kW, and for the first time also the electrolyzer is a PEM type, with a nominal power of 50 kW. The compressed hydrogen storage is able to keep almost 100 kg of hydrogen.

The supposed use in this case for the storage system is to exploit the excess of renewable energy production, it is supposed to have more than two times the energy needs in form of excess and make it available for future uses when needed [16].

The work carried on by Marocco et al., but also the one of Favelpour et al. [17] underlined that the best solution in economic terms to reach the complete independence from the grid is to couple a battery system with a P2P solution avoiding in this way too big batteries whose cost is unfeasible.

Under all these premises the current work aims to determine a suitable control strategy to better optimize the operations of a small battery-P2P system coupled with PV plant in order to satisfy the demand of a small building within the Turin airport.

3. Methodology

This chapter describes the modelling techniques followed to correctly characterize the elements of the system; the characterization is performed to be coherent with the control logics of the system, described in this chapter too.

The last section of the chapter describes the key performance indicators used to quantify the results obtained by the model simulations.

3.1 Components modelling

The first element is the battery that has been modelled within the code considering the nominal capacity, specified in Chapter 4, and the rate of charge and discharge equal to $2C$ accordingly to [18]. The minimum allowed state of charge, SOC_{min}, has been set equal to 0.2 in order to avoid the degradation generated by the deep discharge of the battery.

The alkaline electrolyzer is instead characterized using an efficiency curve that relates the energy in input, electricity, with the energy in output in form of hydrogen flux. This curve is obtained from the one that relates the efficiency and the load percentage presented in [19]; in Figure 2 is reported the graph relating input and output energy. These energies are obtained using (1) and (2), considering that it is possible to set the operating point of the electrolyzer selecting the input power.

$$(1)\ P_{in_{elec}} = \%_{load_{elec}} * P_{elec_{nom}}$$

$$(2)\ P_{out_{elec}} = \eta_{elec} * P_{in_{elec}}$$

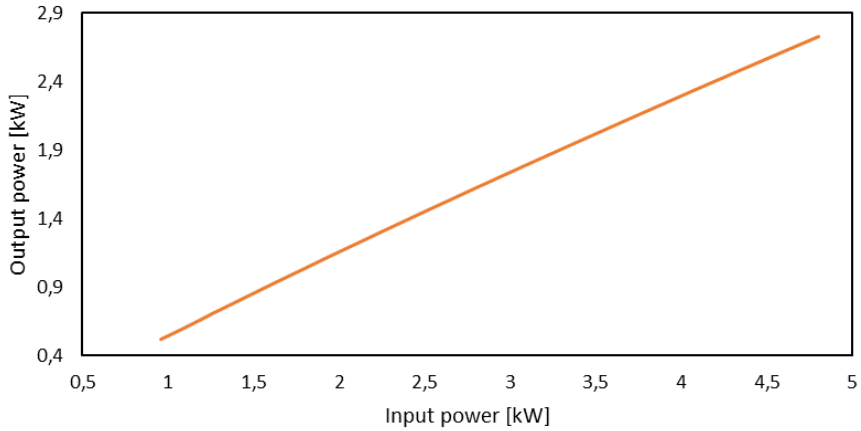

Figure 2. Electrolyzer power curve

The modelling of the fuel cells requires a deeper analysis since one of the most innovative aspects is related to the use of the Solid Oxide Fuel Cell, $SOFC$, for the $P2P$ application in order to cover, for a small fraction, the thermal load. Another interesting aspect to be considered is the possibilities of different blending percentages between hydrogen and methane at the fuel cell input: one of the focuses of the project is indeed the analysis of the performances of the fuel cells while used with different input fuels. The manufacturer has tested the fuel cells with a maximum percentage of input hydrogen equal to $20\ \%$ in blending conditions, mixed with methane, but theoretically it should be possible to work with percentages

of hydrogen between this value and the full hydrogen condition. The project aims to determine the feasibility of these operations and to check which will be the behaviour of the cell characteristic parameters to determine if they are working properly; as a consequence, the modelling of the fuel cells should consider this aspect too.

The fuel cells producer has underlined that this prototype is able to work at its nominal power, equal to 1,3 kW, only if it is completely fed by methane, thanks to the cooling effect generated by the methane reforming reaction, while during the blending operations it is better to provide them a lower input power making them work in derating with a new nominal condition of 1 kW. This additional constraint has to be integrated in the code, considering different nominal conditions on the basis of the different kind of input.

In this case the fuel cells have been modelled referring to [20], the choice has been to directly determine the link between input and output power using the relations expressed by (3), (4) and (5); considering in this case that the driving element is the electric output power and that the fuel cells produce also thermal power. In Figure 3 are reported the curves relating electric, P_{ee}, and thermal, P_{th}, output power as a function of the input power, both for the full power and the derating conditions, the first named as CH_4 and the latter $blend$.

$$(3)\ P_{out\ ee_{cell}} = \%_{out_{cell}} * P_{nom_{cell}}$$

$$(4)\ P_{in_{cell}} = \frac{P_{out\ ee_{cell}}}{\eta_{ee}}$$

$$(5) P_{out\ th_{cell}} = P_{in_{cell}} * \eta_{th}$$

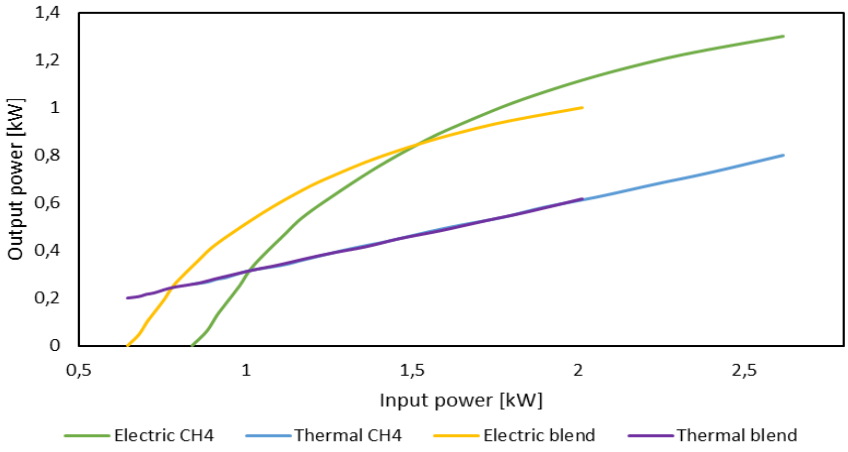

Figure 3. Fuel cells power curves

3.2 Model basic layout

In order to address the possible different alternatives regarding the control logics that can be applied to the system, has been used a power balance approach in which all the different elements are combined to guarantee the satisfaction of the demand (6).

$$(6)\ P_{load} = P_{RES} + P_{storage} + P_{grid}$$

Where:

- P_{load} represents the electricity demand evaluated on a fifteen-minute basis.
- P_{RES} is the power produced by the panels, considered every fifteen minutes.
- $P_{storage}$ is the power provided by the storages either the fuel cells and/or the battery, directly calculated every fifteen minutes.
- P_{grid} is the input power from the grid, assumed as an infinite reservoir.

All the time series that were on an hour basis, the ones of P_{load} and P_{RES} as reported in Chapter 4, have been recalculated with a time step of fifteen minutes thanks to a linear interpolation function that keeps unchanged the total amount of energy. This function considers the value relative to each hour as the one effectively present at the half of that hour, then it is interpolated between these two values. For the first data it is considered that the profile is relative to the whole year, as a consequence the last data can be used to make the interpolation with the first one.

The load profile reported in Figure 17, identifies that there is always the need of power while the PV panels are able to produce only during the daytime and their size determines the impossibility of the coverage of the whole load, as explained in Chapter 4. As a consequence, the grid has to be used in order to compensate the needs when the stored power is not enough.

In all the different analyzed conditions the first use of the power produced by the panels is to directly cover part of the demand. When the PV production is higher than the load, typical condition of the summer days, the excess of energy is firstly used to charge the storages, following different logics explained in Section 3.2, and then, if they are fully charged, it is released to the grid, assuming that it is able to accept all the possible excesses produced by the system. This last assumption is justified by the fact that the grid is linked to all the airport loads, the small quantities produced by this system will always find a load to serve.

The modelling environment used to perform the balance on the whole year and to implement the different possible control logics presented in Sections 3.3, 3.4 and 3.5 is MATLAB. This software allows to write some mathematical models able to perform different calculations.

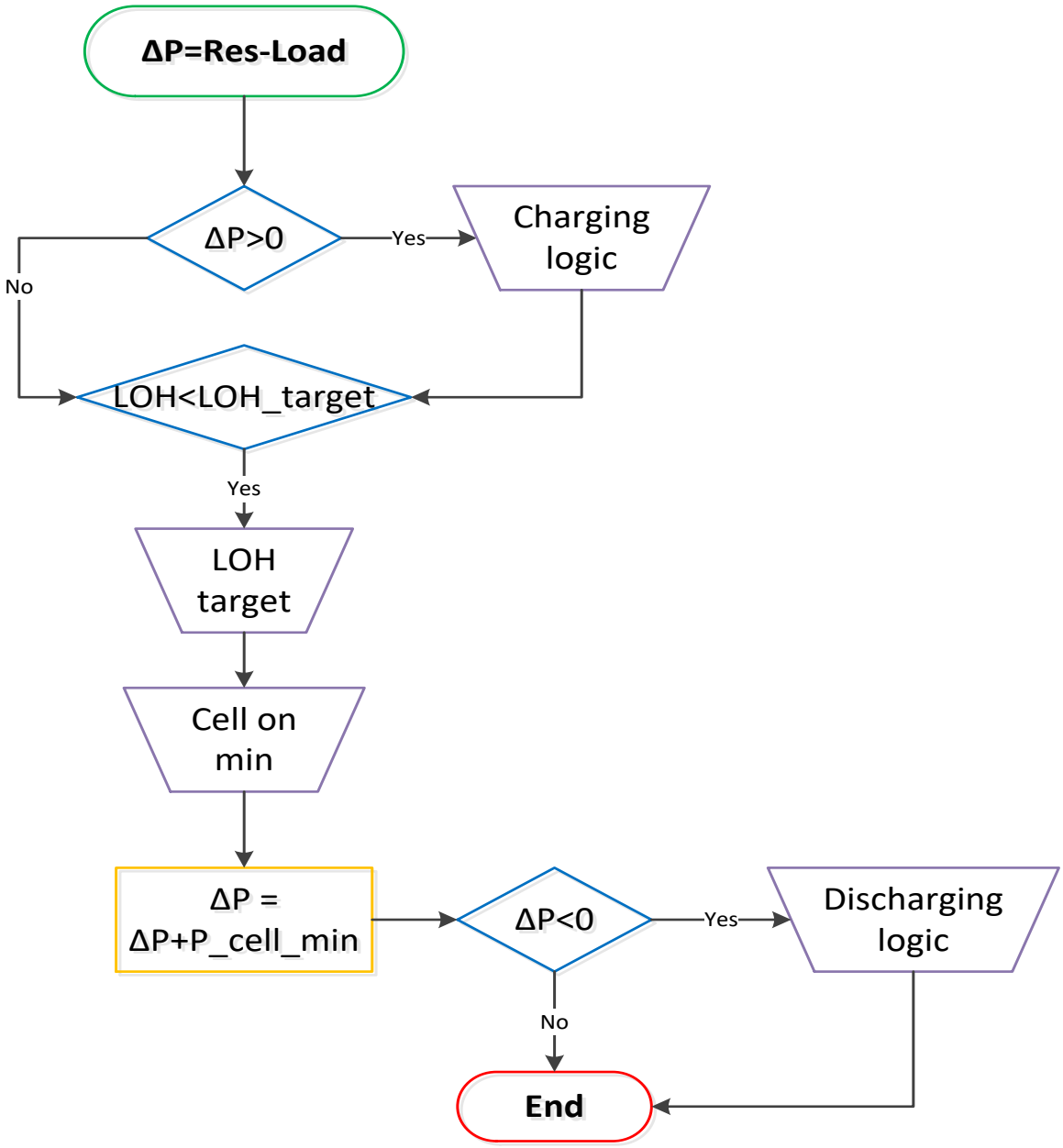

Figure 4. General control logic schematic.

In Figure 4 is presented the general control logic of the system, based on the methodology proposed by Marocco et al. [21], focused on the power balance. The starting point of this analysis is the evaluation of the power gap ΔP between renewable production and load (7).

$$(7)\ \Delta P = P_{RES} - P_{load}$$

If there is power left to be exploited, the system follows one of the charging logics presented in Section 3.3, otherwise, it starts the logic named $LOH\ fixed$, presented in Section 3.5.2, that ensures a minimum level of hydrogen in the storage tank. This last control logic is applied only if the hydrogen tank is not filled enough yet.

The following step is to work the fuel cell at a minimum fixed percentage to avoid thermal cycles generated by continuous switches on/off; this constant work is possible thanks to the function $Cell\ on\ min$ presented in Section 3.5.1. At this point the ΔP is updated by means of the power produced during this guaranteed work of the fuel cells.

The last check is performed analyzing if there is power left to be provided to cover the load, if it is the case the system uses one of the discharging logics presented in Section 3.4, otherwise the system ends the cycle; these passages are repeated every fifteen minutes.

3.3 Charging logics

In this section will be analyzed the different charging logics that can be applied to the system. All of them are characterized by the working condition determined by means of an energy excess, the PV production has to be higher than the load to allow the charging of the storages with the power difference ΔP calculated by means of (7).

3.3.1 Charging logic 1: Battery first

This control logic determines as a priority the charging of the battery while the conversion in hydrogen is performed only when the battery is already fully charged; in this way it is possible to better exploit the higher efficiency of the battery. Figure 5 summarizes the principal steps of this logic.

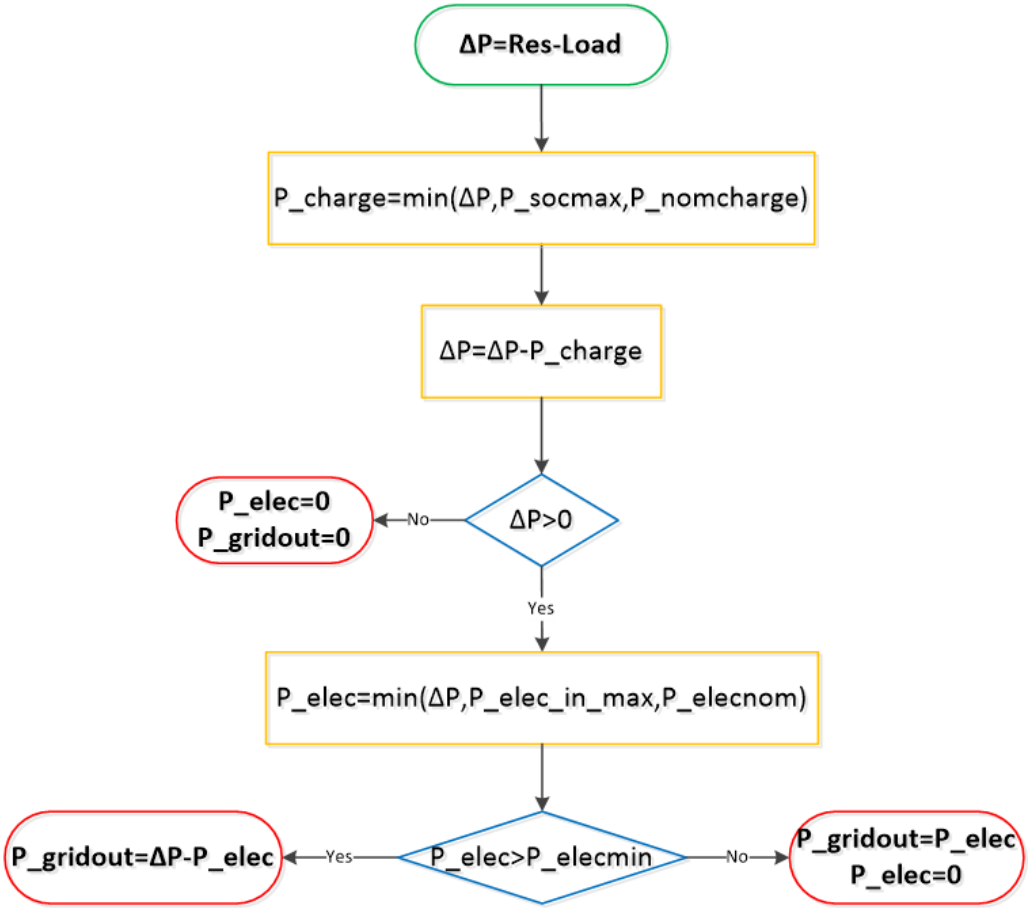

Figure 5. First charging logic schematic, battery first

The first step of the logic consists in the determination of the charging power that has to be provided to the battery, P_{charge}, that is determined as the minimum value between the actual available power, ΔP, the maximum power that avoids an overcharge of the battery, P_{SOCmax}, determined using (8), and the nominal charging power of the battery itself, $P_{nom_{charge}}$, obtained through (9).

$$(8)\ P_{SOC_{max}} = (SOC_{max} - SOC_i) * \frac{Cap}{\Delta t}$$

$$(9)\ P_{nom_{charge}} = Cap * C_{rate_{charge}}$$

Using this definition with the minimum function, it is ensured that the charging power does not overcome the maximum one that can be accepted by the battery, and, at the same time, the battery cannot be overcharged by the entering power. Whit this definition, if the battery is fully charged the $P_{SOC_{max}}$ becomes null determining also a null value for the P_{charge} as a consequence excluding the battery from the charging process.

After this step, the code performs a check on the left power difference, ΔP, once it has been removed the amount of power used to charge the battery; if there is no more power that can be exploited, the logic simply stops there while if there is power left it is used to charge the hydrogen storage.

The determination of the theoretical power that can be used by the electrolyzer is obtained performing the analysis of the minimum value between three different powers, the remaining ΔP, the nominal working power of the electrolyzer $P_{elec_{nom}}$ and the maximum power of the electrolyzer that avoid an overcharge of the hydrogen storage $P_{elec_{in_{max}}}$, determined by the use of the power curve of Figure 6 and by the power output value determined by (10).

$$(10)\ P_{elec_{max}} = (LOH_{max} - LOH_i) * LHV_{H_2} * \frac{m_{H_2max}}{\Delta t}$$

As for the battery, this way of evaluating the power automatically excludes the hydrogen production if the tank is already filled, the $P_{elec_{max}}$ becomes null in this case determining a null value also for $P_{elec_{in_{max}}}$. Once this value is determined it is converted in the correspondent input power, $P_{in_{max-elec}}$ using the inverse of the power curve presented in Figure 2. The formula (10) requires a deeper analysis because of the parameter m_{H_2max} that cannot be directly obtained with the actual information available about the hydrogen storage.

In order to evaluate this parameter, it is required to determine the hydrogen density at the pressure of 16 bar that is the actual operating pressure of the tank. To do so has been assumed to be possible to consider the hydrogen as an ideal gas, applying as a consequence (11). This assumption is verified by [22] where it is underlined that the value of the hydrogen compressibility factor at ambient temperature and pressure level close to the ambient one is almost equal to 1.

$$(11)\ \rho_{H_2} = \frac{MM_{H_2} * p}{R * T}$$

Combining the value of the density obtained in this way with the volume of the storage, data available for the real model and reported in Table 1, it is finally possible to determine m_{H_2max}.

Once the theoretical power required is determined the model performs a check on it to verify that it is higher than the minimum working power of the electrolyzer $P_{elec_{min}}$, determined by means of (12).

$$(12)\ P_{elec_{min}} = P_{elec_{nom}} * \%_{min_{elec}}$$

If the theoretical working power of the electrolyzer P_{elec} is above the value of $P_{elec_{min}}$ the model determines the power released to the grid, $P_{grid_{out}}$, with (13); otherwise, the value of P_{elec} is released to the grid and then this value is set equal to zero in order to do not create errors in the hydrogen storage management. Ones it is determined the value of P_{elec} it is performed the calculation of the effective output power, correspondent to the effective quantity of hydrogen produced, using the curve presented in Figure 2, obtaining the $P_{out_{eff-elec}}$

$$(13)\ P_{grid_{out}} = \Delta P - P_{elec}$$

At the end of all these passages the last step is the update of the storage conditions, evaluating the variations caused by the charging powers. The model always makes this passage, considering the fact that when it is impossible or there is no power left, some of the powers P_{charge} and/or P_{elec} are set with a null value. To calculate the updated SOC is used (14) while (15) is adopted to address the variation within the hydrogen tank.

$$(14)\ SOC_{(i+1)} = SOC_i + P_{charge} * \frac{\Delta t}{Cap}$$

$$(15)\ LOH_{i+1} = LOH_i + \frac{P_{out_{eff-elec}} * \Delta t}{m_{H_2 max} * LHV_{H_2}}$$

3.3.2 Charging logic 2: hydrogen tank first

The second charging logic provides a higher priority to the hydrogen charging, in order to better explore the possibilities related to its use. In Figure 6 is reported the general logic scheme at the basis of this second charging solution.

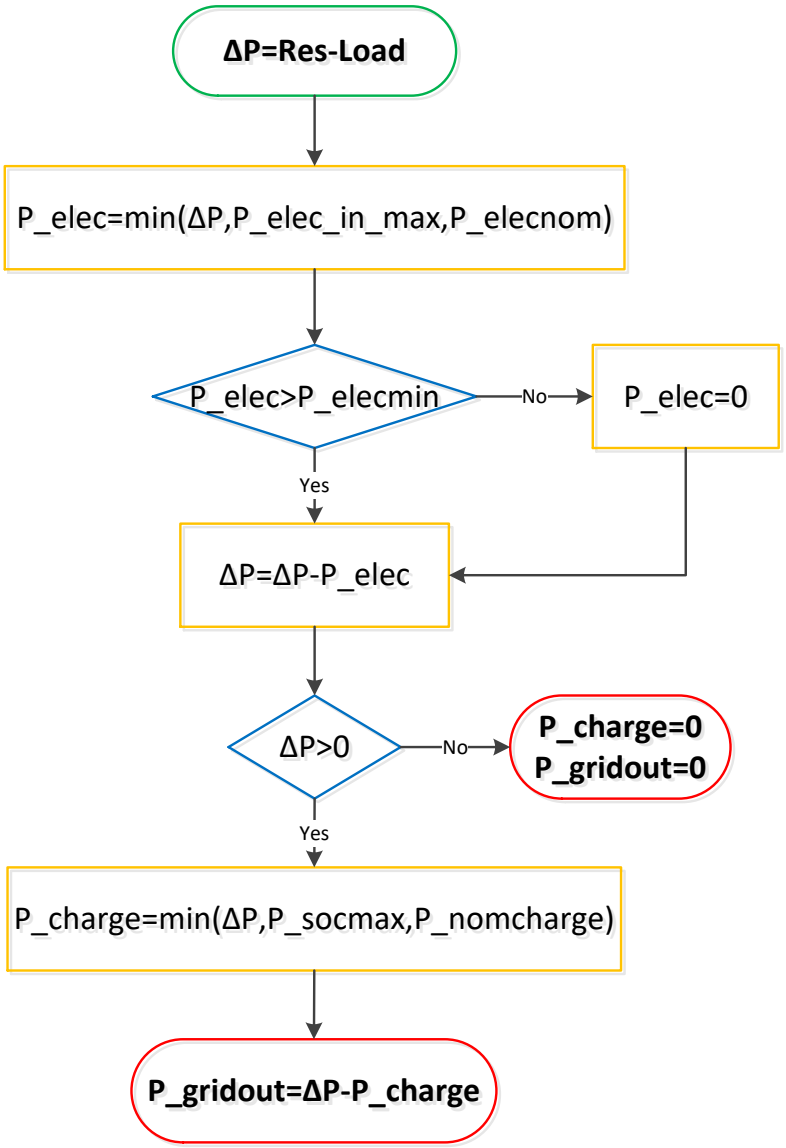

Figure 6. Second charging logic schematic, hydrogen tank first

This second alternative control logic follows the passages explained for the first one in Section 3.3.1 with a different order. It starts with the determination of the P_{elec} obtained as the minimum value between the same three explained in section 3.3.1., ΔP, $P_{elec_{in_{max}}}$, and $P_{elec_{nom}}$.

The check on the $P_{elec_{min}}$ does not determine the end of the cycle if not respected, as in the first charging logic, it simply set the value of the P_{elec} equal to zero. The check to finish the cycle is before the one on the ΔP, it determines the possible exit setting at a null value both the battery charging power and the power released to the grid.

If instead it is possible to operate the electrolyzer at the correct working point determined through P_{elec}, it is filtered by the electrolyzer power curve and converted into $P_{out_{eff-elec}}$ needed to determine the amount of produced hydrogen.

The second part of the calculations determines the power charged within the battery, starting again with the setting of P_{charge} as the minimum value between three powers that, as in the previous case, are the left ΔP to be exploited, $P_{SOC_{max}}$ determined by means of (8) and $P_{disch_{nom}}$ from (9).

In this case the power released to the grid is no longer determined using (13) but instead using (16) since the value of P_{elec} is already removed from the ΔP.

$$(16)\ P_{grid_{out}} = \Delta P - P_{charge}$$

The last step is, also in this case, the updating of the new levels within the battery and the hydrogen storage, obtained using (14) and (15).

3.3.3 Alternative charging logic

In order to better characterize the model, it has been included the possibility of two alternative charging logics in which the electrolyzer can be made work at the minimum power level thanks to the use of the grid input. This logic can help the electrolyzer working at a constant level without many switches on/off that can strongly damage the machine.

In Figure 7 is reported the implemented additional section to the first charging logic, it is not represented the whole flow chart since it is almost equal to the one of Figure 5, anyway, these blocks are linked to the check performed after the definition of P_{elec}.

It is not represented the additional part related to the second charging logic since the added blocks are the same of Figure 7, also in this case located after the definition of P_{elec}.

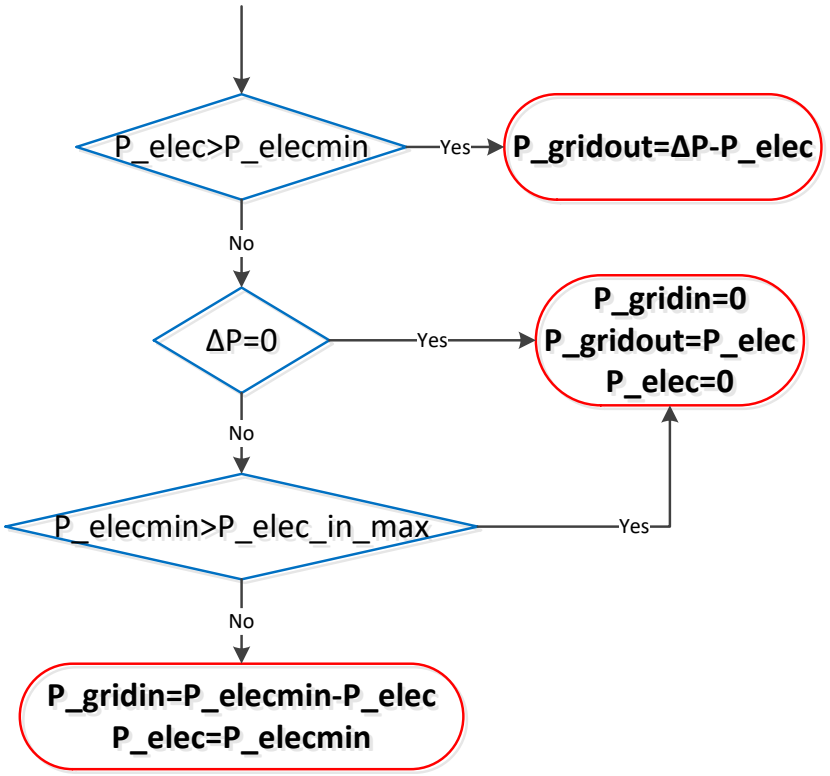

Figure 7. Additional part of the alternative charging strategy

The first step is a check on the value of ΔP, after the one on $P_{elec_{min}}$, to avoid the starting of the electrolyzer using only the power from grid; this possibility is included in the function presented in Section 3.5.2.

If the value of ΔP is null, the logic ends in the same way presented in Section 3.3.1, it is additionally reported the value of the input power from the grid to always have the same kind and number of outputs; this last aspect is important for the modelling in MATLAB.

The second check is instead performed in order to verify that the $P_{elec_{min}}$ does not produce more power than the one that will completely charge the hydrogen tank $P_{elec_{in_{max}}}$. If it is verified that there is no problem in making work the electrolyzer at its minimum the input from the grid, $P_{grid_{in}}$, is used to compensate the required gap between the $P_{elec_{min}}$ and the power already available from the charging, accounted in the variable P_{elec} thanks to its definition.

For sake of simplicity has not been implemented the possibility of using the power stored within the battery to compensate the requirements; this has been done because of the other implemented control logics already accounting for this aspect. Indeed, this alternative pathway becomes almost useless with the implementation of the function $LOH\ fixed$.

3.4 Discharging logics

This Section deals with the different control logics that can be implemented in order to satisfy the demand when there is not enough power provided by the PV panels. In these conditions, in order to deal with positive values, the ΔP is calculated following (17) and not (7) as it has been done for the charging logics.

$$(17)\ \Delta P = P_{load} - P_{RES}$$

In this section the value is assumed positive to correctly apply the definitions of some working points as the minimum value among a series of alternatives.

The discharging logics will be much more complicated since the model should be able to manage both the conditions of blending and full methane operation of the fuel cells, have to consider the presence of both electric and thermal load, and, in the more complex conditions, should be able to guarantee the correct blending operations managing also the electrolyzer.

It is important to consider that before the actual discharging logic it is present the function $Cell\ on\ min$, presented in Section 3.5.1; as a consequence, in these logics is neglected the check on the minimum power of the cells. The analysis performed in all the four discharging logics presented, regards the possibility of exploiting more than this minimum guaranteed power from the fuel cells.

3.4.1 First discharging logic: battery first without electrolyzer

This is one of the simplest discharging logics, in this case the model exploits at first glance the power stored within the battery and then the power available from the fuel cells, in this way it is possible to better use the higher efficiency of the battery.

In Figure 8 is showed the flow chart explaining the different passages followed in the implementation of this control logic.

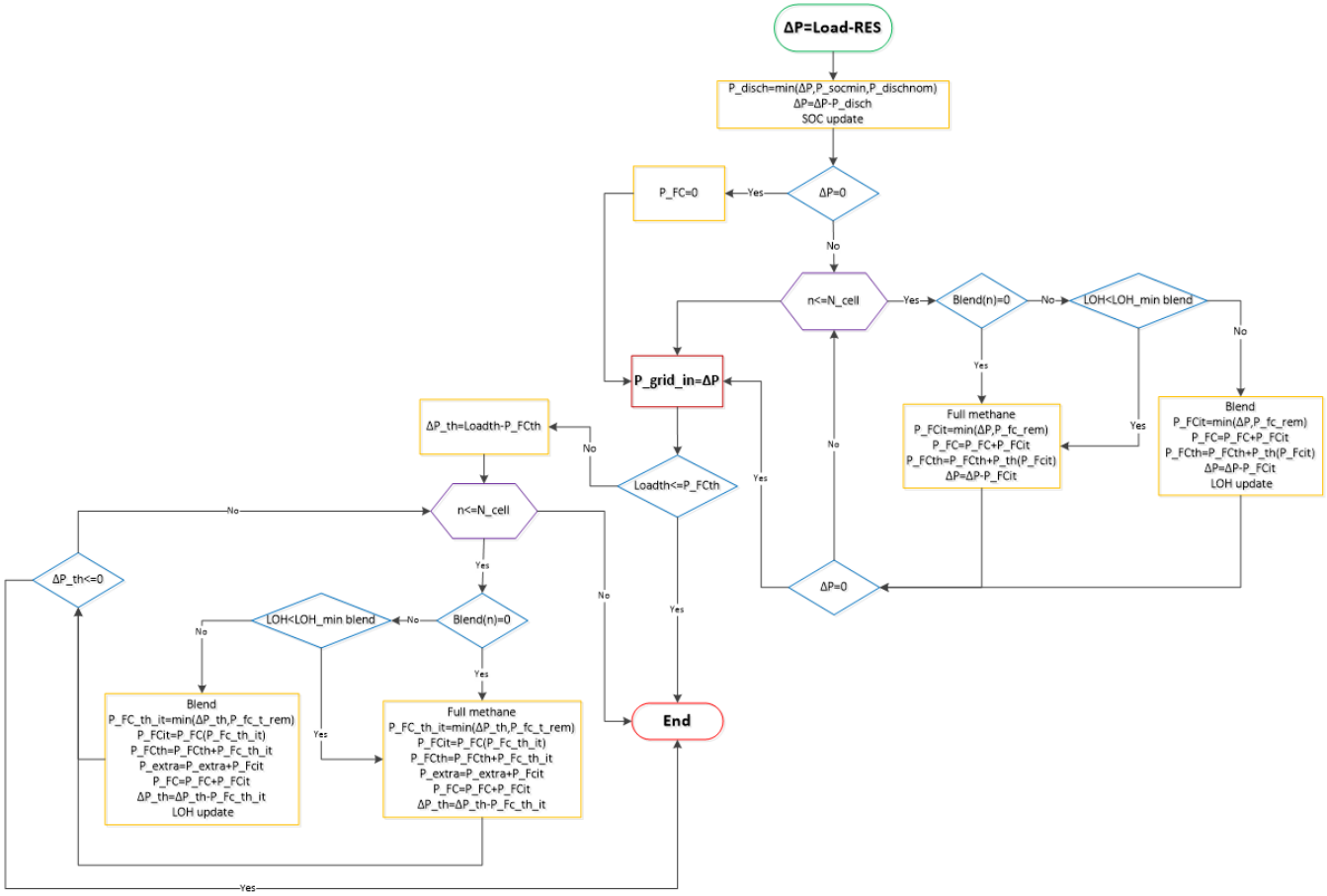

Figure 8. First discharging logic flow chart.

The first step is the evaluation of maximum power that can be extracted from the battery, is adopted, also in this case, the minimum function to define it. This choice is done to obtain the possibility of automatically exclude the battery if there is no more available charge stored.

The discharging power P_{disch} is obtained as the minimum between the power that should be provided ΔP, the nominal discharging power $P_{disch_{nom}}$ obtained from (18) and the maximum power that can be extracted from the battery without damaging it $P_{SOC_{min}}$,i.e., not going below the value of SOC_{min}, determined by means of (19).

$$(18)\ P_{disch_{nom}} = Cap * C_{rate_{discharge}}$$

$$(19)\ P_{SOC_{min}} = (SOC_i - SOC_{min}) * Cap * \Delta t$$

Once it is determined the value of the discharging power it is possible to perform two other passages, the first one is to evaluate the new ΔP removing the power taken from the battery, and the second is to update the value of the battery SOC removing the charge extracted from the battery. This step is performed using (20).

$$(20)\ SOC_{i+1} = SOC_i - P_{disch} * \frac{\Delta t}{Cap}$$

With this definition, if there is no more power stored in the battery, the value of $P_{SOC_{min}}$ becomes null since the value of SOC_i will be the same of SOC_{min}, as a consequence, the value of P_{disch} will be null too.

The next step will be a check performed on the value of the remaining power to be provided to satisfy the demand; if the value of ΔP is null, the model checks if there is required thermal need to be satisfied, following in this case the passages presented below. If instead ΔP is different from zero, the model starts with the operation of the fuel cells to satisfy the electric need.

The analysis of the two fuel cells is performed separately, considering the possibility of a differentiation in the operating conditions of the two. Considering a more generic condition, the model is able to manage separately N_{cell} making an inner loop on each one of them; additionally, the model is also able to consider possible different blending levels for the cells. In the actual case study these conditions cannot be possible due to the presence of a single mixing unit, as a consequence the model considers the fuel cells as a single element.

The first step of the loop relative to each cell is the check performed on the $blend_n$ since the cell will work in different conditions if we are referring to the full methane or the mixed operation, as already underlined in Section 3.1. The equations determining the working point will be the same even if the maximum and minimum allowed powers are different. The following part represents in detail the steps followed for the blending operation, for what concerns the methane one, the powers are defined in the same way.

The second step required to work in blended conditions is to have enough hydrogen within the tank. This check is performed comparing the actual LOH with a parameter named $LOH_{min_{blend}}$ that defines the minimum quantity of hydrogen ensuring to do not overcome the threshold set by LOH_{min} after the fuel cells work; $LOH_{min_{blend}}$ is defined by (21)

$$(21)\ LOH_{min_{blend}} = LOH_{min} + \dot{m}_{H_2} * \frac{\Delta t}{m_{H_2 max}}$$

The main issue comes from the determination of the $\dot{m}_{H_2}$ that can be defined starting from $\dot{n}_{H_2}$ and using the MM_{H_2}. The problem is then shifted to the search of the molar flow rate that can be obtained by means of (22).

$$(22)\ \dot{n_{H2}} = \frac{P_{in_{eff}}}{MM_{H_2} * LHV_{H_2} + MM_{CH_4} * \frac{1 - blend_n}{blend_n} * LHV_{CH_4}}$$

This formula is obtained explicating the $\dot{n_{H2}}$ form equation determining the chemical power of a mixture of hydrogen and methane, (23), and considering that the $blend_n$ represents the ratio between hydrogen and methane in the mixture (24), (25).

$$(23)\ P_{chemical} = \dot{m}_{H_2} * LHV_{H_2} + \dot{m}_{CH_4} * LHV_{CH_4}$$

$$(24)\ \dot{n}_{H_2} = blend_n * \dot{n}_{tot}$$

$$(25)\ \dot{n}_{CH_4} = (1 - blend_n) * \dot{n}_{tot}$$

To determine $P_{in_{eff}}$ it is required to evaluate which will be the theoretical output power of the cells since, as explained in Section 3.1, it is the real determining parameter for this machine. This theoretical output power can be determined as the lower value between the nominal power of the fuel cell and the actual required power ΔP. It is important to underline that in Section 3.5.1 will be presented a function that

determines a guaranteed working point of the fuel cells, to avoid the presence of dangerous thermal cycles, and to do not make any error it is crucial to consider an additional step.

The problem is related to the fact that the efficiency of the fuel cell is different at the different working points, as underlined by Figure 3, as a consequence the point at the guaranteed working level will be characterized by an efficiency different from the real one if the cell works at higher power. To avoid the error caused by this difference, the fuel cell power output will be set to a null value, removing the power production and hydrogen consumption, if the cell is used in this part of the code.

The next passage is to use the inverse of the curve presented in Figure 3, the one determining the input power as a function of the output one, to consider the not-constant efficiency of the fuel cells.

With this series of steps, it is possible to determine if the cell can work in blending conditions without damaging the hydrogen tank with an over-discharge; if this is not so, the cell is made work with a full methane input in this control logic.

At this point can be calculated the power output of the single cell $P_{FC_{it}}$ as equal to the theoretical output power calculated in the preliminary analysis.

The last but one step is the evaluation of the thermal output of the cell, the produced thermal power associated with the electric power production, represented in the flow chart of Figure 8 by means of $P_{FC_{th}}(P_{FC_{it}})$. In order to calculate $P_{FC_{th}}(P_{FC_{it}})$ is used a power curve linking together the electrical and thermal output, this curve is the one represented in Figure 9. In this figure are reported the two curves in the case of a blending or full methane operation, considering the differences underlined in Section 3.1.

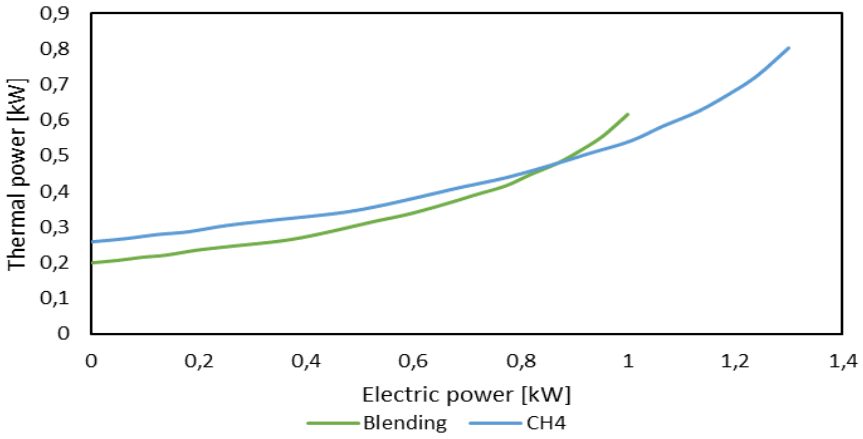

Figure 9. Fuel cell output power curves

As it has been done for the evaluation of the $P_{in_{eff}}$, the correct calculation is performed removing the part already calculated by the function providing the guaranteed working point and using the correct efficiency of the fuel cells.

The obtained thermal power output, $P_{FC_{th}}(P_{FC_{it}})$, is then accounted in the variable $P_{FC_{th}}$ where all the produced thermal power from the fuel cells is considered.

The last step of the fuel cell cycle is the update of the LOH level within the hydrogen storage, it is done using (26). This passage is required if the cell worked in blending conditions, otherwise the LOH is kept unchanged.

$$(26)\ LOH_n = LOH_i - \dot{m_{H_2}} * \frac{\Delta t}{m_{H_2 max}}$$

At the end of each iteration about a single cell, the ΔP is recalculated removing the produced $P_{FC_{it}}$, this last value is also added to the variable P_{FC} in order to account the total power output of the fuel cells. These steps end the part of the electric load that can be covered thanks to the storages, the left ΔP is covered using the grid.

Looking at Figure 8, the left part of the flow chart represents the passages required to supply the thermal load using the available power from the fuel cells. This part of the code is implemented but not used in the real case since the fuel cells are not supposed to work in a thermal load following operation, however the logics behind this part will be explained too.

The first step of the analysis requires to perform a check between the already produced thermal power, $P_{FC_{th}}$, and the thermal load that should be supplied at this iteration, $Load_{th}$. If the already produced power is higher than the load, the cycle ends, otherwise the model calculates which is the thermal power left to be provided in order to satisfy the demand.

Then it is performed again a cycle using the cells not yet exploited to cover the electric load. The performed calculations are the same of the cycle in which the cells are used to cover the electric load, starting with the calculation of the possibility of make the cell work in blending conditions.

The main difference is that the calculations are performed in terms of thermal power, the analyzed power that can be generated is the thermal one also from a theoretical point of view. In this case is determined the theoretical thermal output $P_{FC_{th_{it}}}$ as the minimum between the left $Load_{th}$ and the maximum thermal of the cell, $P_{nom_{th-cell}}$. Also in this case, it is necessaire to reset the fuel cell operating power and the LOH to the level before the working at the guaranteed load to ensure the correct efficiency.

From this power is determined in the same way the required level of hydrogen $LOH_{min_{blend}}$ applying (21), the only difference is that $P_{in_{eff}}$, required to use (22), is obtained using the inverse of the curves of Figure 3 starting from the thermal power in this case, violet and light blue curves in figure.

The curve of Figure 9 is used to determine the correspondent electrical output associated with the thermal output produced by the cell $P_{FC}(P_{FC_{th_{it}}})$, this power is not used to cover the electric demand, as a consequence it is accounted in a proper variable, the P_{extra} used to determine which will be the extra power sent to the grid. The value of P_{extra} is then added to the actual P_{FC} in order to correctly determine the total power output of the cells in the analyzed time step.

The last step is to determine the new level of hydrogen if the fuel cell has been used in blending condition, this evaluation is performed using (26) as for the electric load following loop.

3.4.2 Second discharging logic: fuel cells first without electrolyzer

This second discharging logic is similar to the first one presented in Section 3.4.1, the main difference is related to the choice of using first the fuel cells and only as a second option the battery. This

choice will determine a higher use of the fuel cells avoiding in this way possible damages caused by a not constant use.

In Figure 10 is presented the flow chart containing the main required steps in order to implement the logic; as for Figure 8, the left part of the graph represents the thermal part of the problem. Also in this logic, and for the following ones too, the real model works considering a single cell and neglecting the thermal part.

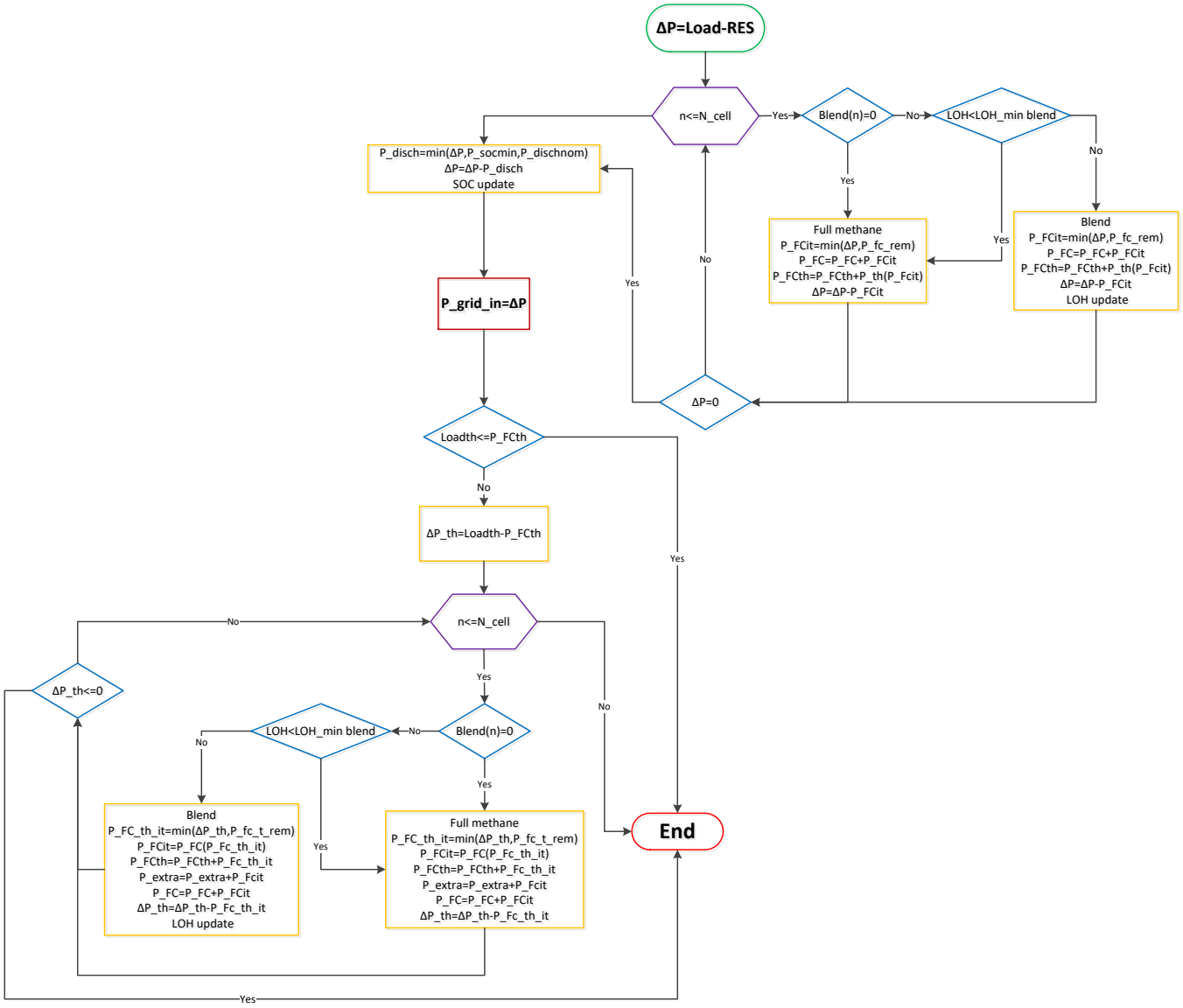

Figure 10. Second discharging logic flow chart.

In this case the logic starts with the cycle used to exploit the fuel cells, it is the same cycle explained in Section 4.3.1 and tries to cover the largest part possible of the ΔP. At the end of these steps, the battery is used to compensate as much as possible the required power.

The power output of the cells is determined again as the minimum value between ΔP and $P_{FC_{nom}}$, considering the same check needed to verify the possible working in blending conditions. As in the previous case, the alternative if there is not enough hydrogen in the tank is to use a full methane operation.

The power exploited from the battery is equal to the minimum value between the remaining ΔP, considering the power produced by each single cell, $P_{SOC_{min}}$, also in this case obtained by means of (19), and $P_{disch_{nom}}$, from (18).

As in the previous case the left load to be covered, if present, is totally supplied by means of the grid; after this part the thermal one is exactly equal to the one of the first discharging logic since also in this case is used a cycle to use the left power from the fuel cells if the already produced thermal output is not enough to cover the demand.

3.4.3 Third discharging logic: battery first with electrolyzer

This control logic is an alternative version of the first one presented in Section 3.4.1; the difference is that, in this case, if the cell is supposed to work in blending conditions and the amount of hydrogen stored in the tank is not enough to allow the correct operation of the cell, the electrolyzer is switched on to produce the correct level of hydrogen.

This aspect cannot be representative of a real case, since we have to consider the ramp rates of the switch on/off of the electrolyzer, that will not produce instantaneously hydrogen; however, with this control logic it is possible to verify how much this switch on will happen and act in order to guarantee the correct level of hydrogen in the tank in order to avoid this necessity. The control logic presented in Section 3.5.2. will ensure this correct level of hydrogen.

In Figure 11 is presented the set of additional steps that should be applied to the flow chart of Figure 8 to allow the possible switch on of the electrolyzer. For a better comprehension of the changed part, it is represented the whole cycle relative to the fuel cells, even if not all the parts are changed.

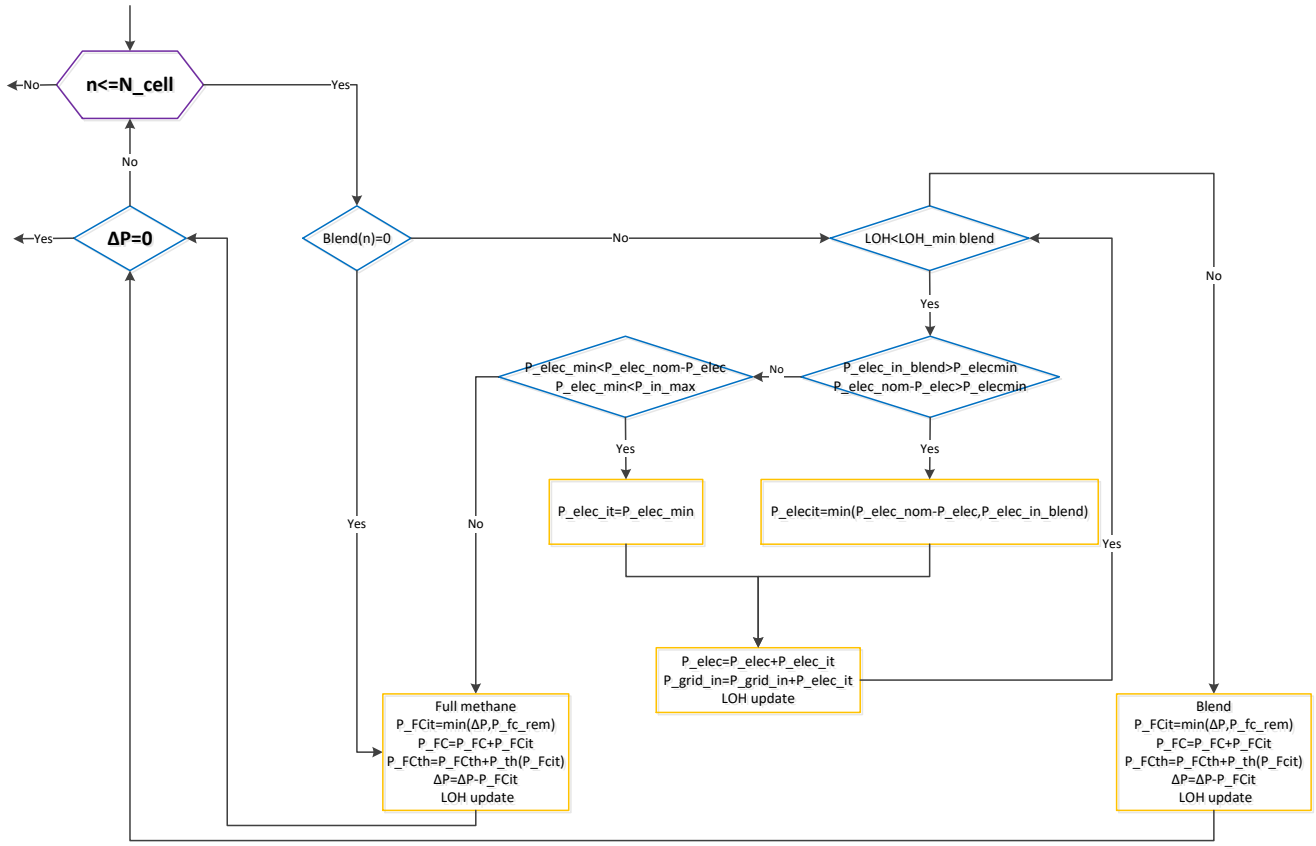

Figure 11. Third discharging logic fuel cell loop

Before this loop the passages are exactly the same of the first control logic, it starts with the exploitation of the battery to cover the demand as much as possible.

The loop starts with the check of the possibility for the cell to perform blending, if it is so, is used (21) to determine the value of $LOH_{min_{blend}}$ following the series of passages listed in the previous analysis. Then is determined the theoretical output as $P_{FC_{it}}$ and from it is derived the necessaire input from the power curve, showed in Figure 3; starting from this value is obtained the required mass flow rate of hydrogen that has to be provided to the fuel cell.

If the required level of hydrogen is not available in the storage, the model check if it is possible to operate the electrolyzer in order to produce the required quantity of hydrogen. The steps to address this possibility are relative to the determination of the actual power able to satisfy the hydrogen demand.

In this case it is required to start from the power output, representative of the amount of produced hydrogen, that can be evaluated using (27).

$$(27)\ P_{elec_{blend}} = \left(LOH_{min_{blend}} - LOH_i\right) * LHV_{H_2} * \frac{m_{H_2 max}}{\Delta t}$$

From this obtained power output is then used the inverse of the power curve presented in Figure 2 to determine the correspondent necessaire input, $P_{elec_{in_{blend}}}$. The following step is to determine if this power is higher than the minimum working point of the electrolyzer, otherwise cannot be feasible to safely operate the machine at that power level.

It is required to perform a simultaneous check on the value of $P_{elec_{in_{blend}}}$ since we have to be sure that there is the possibility of exploiting it. The electrolyzer is used in different parts of the code and, as a consequence, it is necessaire to verify that the total power taken from it during the single iteration is not higher than the nominal power. To address this aspect is used the difference between $P_{elec_{nom}}$ and the already used in the iteration P_{elec}; if it is higher than the $P_{elec_{min}}$ there are no problem in the selected working point of the electrolyzer.

In the case in which $P_{elec_{in_{blend}}}$ is lower than $P_{elec_{min}}$, a second check is performed defining the $P_{elec_{in_{max}}}$ equal to the maximum power input that can be provided to the electrolyzer that avoid an overcharge of the hydrogen storage. This power is again obtained from an output power, from $P_{elec_{max}}$ defined trough (28).

$$(28) P_{elec_{max}} = (LOH_{max} - LOH_i) * LHV_{H_2} * \frac{m_{H_2 max}}{\Delta t}$$

The input power obtained from this, using again the inverse of the electrolyzer power curve, is then compared with the $P_{elec_{min}}$, if the minimum power is lower than this input power the electrolyzer is worked at the minimum power, $P_{elec_{it}} = P_{elec_{min}}$, producing a bit more hydrogen than the necessaire but always avoiding overcharging the tank.

Also in this case, it is required the check on the power left of the electrolyzer, it is performed with the same principle used in the previous part, even if it is used the relationship seen from the opposite point of view, the value of $P_{elec_{min}}$ has to be bigger than the difference $P_{elec_{nom}} - P_{elec}$.

If instead the $P_{elec_{in_{blend}}}$ is higher than the $P_{elec_{min}}$, the effective electrolyzer working point, $P_{elec_{it}}$ is set equal to the minimum value between this calculated $P_{elec_{in_{blend}}}$ and the difference between the nominal power of the electrolyzer, $P_{elec_{nom}}$, and the already exploited P_{elec} during the analyzed iteration.

The last step of this analysis is to determine the new LOH after the electrolyzer work, it is obtained using (15); the $P_{out_{eff-elec}}$ in this case is obtained using the power curve of Figure 2 with the value of $P_{elec_{it}}$ as input power.

This procedure is performed as a loop since it is supposed possible to operate more times the electrolyzer in order to reach the correct hydrogen level within the storage, always checking that the working point of the electrolyzer does not overcome its nominal value that is assumed to be the maximum working point of the machine.

On the other hand, it is considered the hypothesis in which the required level of hydrogen in the storage cannot be reached since the $P_{elec_{in_{blend}}}$ is lower than $P_{elec_{min}}$ and also $P_{elec_{in_{max}}}$ is lower than the minimum allowed power. In this case the only possibility is to work the fuel cell in full methane conditions; this is considered as the worst alternative, chosen only if there is no possibility of producing enough hydrogen.

The solution in which the system automatically reduces the blending percentage in order to allow the cells to still work using hydrogen has not been kept in consideration, assuming that as a solution not compliant with the possible tests that can be done on the system.

The power used by the electrolyzer in each iteration of the loop is then accounted by means of a proper variable in order to determine how many times it is used in this part of the code, allowing a deeper analysis on the electrolyzer performances. The power to work the electrolyzer is provided by the grid, supposed as an infinite power reservoir.

The passages determining the operating point of the fuel cell are the same ones of the cycle presented in Section 3.4.1. without any variation, this loop for the operation of the electrolyzer during the discharging phase is replicated, with the same passages, in the thermal part of the cycle.

3.4.4 Fourth discharge logic: fuel cells first with electrolyzer

This last discharging logic applies the variation of the fuel cell loop presented in Section 3.4.3. to the flow chart of the second discharging logic, with the additional possibility of using the power stored within the battery in order to drive the electrolyzer.

In Figure 12 is reported the varied loop with the additional blocks relative to the possibility of the exploitation of the battery power.

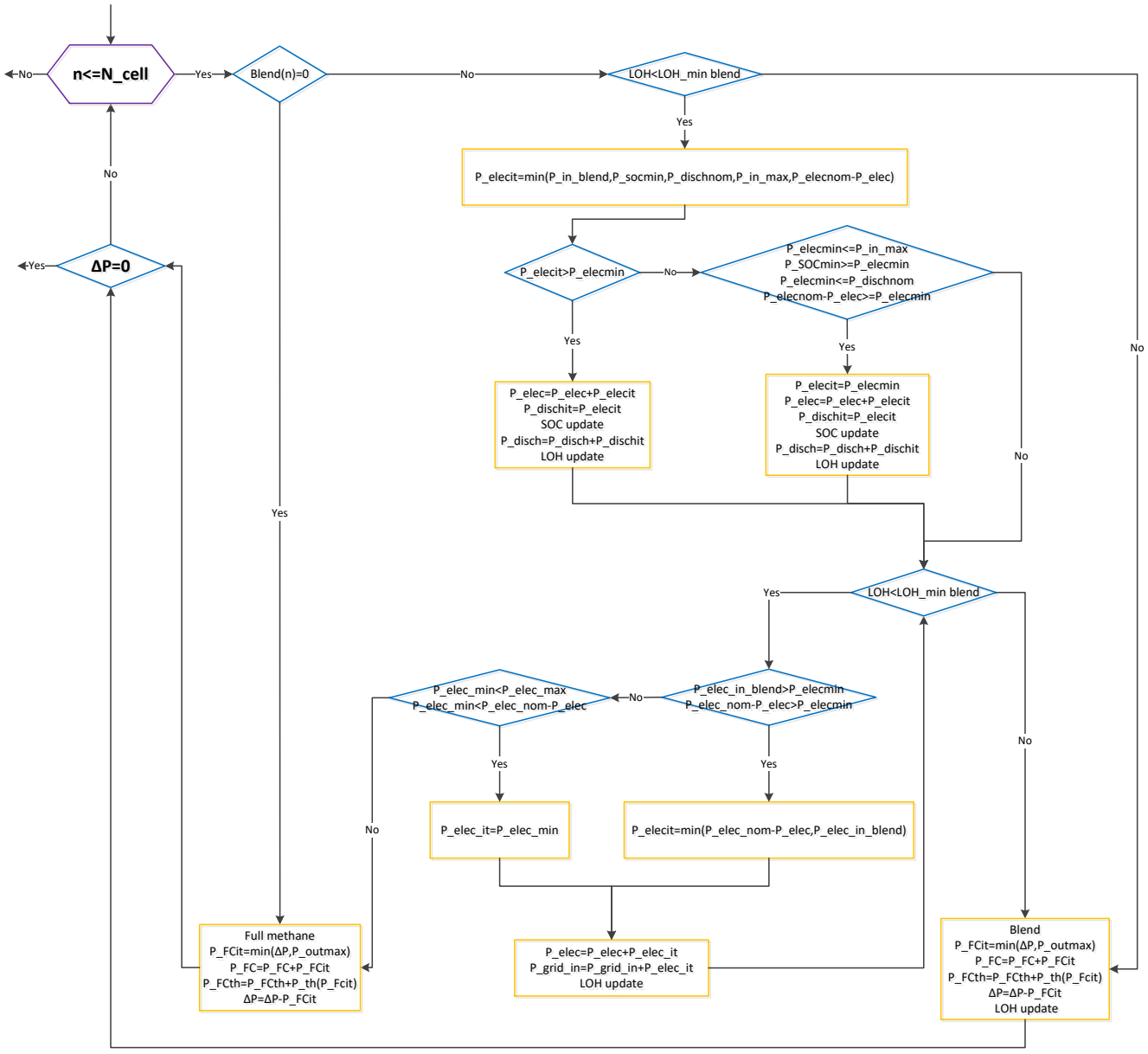

Figure 12. Fourth discharging logic fuel cell loop.

The choice has been to model use of the battery as the first element to be considered to drive the electrolyzer, in order to exploit the energy produced by the panels as much as possible, since they are the only way to charge the battery.

In this loop the first check is the one on the LOH, ensuring the possibility of safe operation in blending mode through $LOH_{min_{blend}}$, as in the other discharging logics, but after it is defined the theoretical working point of the electrolyzer $P_{elec_{it}}$ to verify if the results are suitable. Indeed, the analysis should be performed considering more constraints than before.

The value of $P_{elec_{it}}$ is chosen as the minimum value among the $P_{elec_{in_{blend}}}$, obtained from the electrolyzer power curve and the use of (27), $P_{SOC_{min}}$ defined by (19), $P_{disch_{nom}}$ form (18), $P_{elec_{in_{max}}}$ obtained considering the value obtained from the curve of Figure 2 and the power resulting from (28), and the difference between the values of $P_{elec_{nom}}$ and the already used P_{elec}. In this way it is ensured at the same time that the electrolyzer does not overcharge the storage, does not exceed its nominal power, and does not exploit from the battery a power that can damage it.

The following step is the check of the suitability of such an obtained theoretical value verifying that it is higher than the minimum allowed working point of the electrolyzer $P_{elec_{min}}$. If it possible to use this value, the same amount of power is also added to the discharging power, considering that it is taken from the battery, and then the SOC and LOH are updated by means of (20) and (15), considering also in this case the passage using the electrolyzer power curve in order to determine $P_{out_{eff-elec}}$.

If instead it is not possible to directly use the calculated $P_{elec_{it}}$, it is performed a multiple check in which four different conditions should be verified in order to allow the next step. The first check is on the $P_{elec_{min}}$ that should not overcome the value of $P_{elec_{in_{max}}}$, in this way if the electrolyzer is worked at its minimum, the tank will not be overcharged by the produced hydrogen.

The second check is instead used to verify if the minimum operating point of the electrolyzer is compliant with the operating point of the battery, avoiding the possible extra discharge of it, check performed using $P_{SOC_{min}}$; the third comparison is performed always on the battery checking that the value of $P_{elec_{min}}$ is not higher than the nominal discharge value of the battery.

The last check is performed in order to verify if in the iteration considered there is enough power left to be exploited from the electrolyzer to make it work at the minimum allowed power, using the value obtained as $P_{elec_{nom}} - P_{elec}$. If all these four conditions are respected the electrolyzer is made work at the minimum power considering, then, the same passages of updating of SOC and LOH, but with the value of $P_{elec_{min}}$ in place of P_{disch} and used to determine the respective $P_{out_{eff-elec}}$, are followed.

If the check over these conditions is not respected instead, the battery is bypassed and the $LOH_{min_{blend}}$ is tried to be reached by means of the same loop described in Section 3.4.3; this loop is activated also if the power taken from the battery was not enough to guarantee the correct level of hydrogen and there is still the possibility to increment the working level of the electrolyzer.

The part of the cycle dealing with the amount of power produced by the fuel cells is not changed from the previous case, the solution regarding the use of methane only is adopted if there isn't the possibility of working at the correct blending percentage. As for the loop presented in Section 3.4.3, it is replicated exactly as it is in the thermal part of the code.

3.5 Additional logics

This section analyzes the other implanted logics that are not strictly related to the power balance between the produced PV power and the electric load. These functions are used to simulate the possibility of imposing some external constraints on the system working conditions and decoupling it from the power balance.

The proposed additional logics are two: the first one determines a minimum guaranteed working level of the fuel cells, it is named $Cell\_on\_min$, while the second instead the electrolyzer to try to reach a chosen LOH within the tank, is the LOH_target function.

3.5.1 $Cell\_on\_min$: minimum guaranteed working point of the cells

This control logic determines that all the cells present in the simulation are forced to work at a minimum working percentage in all the different considered iterations. This function is used to simulate the possible choice of using the cells always at a minimum working point in order to guarantee to avoid the thermal cycles that can strongly damage the cells.

This function is so called before the chosen discharge logic and after the function called LOH_fixed presented in Section 4.4.2; it is totally independent from the effective power balance. In Figure 13 is presented the flow chart relative to this part of the code. As for the discharging logics, it is presented a loop to consider separately the fuel cells with different operating conditions, but the real model considers only one fuel cell.

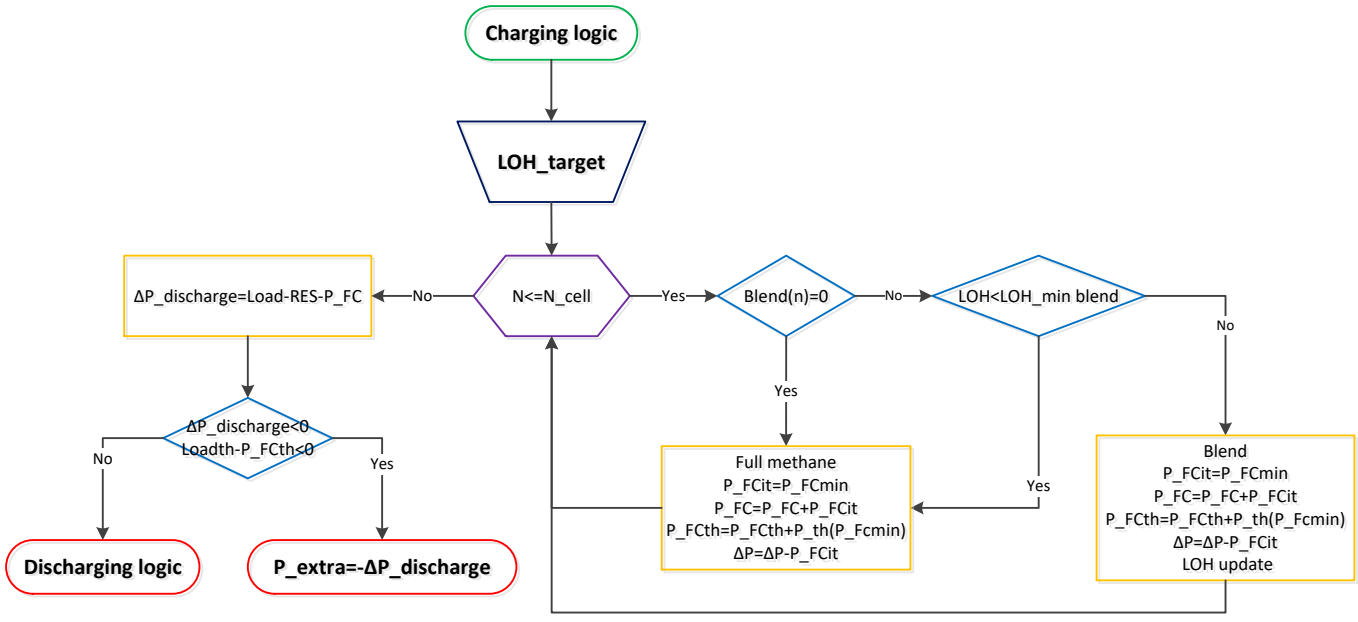

Figure 13. Additional cells control logic flow chart.

This control logic performs a cycle on the different available cells to guarantee them a minimum working condition. The first element of the loop is the check on the type of working point that can be set

for the cell, if it works in blending conditions, so with a defined blending percentage, or in full methane condition.

The second check is the one performed on the LOH verifying the availability of hydrogen within the storage to correctly operate the cell in that specific blending condition. In this case, if the LOH is not high enough to reach $LOH_{min_{blend}}$, the cell is operated in full methane conditions.

In this loop has been supposed not useful to allow the use of the electrolyzer, because the control logic presented in Section 3.5.2, ensures that there is a required LOH exactly before this logic; as a consequence, it has been supposed that the level is set in order to guarantee the correct operation of the cells.

In this section the output power is set equal to $P_{FC_{min}}$ determined by means of (29), this power output is the one removed in the discharging logics if there is more power required from the cells to correctly evaluate the working point.

$$(29)\ P_{FC_{min}} = P_{nom_{cell}} * load_{gua_{FC}}$$

The value of $load_{gua_{FC}}$ is a free choice of the modeler, it can be set in the range between the minimum allowed working percentage for the cells, assumed equal to 40% according to [20] and the value of 100% that forces the cells to work always at their nominal power.

At this value of the electric power output is then associated a thermal power output, $P_{FC_{th}}(P_{FC_{min}})$, using the power curve present in Figure 9 and, if the cell worked in blending conditions, the value of LOH is updated by means of (26) determining the correct mass flow rate on the basis of the working point selected. The update of the LOH is then removed when the fuel cells are used at a higher working point.

After the end of the loop, when all the cells are exploited at this fixed working percentage, the produced power is used to reduce the required ΔP that has to be compensated, evaluated by means of (17), obtaining the $\Delta P_{discharge}$ that represents the electric power that still has to be compensated by means of the discharging logic selected.

At this point is performed a double check on the required powers, if the $\Delta P_{discharge}$ is lower than zero, the extra power produced is accounted as a P_{extra} and sent to the grid. This condition is applied only if the thermal load is absent otherwise the normal discharging logic is applied and the P_{extra} is determined in it, as explained in Section 3.4.1 and equal also in the other three logics. This last aspect is considered from a theoretical point of view since the thermal load is not considered in the results presented in Chapter 5.

3.5.2 LOH_target minimum guaranteed level of hydrogen in the tank

This second additional logic is used to address the possibility of charging the hydrogen storage always at a predefined level, even if there is no power available from the panels. In this way can be reached a more constant operation of the electrolyzer that, if it is kept always working, is not affected by the ramp rates and thermal cycles.

In Figure 14 is shown the flow chart relative to this section of the code that is called by the model at each iteration considered after the charging logic, in this way the electrolyzer is worked using the panels production if possible.

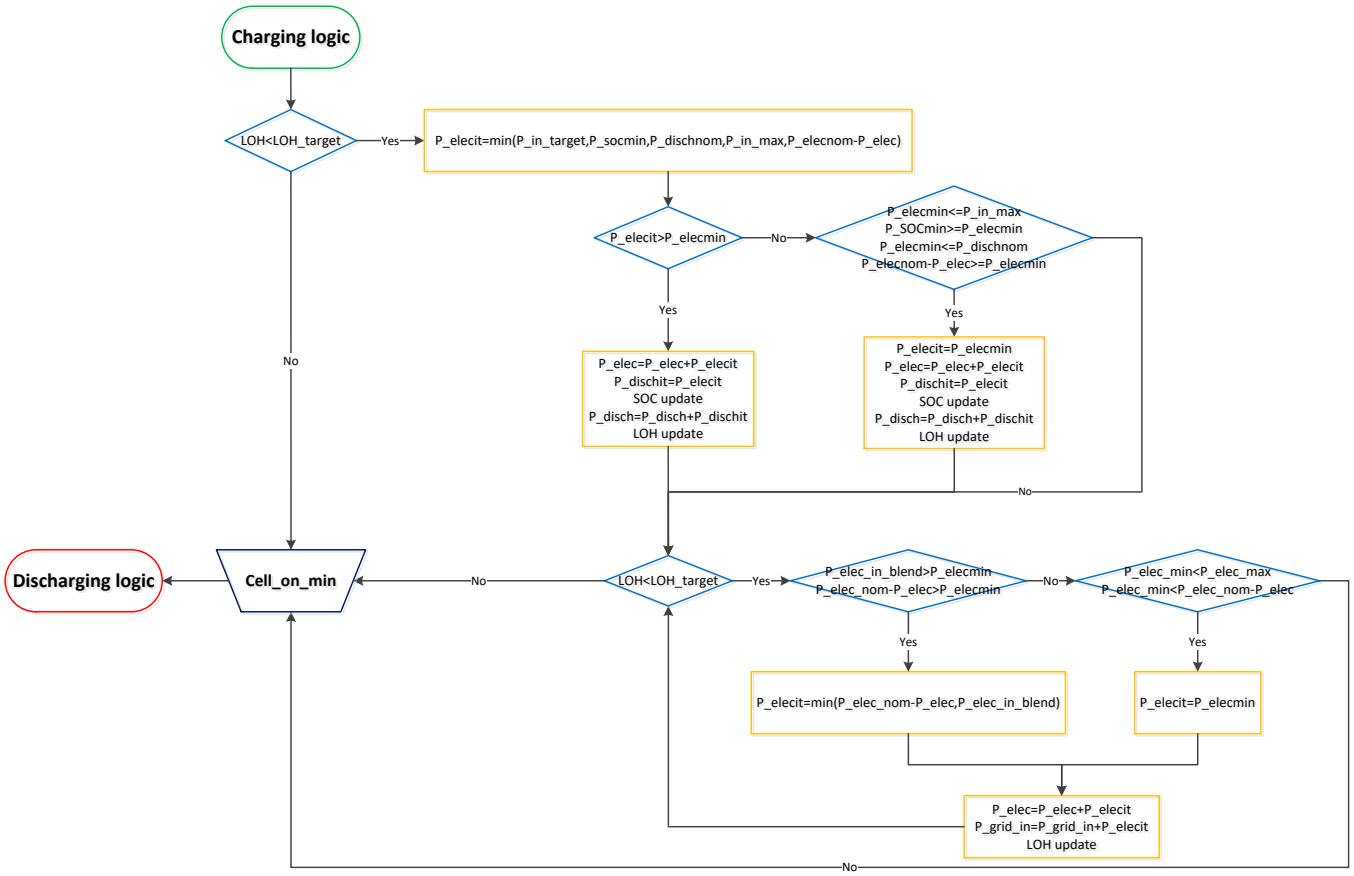

Figure 14. Flow chart of additional control logic on LOH

This control logic requires the definition of the parameter LOH_{target} that represents the level of hydrogen within the storage that should be guaranteed according to the willingness of the modeler. Indeed, this parameter can be freely set in the range that can vary between the minimum allowed level in the tank, assumed equal to 5% and the maximum level correspondent to 100 %.

The first check will be on the actual LOH since if it is already compliant with the target level, all the steps are not required. If instead the value is not reached yet the passages followed are close to the ones listed in Section 3.4.4. while considering the steps required for the working of the electrolyzer.

The first step is the determination of the actual input power of the electrolyzer, from a theoretical point of view. The value of $P_{elec_{it}}$ is determined as the lowest value among five powers, the first is the required input power $P_{elec_{in_{target}}}$ correspondent to the output generating the required quantity of hydrogen obtained using the power curve of Figure 6 and the value of $P_{elec_{target}}$ determined by (30).

$$(30)\ P_{elec_{target}} = \left(LOH_{target} - LOH_i\right) * LHV_{H_2} * \frac{m_{H_2 max}}{\Delta t}$$

The other four powers are instead equal to the ones of the loop in Section 3.4.4., they are $P_{SOC_{min}}$, $P_{disch_{nom}}$, $P_{elec_{in_{max}}}$ and the difference between the nominal electrolyzer power and the already used power. Choosing the lowest among these values it is ensured that the electrolyzer works respecting the technical constraints related both to the storages and to the electrolyzer itself.

If it is not possible to work the electrolyzer at this operational point, the model tries to make it work at the value of $P_{elec_{min}}$ performing also in this case the checks on the possibility of using this power level considering the different values of the battery, $P_{disch_{nom}}$ and $P_{SOC_{min}}$, of the hydrogen tank, $P_{elec_{in_{max}}}$, and the power left of the electrolyzer.

If one of these possibilities is verified, the following step is to update the values of LOH and SOC, using (15) and (20) with the correct power level of the electrolyzer.

This first part of the code is the one relative to the possible exploitation of the battery power, in this way is still used the PV panels production in a undirect way; if it is not possible to use it, or the level of hydrogen is not reached yet, the next step of the simulation is to try to use the grid to reach the target, always checking that there is still the possibility of exploiting more the electrolyzer.

After a check performed on the LOH, in order to exclude part of the passages if there is no need, the following step requires again the definition of the theoretical power needed to correctly feed the tank, $P_{elec_{in_{target}}}$, that is then compared to the minimum value $P_{elec_{min}}$; simultaneously, there is the check about the electrolyzer power left.

If one of these conditions is not respected there is the check on the value of $P_{elec_{min}}$ to verify if it is possible to make the electrolyzer work at this power level. Once it is determined which is the effective operative power of the electrolyzer, the value of LOH is update by means of (15).

If it is not possible to work the electrolyzer in any condition, since the gap between the LOH_i and LOH_{target} is too small or the electrolyzer already works at its nominal power, this function is not used and the LOH remains as it is.

After this series of step is called the function $Cell\_on\_min$ that represent the minimum guaranteed working condition of the cells presented in Section 3.5.1.

It is important to underline that this LOH is guaranteed only in this part of the code, at the end of each iteration the reached value can be different from it.

3.6 Key performance indicators

The results obtained in the different sections of Chapter 5 are evaluated using some specific key performance indicators useful to summarize the large quantity of data determined by the model.

The first one is the $Number\ of\ electrolyzer\ switch\ on$ that represent the number of times in which the electrolyzer is switched on during the simulation, it is determined as a counter that starts from a null value and rises every time that the electrolyzer power is equal to zero at the previous iteration and then it becomes positive at the following one.

This parameter is coupled with the one named $Hours\ elec\ on$, that is a counter considering the number of times in which the electrolyzer is different from zero, then this number is multiplied for the time step of $15\ min$, to obtain a time. Considering these two parameters together it is possible to determine the effective performances of the electrolyzer. This component should work in the most constant way, as a consequence its performances has to be carefully analyzed.

To determine the operations of the fuel cells, have been used two parameters checking how long are them able to work at the correct level of blending and how much is instead required for them to work with methane, these two aspects are accounted respectively in $Hours\ FC_{blending}$ and $Hours\ FC_{CH4}$. These parameters are determined as some counters multiplied for the time step as for $Hours\ elec\ on$.

These parameters are related to the specific technical aspects related to one of the components of the total $P2P$ system, the other used parameters are instead related to the different share of power used by the different components of the system both during the charge and the discharge of the system.

Considering the charging process, the share is determined by means of three percentages named $Battery\ charge_{\%}$ (31), $Electrolyzer\ charge_{\%}$ (32) and $Grid\ reject_{\%}$ (33) considering how much of the total charging energy is respectively used to: charge the battery, to drive the electrolyzer and so producing hydrogen or is simply sent to the grid. In order to determine the total energy, it is used the sum of the power at the single iteration multiplied for the Δt.

$$(31)\ Battery\ charge_{\%} = \frac{\sum P_{charge} * \Delta t}{\sum \Delta P_{charge} * \Delta t}$$

$$(32)\ Electrolyzer\ charge_{\%} = \frac{\sum P_{charge} * \Delta t}{\sum \Delta P_{charge} * \Delta t}$$

$$(33)\ Grid\ reject_{\%} = \frac{\sum P_{charge} * \Delta t}{\sum \Delta P_{charge} * \Delta t}$$

In these formulas the value of ΔP_{charge} is obtained as the value of ΔP, obtained by means of (7), when it is positive while if it is negative, it will be set equal to zero; in this way it is possible to evaluate the amount of energy that can be effectively exploited to charge the storages. These calculations consider only the power directly taken from the one available from the PV panels production, as a consequence it is specified the term "charge" in both P_{elec} and $P_{grid_{out}}$; for the battery power this is not needed since the battery can only be charged by the panels.

The last three parameters used are related to the discharging process and are also in this case some energy related percentages, in detail they are: $Battery\ discharge_{\%}$ (34), accounting the amount of energy taken from the battery to cover the demand, excluding the energy taken to drive the electrolyzer, $Fuel\ cell_{\%}$ (35), considering all the power produced by the fuel cells that is used to cover part of the demand, it excludes the extra power produced, and the $Grid\ input_{\%}$ (36) that considers the energy input required to cover the remaining part of the load, also in this case is neglected the part of the energy required to drive the electrolyzer.

$$(34)\ Battery\ discharge_{\%} = \frac{\sum P_{discharge} * \Delta t}{\sum \Delta P_{discharge} * \Delta t}$$

$$(35)\ Fuel\ cell_{\%} = \frac{\sum P_{FC_{discharge}} * \Delta t}{\sum \Delta P_{discharge} * \Delta t}$$

$$(36)\ Grid\ input_{\%} = \frac{\sum P_{grid_{in_{discharge}}} * \Delta t}{\sum \Delta P_{discharge} * \Delta t}$$

As for the charging percentages, the values of fuel cell and grid input power have the specification "discharge" to account the fact that are considered only those powers and not the whole fuel cell output or grid input. The value of $\Delta P_{discharge}$ is determined in a way similar to ΔP_{charge} but in this case the value is determined as the opposite of ΔP, always determined with (7), when it is negative and with a null value if instead the power gap is positive, in this way is determined the effective power gap that has to be closed by the storages. The percentual key performance indicators are evaluated on a yearly basis.

4. Case study analysis

The application an innovative technology as a hybrid energy storage system to an important infrastructure as an airport is justified by the TULIPS, demonsTrating lower pollUting soLutions for sustaInable airPorts acrosS Europe, project joined by the Turin airport. Within this project the point 3 is the one focused on the energy and it requires each airport participating to TULIPS to address at least two points of the five presented [23].

The Turin airport, represented by the company SAGAT, "Società Azionaria Gestione Aereoporto Torino", has joined the points 3.1, regarding the analysis of current and future situations in order to determine a model for the simulation of the whole airport system, the 3.2, focused on the integration and monitoring of a proper energy strategy, and the 3.4 characterized by the demonstration of heat supply facilities. The last element of the Energy related part is linked to the information exchange between airports to allow an easier integration of the different solutions.

The specific part analyzed within this work is related to the point 3.4, indeed it is studied a possible application in which the fuel cells are used also to supply part of the building heat load.

Going in detail, the chosen building is the fire station of the airport that is sited close to the runway in the Turin airport, as shown in Figure 15; in Figure 16 is presented a closer view of the area near to the fire station.

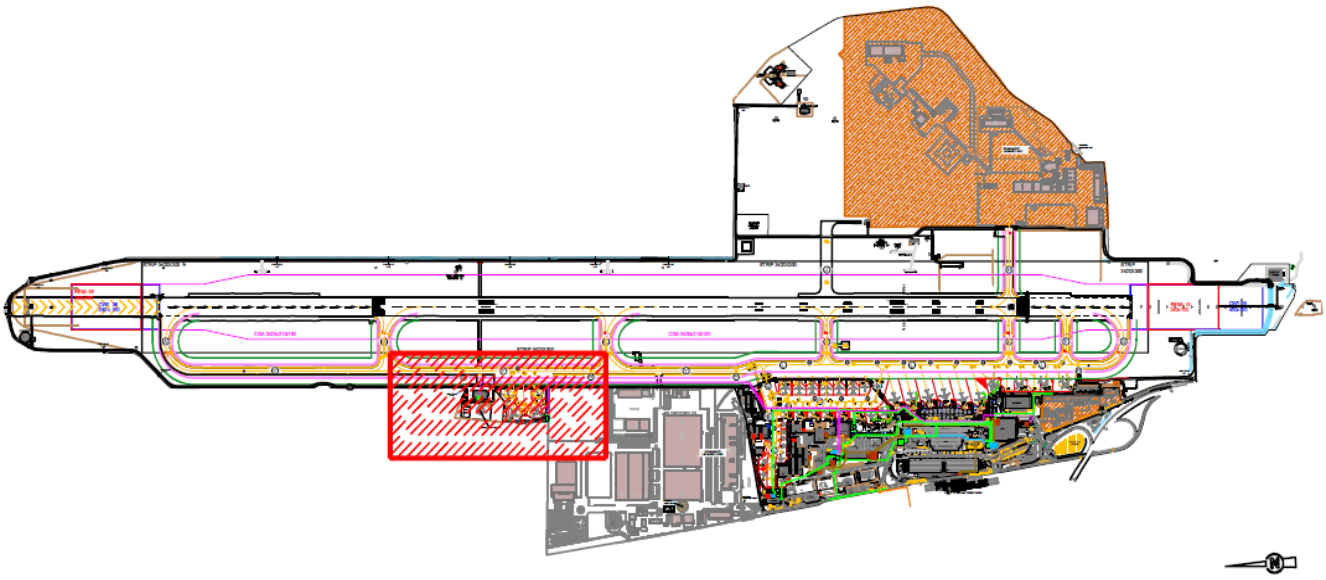

Figure 15. Wide view of the Turin airport with underlined the fire station area [24]

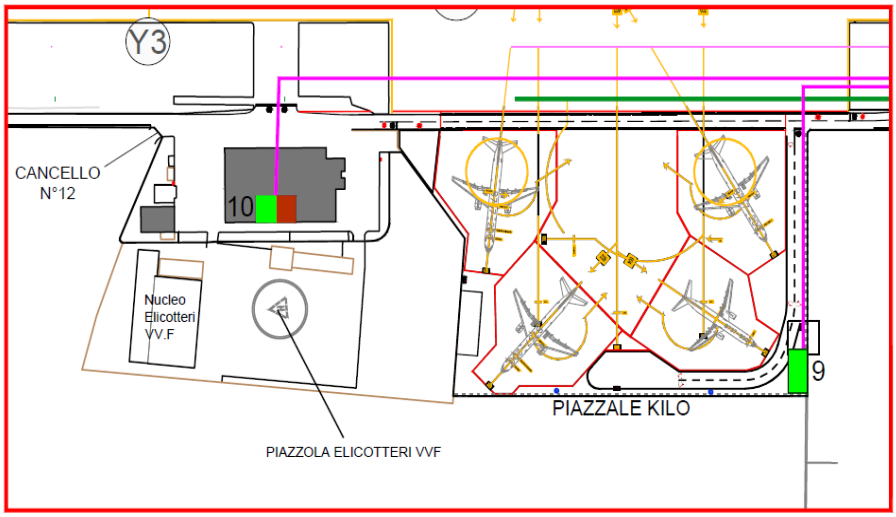

Figure 16. Closer view of the airport fire station (10 in figure) [24]

This small building is characterized by a power and a heat demand reported respectively in Figure 17 and 18. The power load profile has been determined using the available data taken from the meter on an hour basis, obtaining a maximum load of 54 kW and an average value of 25 kW. The winter heat demand profile, i.e., the higher flat profile characteristic of the whole heating period from 15th October to 15th April, has been determined in the same way; it is characterized by a base value of 65,1 kW.

The thermal demand is characterized by an additional load represented by the heat needed, in form of domestic hot water, by the fire fighters to take a shower after their working. This load cannot be directly measured from the meter, as a consequence it has been determined supposing that the showers are taken one hour after the turn end, assuming the amount of hot water needed on the basis of the number of fire fighters present in the fire station. This supposed load is equal to 20,3 kW and is added two times every day; it is considered not only during the heating period but it is present the whole year.

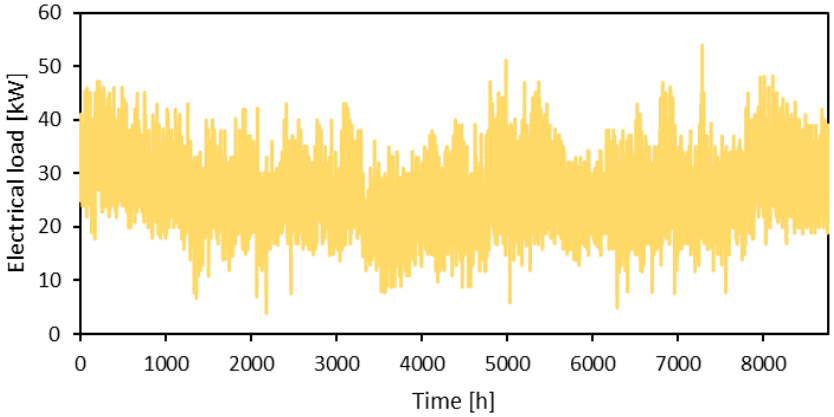

Figure 17. Electrical profile of the fire station

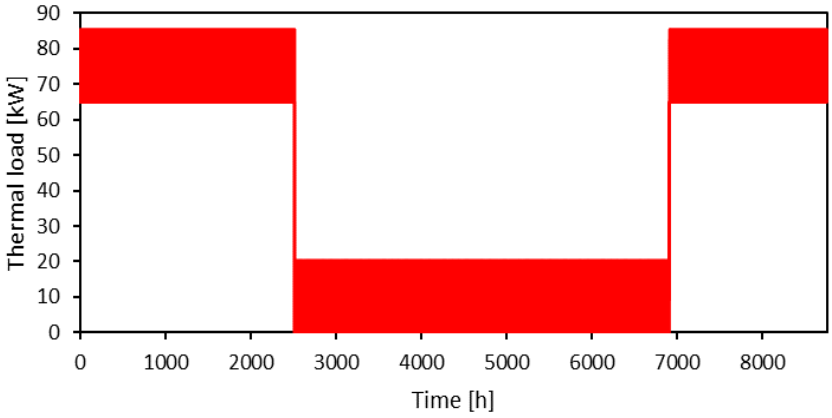

Figure 18. Thermal profile of the fire station

These loads have to be covered by means of a hybrid system comprehensive of a Li-ion battery and a small $P2P$ system made by an alkaline electrolyzer, a small hydrogen storage tank and two $SOFC$. The conceptual layout is showed in Figure 19.

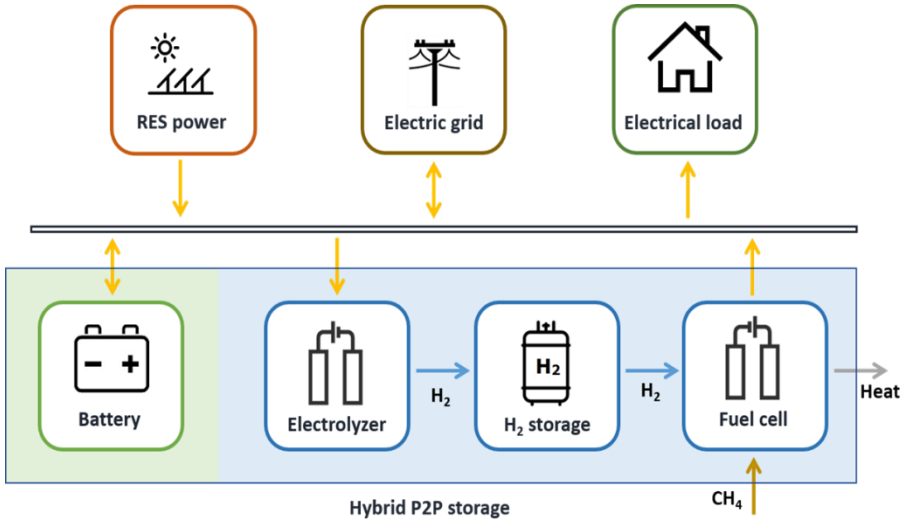

Figure 19. Conceptual layout of the hybrid storage system [25].

As shown in Figure 19, the renewable electricity production is generated by the means of a series of PV panels that are installed on the fire station roof as showed in Figure 20. This PV plant is characterized by a total peak power of 88,4 kW that can generate yearly around 105,7 MWh, according to the analysis performed by Syspro Engineering [26], while the annual load is estimated equal to 220,5 MWh. Analyzing the power production profile showed in Figure 21, the maximum level is equal to 67,9 kW with an average production, also considering the nights, of 12 kW.

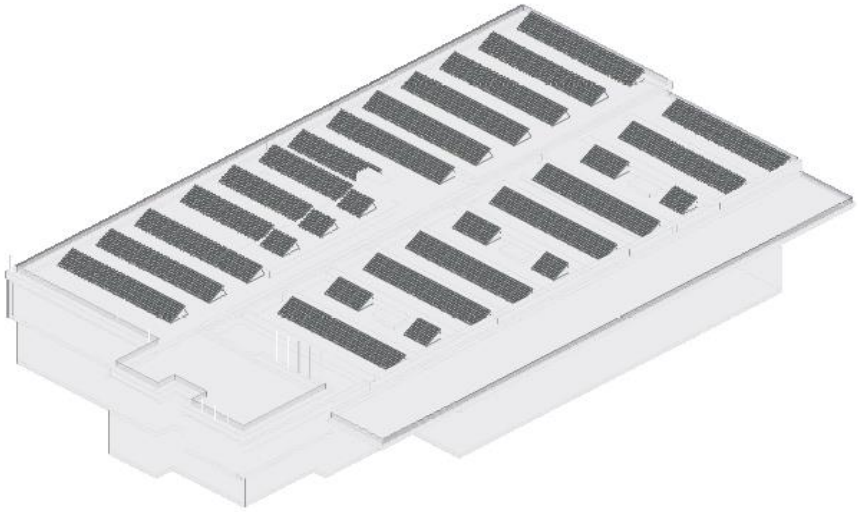

Figure 20. Rooftop panels schematics

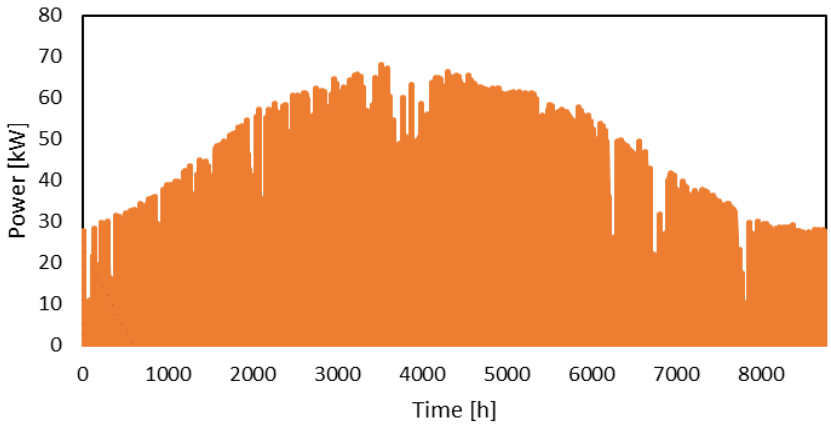

Figure 21. PV panels power profiles

The storage system is composed by a 100 kWh Li-ion battery, mainly used for the short-term storage of electricity, and by a system composed by a small alkaline electrolyzer, with a nominal power of 4,8 kW, a storage tank with a capacity of 0,7 m^3, by two fuel cell stacks of 1,3 kW .

In Table 1 are summarized all the technical parameters and the decision variables necessaire for the control logics presented in Chapter 4 relative to the base case scenario analyzed. The larger part of the results presented in Chapter 5 are based on this scenario, the sensitivity analysis presented are performed modifying the data listed in Table1.

Battery			**Tank and electrolyzer**		
Cap	100	kWh	$V\_storage$	0,70	m^3
$C_{rate_{charge}}$	2	/	m_{H_2max}	0,90	kg
$C_{rate_{discharge}}$	2	/	$P_{elec_{nom}}$	4,8	kW
SOC_{min}	20%	/	LOH_{min}	5%	/
SOC_{max}	100%	/	LOH_{max}	100%	/
			LOH_{target}	30%	/
Fuel cells			**Other parameters**		
N_{cell}	2	/	LHV_{CH_4}	13,9	kWh/kg
$blend_n$	60%	/	LHV_{H_2}	33,33	kWh/kg
$P_{nom_{CH_4}}$	1,3	kW	MM_{CH_4}	16	$kg/kmol$
$P_{nom_{blend}}$	1	kW	MM_{H_2}	2	$kg/kmol$
$load_{gua_{FC}}$	60%	/	Δt	15	min

Table 1. Base case scenario parameters.

Going more in detail about the decision parameters, the chosen value of $LOH\ target$ is justified by the fact that the fuel cells are small, as a consequence even such a not so high quantity of stored hydrogen, equal to 30 % of the total mass, is able to allow them to work in blending conditions.

The blending level instead has been set at 60 % considering it has an average value within the testing conditions, at the same time the value of $load_{gua_{FC}}$ has been chosen assuming a scenario in which the fuel cells are tested close enough to they nominal conditions, due to the low nominal power. The only parameter not reported is the $load_{min_{elec}}$ that is fixed at 20 % considering the electrolyzer power curve. This last parameter will be subject to a sensitivity analysis assuming the possibility of forcing the system to make the electrolyzer work only at higher loads.

In this work have been considered two different alternative sizes of the storage elements for the analysis of the daily simulations performed in Chapter 5.1:

- *Base Case Scenario*: scenario characterized by the real sizes of the elements that will be installed in the Turin airport.
- *Optimized Scenario*: scenario in which the sizes have been assumed equal to the ones proposed by Marocco et al. in [25]. These sizes have been determined in a preliminary study with a CAPEX constraint of 280 k€ imposed by SAGAT and have been taken as the best combination of the storage elements able to minimize the grid requirement.

In Table 2 are reported the sizes of the storage elements for both the scenarios, the decision parameters instead are kept equal, as a consequence they have not been reported there.

	Parameter	*Base case scenario*	*Optimized scenario*	
Battery	Cap	100	46,5	kWh
Electrolyzer	$P_{elec_{nom}}$	4,8	6,4	kW
Hydrogen tank	$V_{storage}$	0,7	0,7	m^3
Fuel cells	$P_{FC_{nom}}$	2,6	19,2	kW

Table 2. Optimized and base case scenario technical parameters comparison.

5. Results

The aim of this chapter is to present some of the possible model outcomes and analyze them to determine which are the most relevant parameters affecting the performances of the system.

All the analyzed simulations are performed considering only the second charging logic, presented in Chapter 3.3.2, that prioritizes the electrolyzer over the battery, and the fourth discharging logic, showed in Chapter 3.4.4, characterized by a higher priority of the fuel cells. When other charging or discharging logics will be implemented it will be explicitly specified.

In Section 5.1 will be presented the analysis of some typical days, a winter day and a summer day, with a detailed description of the way in which the model is able to manage the different components to satisfy the loads and charge the storages. The analysis will be reported both for the base case scenario and for a scenario considering the sizes of the storage components determined in the preliminary analysis of Marocco et al. [25].

Section 5.2 will be dedicated to the description of the sensitivity analysis related to the sizes of the different components of the $P2P$ system; the focus of this part will be set on the determination of the most relevant components to obtain a system more capable to satisfy the load and to find out some sizes able to reach specific targets in the different proposed key performance indicators.

The last Section, 5.3, will analyze the impact of the decision parameters of the model on the performances of the system, with the aim of determining some optimal working points to reach specific targets of the system.

5.1 Typical days analysis

The typical days analyzed have been chosen as representative of their season, assuming that the characteristics of the loads does not vary so much.

For the winter period the analyzed day is the 15^{th} of January, this day will be characterized by the presence of a constant load both for the electrical and thermal part with a small contribute of the PV panels.

The selected summer day is instead the 15^{th} of July, in this day the thermal load for the house heating is absent and the presence of the photovoltaic panels determines a much bigger contribute to the load satisfaction.

5.1.1 Winter day: base case scenario

In order to describe how the different elements of the system contribute to the satisfaction of the demand, in Figure 22 are reported the discharging powers of the different components.

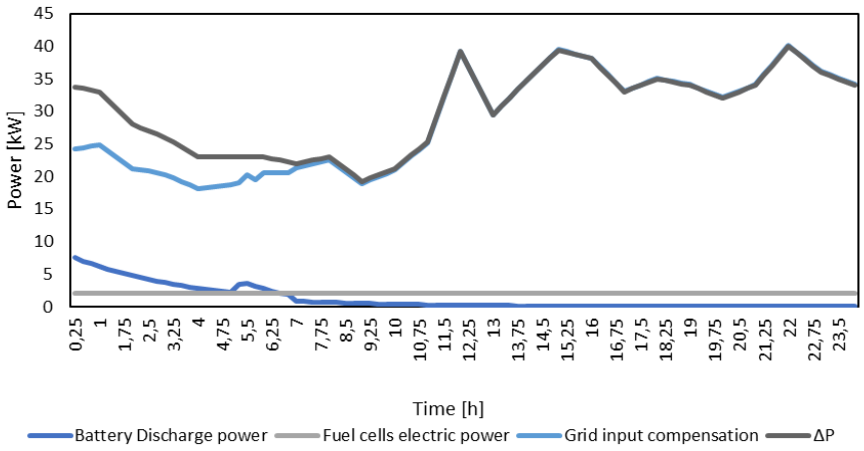

Figure 22. Winter day: discharging powers, base case scenario

The graph shows four different lines, the dark grey one represents the power gap that has to be filled by the different storages, it is the ΔP calculated using (17); this power is provided by means of a constant power production from the fuel cells, working at their nominal power in blending condition, with a uniform output of $2\ kW$, and by the power stored in the battery together with the input form the grid, that is assumed as the infinite reservoir always able to provide enough power to satisfy the demand. Considering the energy needed for the whole day, $\sim 89{,}6\ \%$ is provided by the grid, $\sim 6{,}6\ \%$ is taken from the fuel cells and the remaining $\sim 3{,}8\ \%$ is satisfied by the battery.

The power provided by the battery, dark blue line in Figure 22, follows this decreasing trend due to the definitions of the maximum power output provided, and because of the imposed initial level of the SOC set by the modeler at $50\ \%$. It is important to underline that the reported battery power is not only the one used to satisfy the demand but also the one that can be used to feed the electrolyzer in the function $LOH\ fixed$; this latter element determines that there is a rise in the power curve of the battery when the electrolyzer is switched on around 5 A.M.

The plot of Figure 22 is strongly influenced by the chosen discharging logic, in this case the prioritization of the fuel cells determines a lower exploitation of the battery in the first iterations.

The plot of Figure 23 shows the trend of the state of charge during the analyzed twenty-four hours.

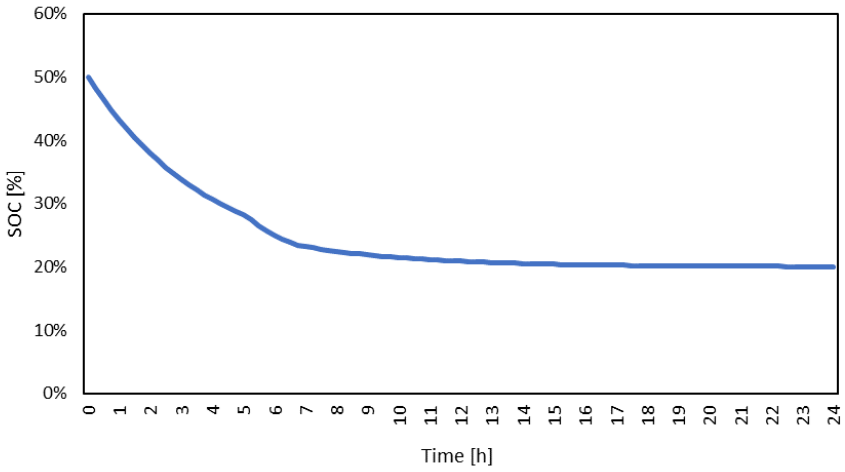

Figure 23. Winter day: SOC trend, base case scenario

The trend showed in Figure 23 underlines that the battery is exploited until it reaches the flat value of 20 % that is the defined level of minimum allowed SOC in the battery.

In Figure 24 are reported the different charging powers intended as the power sent to the different storages. It is important to underline that the power sent to the electrolyzer considers not only the power sent to it from the extra power produced by the PV panels.

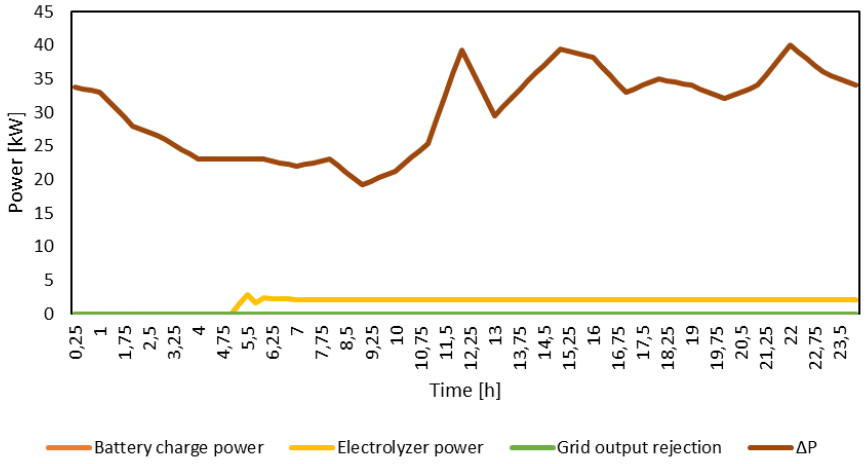

Figure 24. Winter day: charging powers, base case scenario

In this case the electrolyzer is totally fed by the grid since there is no extra power available from the photovoltaic panels, as can be seen in Figure 24 where there are no negative values for the ΔP. The presence of some power sent to the electrolyzer is determined by the function $LOH\ fixed$ that forces it to work to guarantee the presence of hydrogen in the tank; in Figure 25 is showed the trend of the level of hydrogen within the tank.

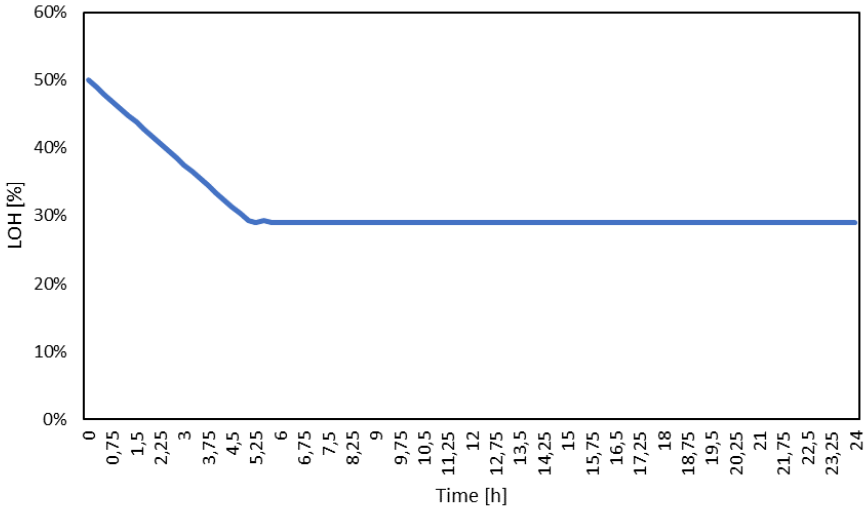

Figure 25. Winter day: LOH trend, base case scenario

The initial value of the LOH is fixed by the modeler at $50\ \%$ in order to have an initial trend in which there is some hydrogen within the storage. The change in the slope of the level of hydrogen trend is determined by the switch on of the function $LOH\ fixed$ that determines a constant value within the storage, it is important to underline that the value in figure is slightly behind the set value of $30\ \%$ since the function $LOH\ fixed$ is called before the functioning of the fuel cells determining a use of the hydrogen after the reach of the guaranteed level while the reported LOH is the one at the end of the fifteen minutes iteration.

In Figure 26 is then reported the thermal load together with the thermal power produced by the fuel cells even if the model does not work in a thermal load following way.

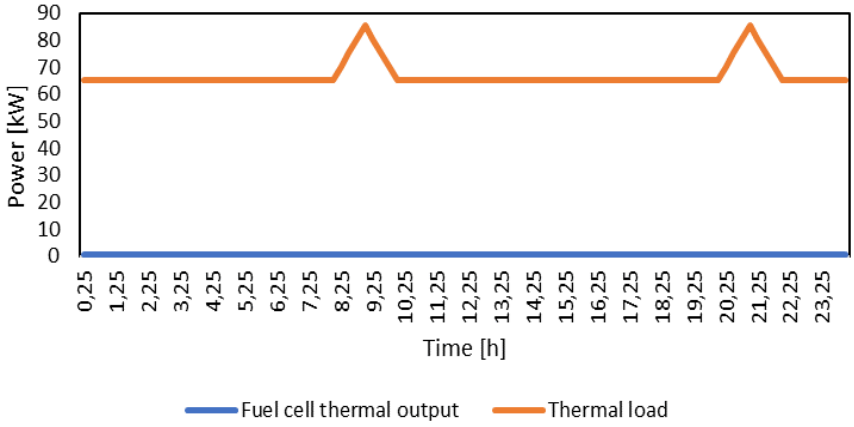

Figure 26. Winter day: thermal powers, base case scenario

Looking at Figure 26 it is possible to identify that effectively the contribute of the fuel cells to the satisfaction of the thermal demand is almost negligible due to the small size of the fuel cells themselves. Indeed, the produced power of the two fuel cells in such conditions is constantly equal to $0{,}55\ kW$ while

the thermal power is more than one hundred times higher. Considering the thermal energy needed for the whole day, the fuel cells are only able to cover ~ 0,8 % of the total.

5.1.2 Winter day: optimized scenario

In this section will be analyzed the same day showed in Section 5.1.1 but with the storages sizes equal to the ones presented in Table 2.

The first analysis is relative to the way in which the load is satisfied by the different elements of the storage system, the discharging powers are showed in Figure 27.

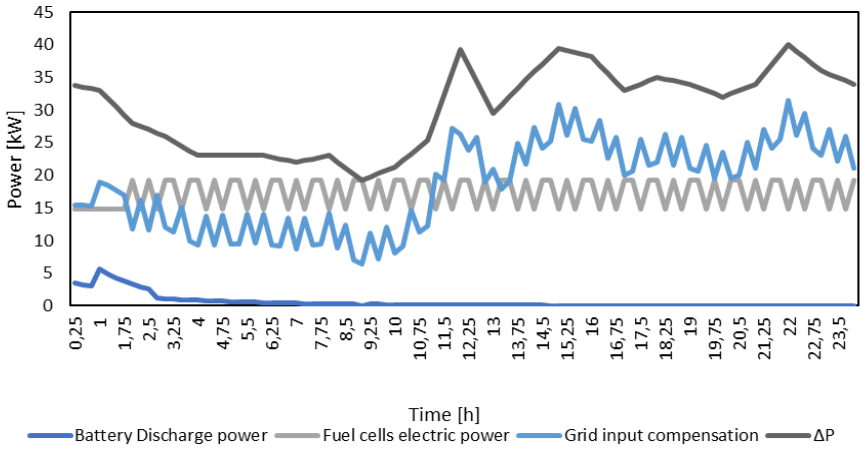

Figure 27. Winter day: discharging powers, optimized scenario

Comparing the plot of Figure 27 with the one of Figure 22 it is evident that the bigger size of the fuel cells in the optimized scenario determines a larger satisfaction of the demand from this element of the system. Indeed, the percentage of the daily load covered by the fuel cells passed from the ~ 6,6 % of the base case scenario to ~ 57,4 % in the latter.

The battery discharging power is less impacting in this case since the size of the battery is smaller than in the base case scenario. Also in this case, the rise in the output around 1 A.M. is determined by the switch on of the electrolyzer.

Another big difference is relative to the not constant power output of the fuel cells that oscillates between ~14,8 kW and 19,3 kW; this behaviour is justified by the different operating conditions of the $SOFC$s that some hours are working in blending conditions, with a lower power output, and in some others instead with only methane.

The switch between the two operating conditions is determined by the smaller size of the electrolyzer that is not able to provide enough hydrogen to make the cells always work with the correct amount of hydrogen in input. Looking at the charging powers of Figure 28 is indeed evident that the electrolyzer is constantly working at its nominal power.

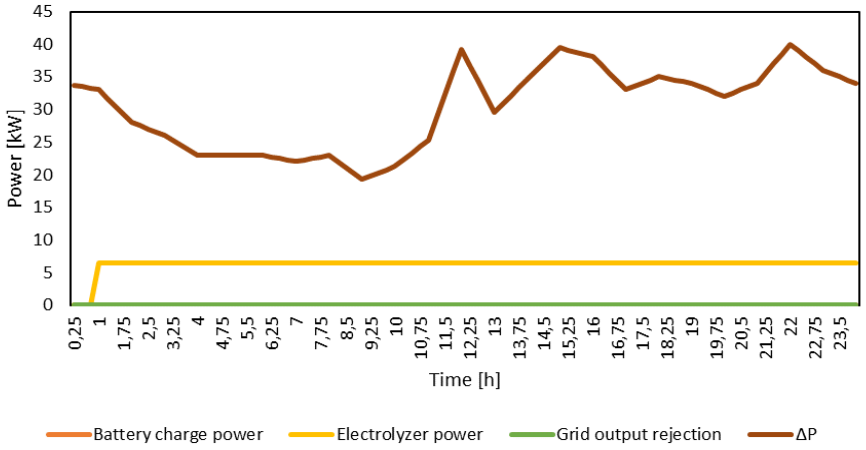

Figure 28. Winter day: charging power, optimized scenario

The trend of the level of hydrogen in the storage presented in Figure 29 is different from the one of Figure 25 since the consumed hydrogen is higher than the produced one.

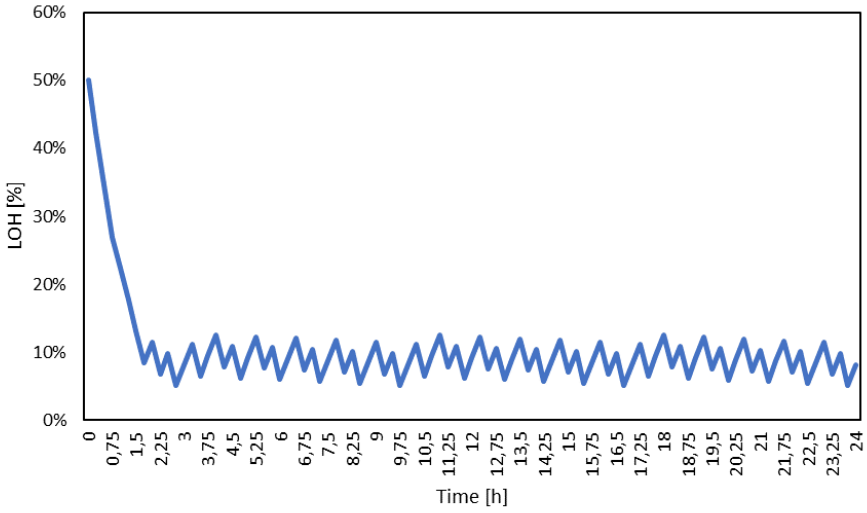

Figure 29. Winter day: LOH trend, optimized scenario

The LOH never reaches the target level imposed by $LOH\ fixed$, even if the function is called also in this simulation with a level of 30 %, since the electrolyzer is too undersized with respect to the fuel cells. After the initial level imposed by the modeler, the LOH varies constantly between the values of ~ 6% and ~11 %. When the first level is reached the cell can only work in methane operation, while with the latter can work in blending conditions.

The same oscillating trend can be found also in the thermal powers showed in Figure 30.

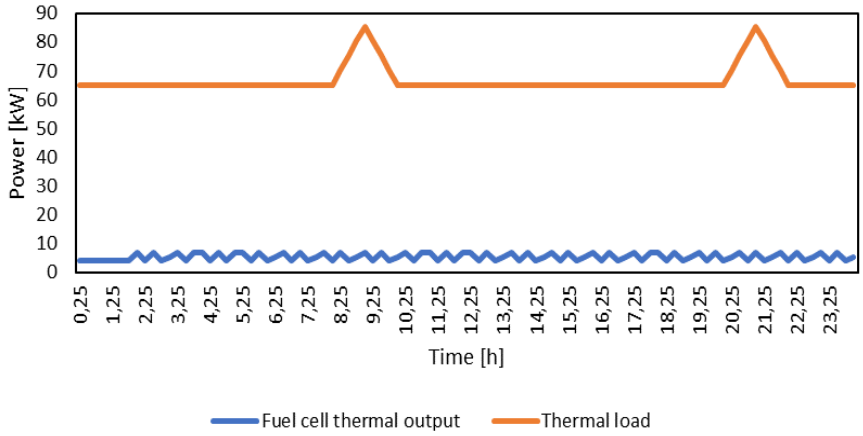

Figure 30. Winter day: thermal power, optimized scenario

In this case the bigger size of the fuel cells determines a larger satisfaction of the thermal demand thanks to the produced heat that varies in this case between $\sim 4{,}1\ kW$ and $\sim 6{,}9\ kW$. In this case the fuel cell system is able to cover a percentage of around the 8% of the total thermal energy needed.

In Table 3 are reported the different percentages of the electrical and thermal loads characteristic of the chosen winter day that are covered by the different elements of the storage system in both the base case and the optimized scenarios.

	Base case scenario	*Optimized scenario*
Battery load coverage	3,8 %	1,4 %
Fuel cell load coverage	6,6 %	57,4 %
Grid load coverage	89,6 %	41,2 %
Battery charging	0 %	0 %
Electrolyzer charging	0 %	0 %
PV power rejected to grid	0 %	0 %
Thermal load coverage	0,8 %	8,1 %

Table 3. Winter day: load coverage comparison.

The charging percentages are null in this case since there is no available extra power produced by the PV panels, all their produced power is sent to the load in the winter period. For what concerns the capacity factors of the fuel cells and electrolyzer, they have not been reported since both the machines are forced to constantly work due to the presence of the functions $LOH\ fixed$ and $Cell\ on\ min$.

5.1.3 Summer day: base case scenario

The summer day is characterized by a significant power production from the PV panels, as a consequence the storages can be charged during the daytime.

In Figure 31 are reported the discharging powers during the whole day.

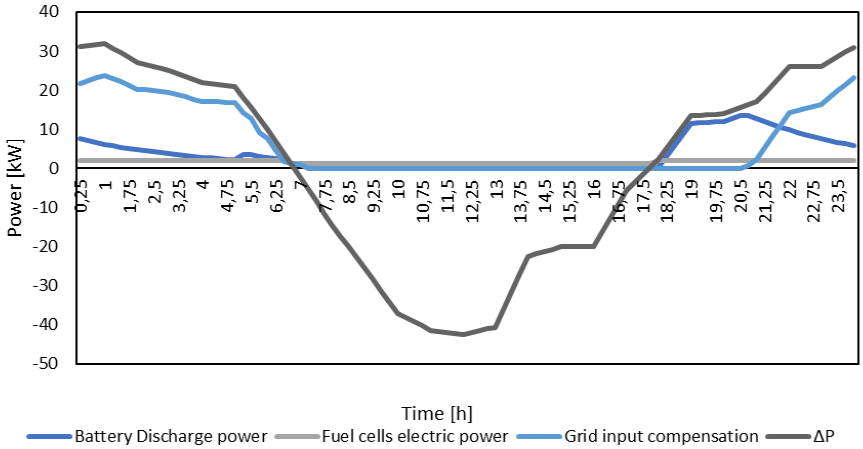

Figure 31. Summer day: discharging powers, base case scenario

Analyzing the plot of Figure 31, the ΔP is not only positive since during the central hours of the day the panels are producing more than the load to be satisfied.

Analyzing the left and right parts of the graph, it is possible to visualize a constant contribute of the fuel cells providing $2\ kW$ working in blending conditions, for a total $\sim 9{,}8\ \%$ of the daily load covered. With respect to the winter day, showed in Figure 22, the battery covers a much higher percentage of the load, up to $\sim 31\ \%$, due to its charging during the excess of the power produced by the panels. This last element determines the necessity of lower power taken from the grid; it is required only to cover $59{,}4\ \%$ of the daily load.

The fuel cell power output is no longer constant as it was in the winter day but varies between two values, $2\ kW$ when there is power needed and $1{,}2\ kW$ when instead the fuel cells are forced to work at the guaranteed percentage of $60\ \%$ by the function $Cell\ on\ min$.

The battery power is determined by the trend of the state of charge within it showed in Figure 32.

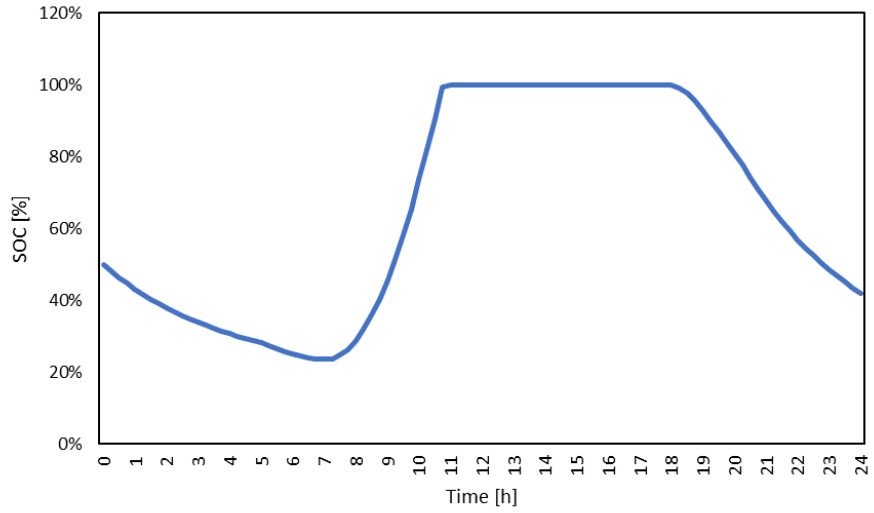

Figure 32. Summer day: SOC trend, base case scenario

The battery starts the charging after the electrolyzer due to the choice of the second charging logic, but the extra power is enough to totally charge it at its nominal power. After the daytime, the battery is discharged at its nominal power providing more than 11 kW almost constantly.

The trend of the level of hydrogen within the tank is shown in Figure 33.

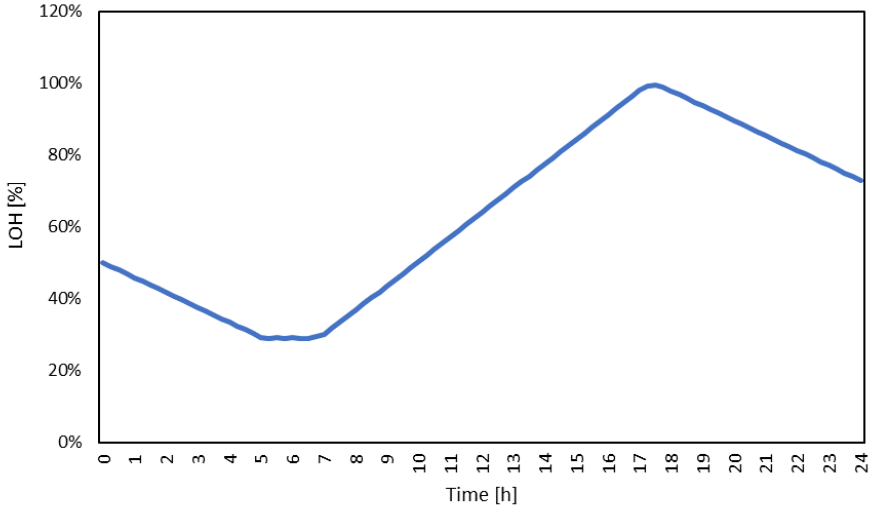

Figure 33. Summer day: LOH trend, base case scenario

The hydrogen storage is charged before the battery, however the energy provided by the fuel cells does not increase since they are already working at the nominal power, the positive effect can be seen in a lower use of the grid to drive the electrolyzer.

In Figure 34 can be seen the different share of the charging percentages when there is power excess.

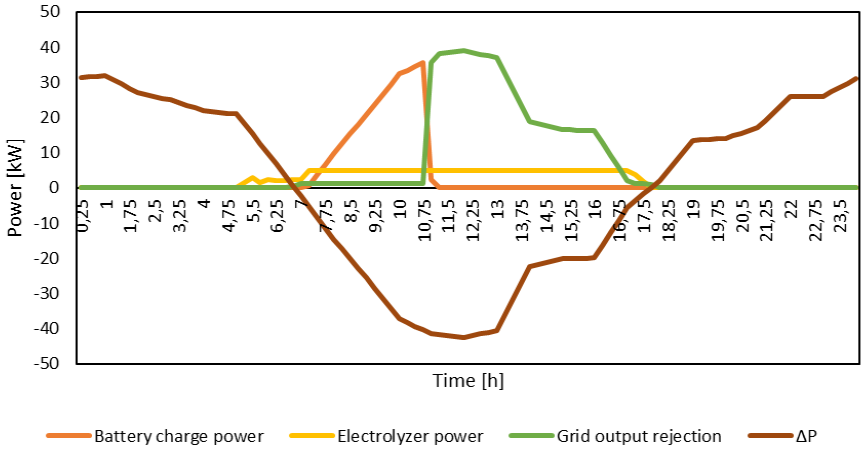

Figure 34. Summer day: charging percentages, base case scenario

The choice of the second charging logic determines a first rise in the working point of the electrolyzer with the battery charged only in a second time. This is evident looking at the yellow and orange curves showed in Figure 34.

Analyzing the share of the available extra power, the ~ 18,4 % is sent to the electrolyzer, the ~ 28,2 % is sent to the battery and the remaining ~ 53,3 % is instead released to the grid.

During the summer days the only thermal load present is the one for the domestic hot water shown in Figure 35.

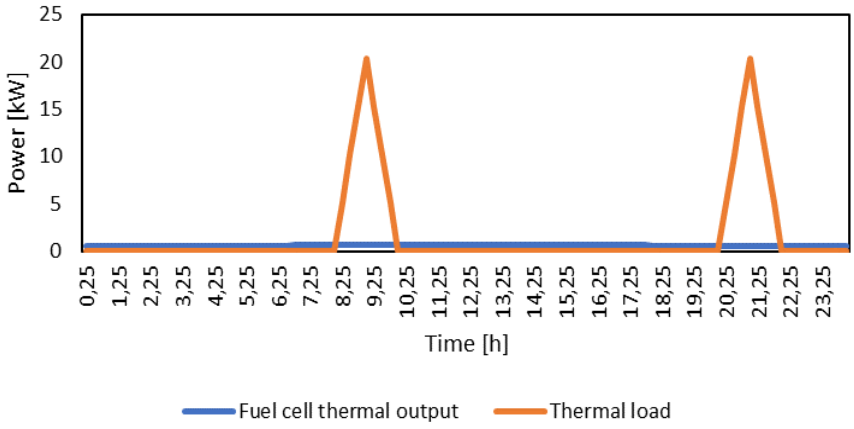

Figure 35. Summer day: thermal powers, base case scenario.

Considering the energy analysis, the fuel cells are able to provide ~ 36% of the total needs. It is important to underline that the thermal energy is constantly provided by the fuel cells thanks to the function *Cell on min*, while the thermal load is limited to two hours, as a consequence it is required a heat storage system to effectively exploit the thermal energy produced.

5.1.4 Summer day: optimized scenario

The analysis of the discharging powers is performed in Figure 36.

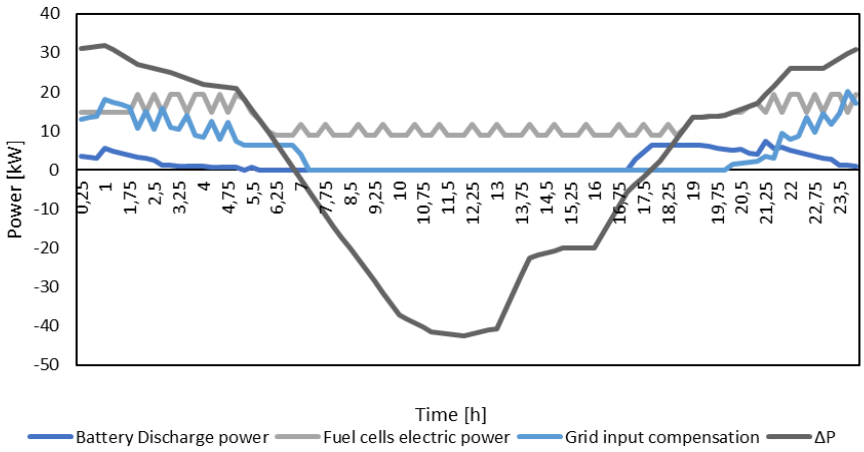

Figure 36. Summer day: discharging powers, optimized scenario

The graph of Figure 36 is characterized by a significantly higher level of power produced by the fuel cells, if compared to the graph of Figure 31. Indeed, the fuel cells are able to cover almost 72,3 % of the load, the battery provides ~ 5,3 % of it and the remaining part of the load is satisfied by the grid.

As already explained in Section 5.1.2, the battery is able to provide less power than in the base case scenario since it is significantly smaller than in the base case scenario, however even if it is almost a half in terms of capacity in this optimized scenario, the satisfied percentage is a sixth of the one in the base case scenario. This behaviour is determined by the bigger fuel cells and by the choice of the fourth discharging logic that prioritizes them over the battery.

The fuel cells operation in this case varies between four operating points, two couples determined by the full load or partial operations at 60 % and another couple is determined, as in Section 5.1.2, by the necessity of the operations in methane conditions due to the smaller size of the electrolyzer. When the cells are working at nominal power they are producing 14,8 kW or 19,3 kW as in the winter day for the optimized scenario, if instead the operation is forced by the function $Cell\ on\ min$ the two power levels are 8,9 kW in blending conditions and 11,6 kW when the fuel cells are fed by methane only.

In Figure 37 is showed the trend followed by the level of hydrogen within the storage.

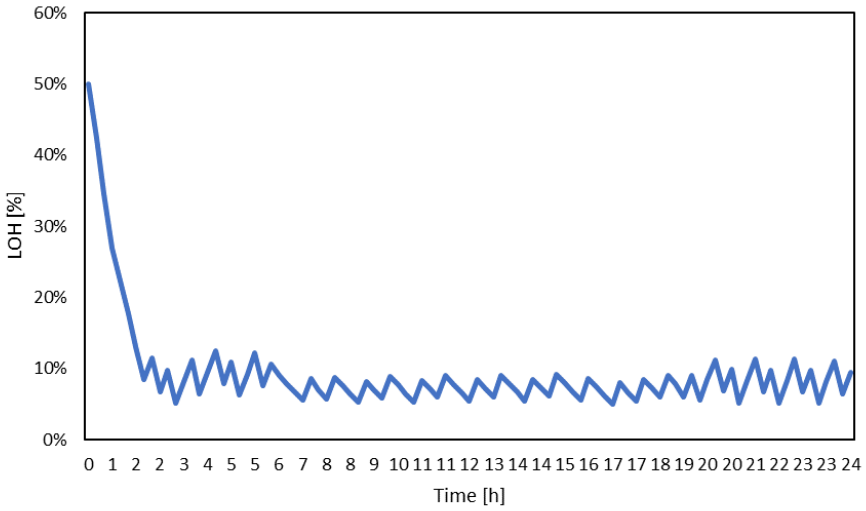

Figure 37. Summer day: LOH trend, optimized scenario

The plot of Figure 37 is close to the one of Figure 29 since the presence of extra power from the PV panels cannot determine a larger production of hydrogen since the main problem is related to the undersized electrolyzer. The only difference with the winter day profile is determined by a different slope of the oscillation during the day hours since there the fuel cells are operating at 60 % of nominal power while in Figure 29 they were constantly at their nominal power.

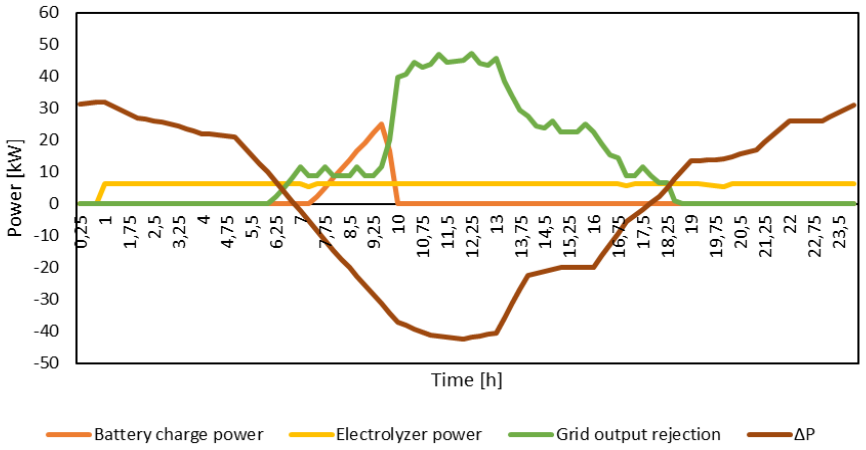

Figure 38. Summer day: charging powers, optimized scenario

In Figure 38 are presented the charging powers; comparing the trend of the *Grid rejection* above with the one of Figure 34, there are some peaks determined by the variable operation of the fuel cells that determines a not constant value. For what concerns the battery charging power it is smaller in this case since the battery capacity is smaller too.

The last analysis can be done looking at the thermal powers presented in Figure 39.

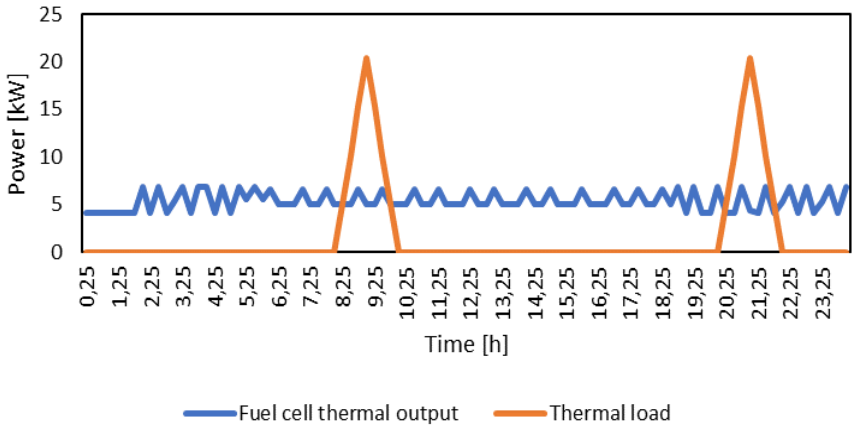

Figure 39. Summer day: thermal powers, optimized scenario

The oscillations in the thermal output of the fuel cells are determined by the variable power production since the thermal and electrical production are coupled. Analyzing the energy accumulated during the day, the fuel cells are able to provide more than 3 times the thermal energy needed, if instead we analyze the instantaneous power need, the system cannot cover the demand. In this case will be required a way to dissipate the extra heat during the summer days.

In Table 4 are reported the different percentages of the summer day thermal and electrical loads covered by the different elements of the storage system with a comparison between the base case and the optimized scenario. With respect to Table 3 there are also reported the charging percentages of the storages.

	Base case scenario	*Optimized scenario*
Battery load coverage	30,9 %	5,3 %
Fuel cell load coverage	9,7 %	72,3 %
Grid load coverage	59,4 %	22,4 %
Battery charging	28,3 %	12,9 %
Electrolyzer charging	18,4 %	24,2 %
PV power rejected to grid	53,3 %	62,9 %
Thermal load coverage	36,2 %	310 %

Table 4. Summer day: load coverage comparison.

5.2 Power to Power system variation

In this part of the chapter are reported the results of a series of sensitivity analysis performed on the sizes of the hydrogen section of the storage system; all the analysis are performed with the same control logics used in the typical day simulations.

It can be already underlined that this initial hypothesis will strongly affect the final results of the analysis, the choice of the control logic determines which of the two storage technologies is more or less used, as a consequence, the performances of the different components will vary.

5.2.1 Fuel cell installed power

The first sensitivity analysis is performed on the fuel cell installed power, making it vary accordingly to the nominal power of a single cell, as a consequence the studied points of the system will be the ones determined by an integer multiple of $1{,}3\ kW$. The analyzed range considers the installation from two to twenty cells, corresponding to a power range from $2{,}6\ kW$ to $26\ kW$, always characterized by the same blending percentage of $60\ \%$.

All the parameters that are different from the number of cells are exactly the ones showed in Table 1, these data will be the ones used for all the simulations, unless differently specified, to obtain consistent results.

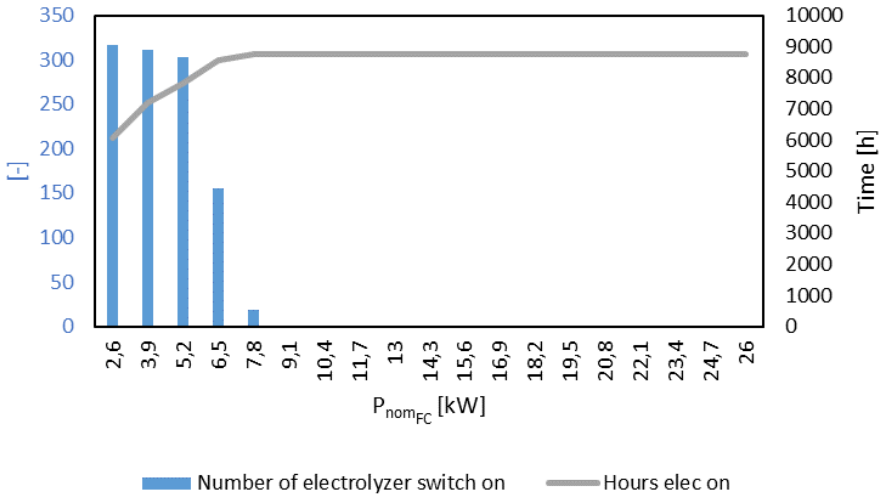

Figure 40. Electrolyzer working conditions, fuel cell power variation

The graph in Figure 40 shows the trend of the two electrolyzer key performance indicators with respect to the installed fuel cell power. This graph is characterized by two axes: on the left one is represented the number of times in which the electrolyzer is switched on while on the right axis are reported the hours in which it is effectively worked.

This Figure shows how the rising fuel cell power causes a higher use of the electrolyzer. This is evident considering that a rising power of the fuel cells causes a greater requirement of hydrogen and, as a

consequence, the electrolyzer is more constantly worked. More in detail, the electrolyzer will remain always on if the installed fuel cell power is above 7,8 kW.

This is a positive aspect considering the highly reduced thermal cycles at which the electrolyzer will be subject under these working conditions, on the other hand it requires to check how the operations of the fuel cells themselves will be affected.

Analyzing Figure 41 it is possible to address this aspect.

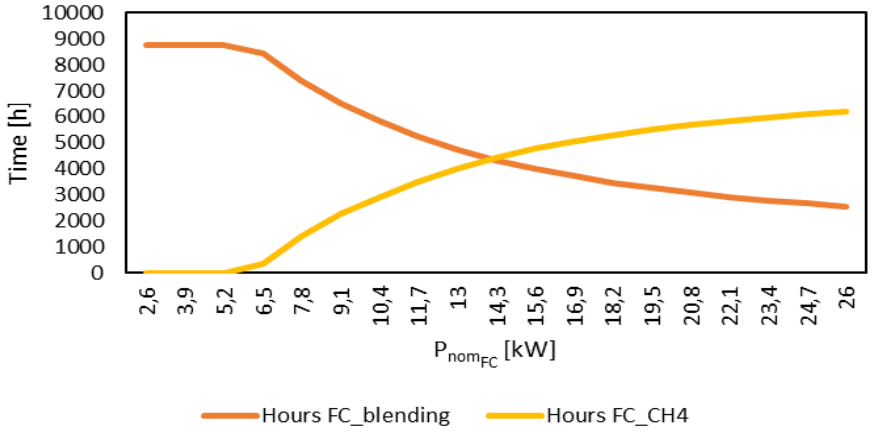

Figure 41. Fuel cell functioning, fuel cell power variation

From the graph in Figure 41, there is evidence of the fact that the rising fuel cell installed power causes a lowered time in which the system can be worked at the correct blending conditions and so rises the number of hours in which the fuel cells are forced to use methane only.

The rising installed power requires higher amount of hydrogen and when the electrolyzer is no longer able to satisfy it, starting form an installed power of 5,2 kW, the fuel cells will operate for more hours using the methane. At this point the electrolyzer remains off in some iterations, as showed in Figure 40, but in some others, it will not be able to constantly produce enough hydrogen to satisfy the demand.

When the installed power rises more, above 7,8 kW, the electrolyzer is already fully exploited, as underlined by Figure 40, and so the number of hours in which the correct blending percentage is used reduces more and more.

In Figure 42 are presented the three charging percentages.

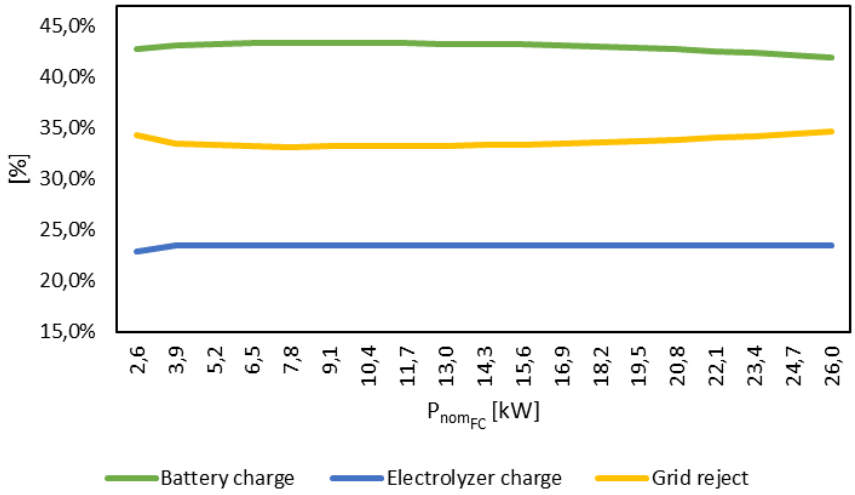

Figure 42. Charging percentages, fuel cell power variation

Figure 42 represents the different share of the two storages charged and the grid rejection, in this case it is evident that the impact of the fuel cell power is not so significative even if it causes at small powers a reduction of the grid rejection according to the higher power required to charge the hydrogen storage that will generate a better exploitation of the extra power.

This trend ends when becomes predominant the working operation of the fuel cells in methane that reduces the possibility of storing hydrogen on one side and it reduces also the power exploited from the battery due to the higher power production form the fuel cells that covers the load, as a consequence the battery remains full reducing the possibilities of its charging. Indeed, it is possible to visualize a rising trend of the $Grid\ reject_{\%}$ at higher values of the installed power of the fuel cells.

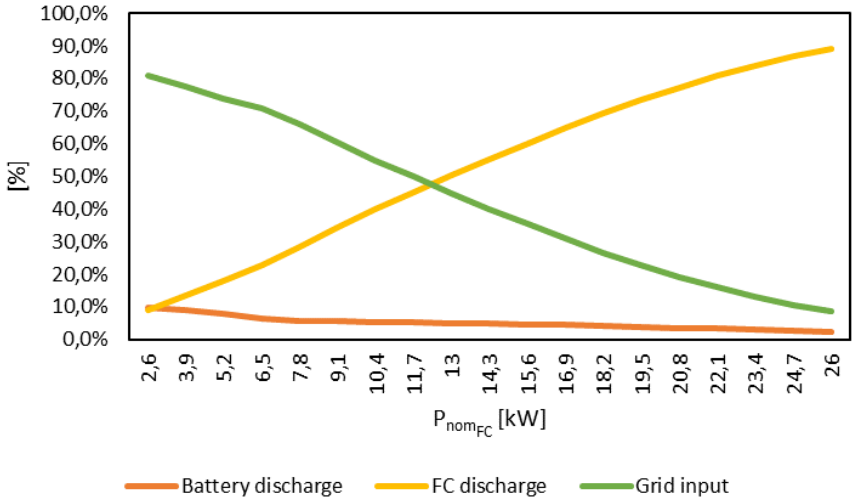

Figure 43. Discharging percentages, fuel cell power variation

The plot in Figure 43 represents how the load is differently satisfy, in a percentual term, by the different element of the system, considering the two storages and the grid input. As already mentioned, the rising power of the fuel cells not only reduces the required input from the grid, that is surely positive, but at the same time, reduces how much the battery contributes to the final load coverage.

The fuel cells are able to satisfy half of the yearly load if the installed power is of 13 kW, in this case the battery provides 5 % of the total while the remaining 45 % should be still satisfied by the grid. When the installed power is instead equal to 26 kW, the fuel cells cover ~ 90 % of the load and the battery only 2 %.

5.2.2 Electrolyzer nominal power

In this section will be analyzed the impact of a bigger electrolyzer on the actual configuration, considering a range from 2 kW to 20 kW.

In Figure 44 are presented the electrolyzer operative conditions with respect to the nominal power of the electrolyzer.

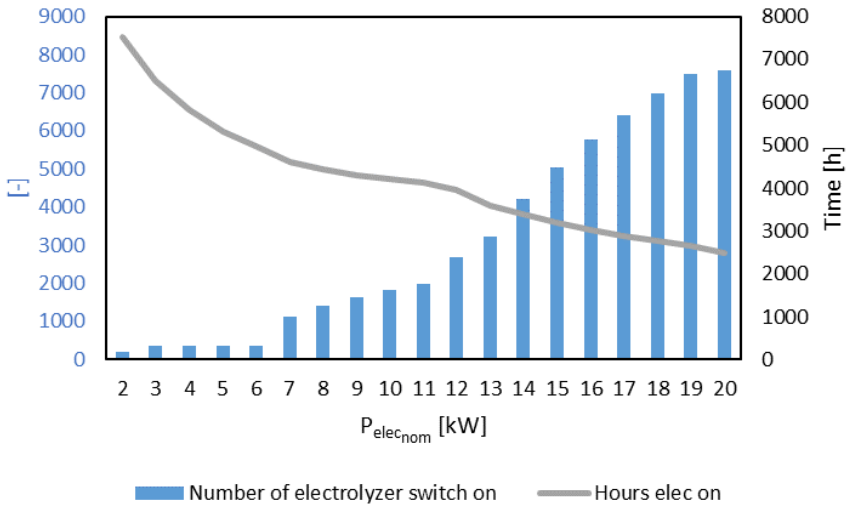

Figure 44. Electrolyzer working conditions, electrolyzer power variation

The plot shown in Figure 44 underlines that the bigger is the electrolyzer the less it will be used and so the more it will be switched on, causing worst operating performances of the machine itself. This behaviour is caused by the fact that the electrolyzer becomes too oversized with respect to the storage and to the fuel cells.

Additionally, the fact of having an oversized electrolyzer determines a higher power demand even at the minimum allowed load, determining a higher minimum production of the hydrogen, so in some cases will not be possible to charge the storage if the quantity that should be produced is too small.

Another relevant comment can be done looking at the flat area of the $Number\ of\ electrolyzer\ switch\ on$ when the $P_{elec_{nom}}$ varies from 3 kW to 6 kW that is coupled with a significant reduction of the total hours in which the electrolyzer is on. This is caused by the fact that a

bigger electrolyzer is able, in some cases, to produce more hydrogen and so even if it is not operated for a while the hydrogen in the tank will be present.

However, this last element can determine that the electrolyzer is less worked at its nominal power and more at a partial load, causing losses in the performances.

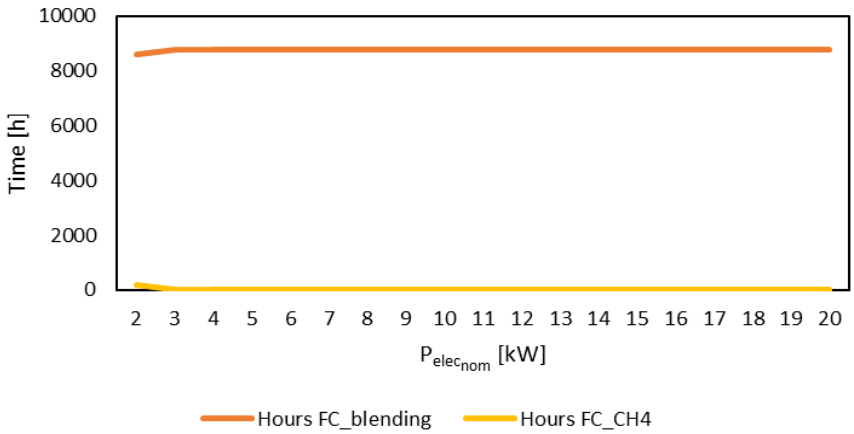

Figure 45. Fuel cell functioning, electrolyzer power variation

The plot shown in Figure 45 underlines that the kind of operation of the fuel cells is almost independent from the size of the electrolyzer if it is big enough. Indeed, the case whit a 2 kW electrolyzer determines a too low hydrogen production not able to make the fuel cells always work in blending conditions, that are forced to operate for some hours with methane only.

The graph of Figure 46 presents the different charging share.

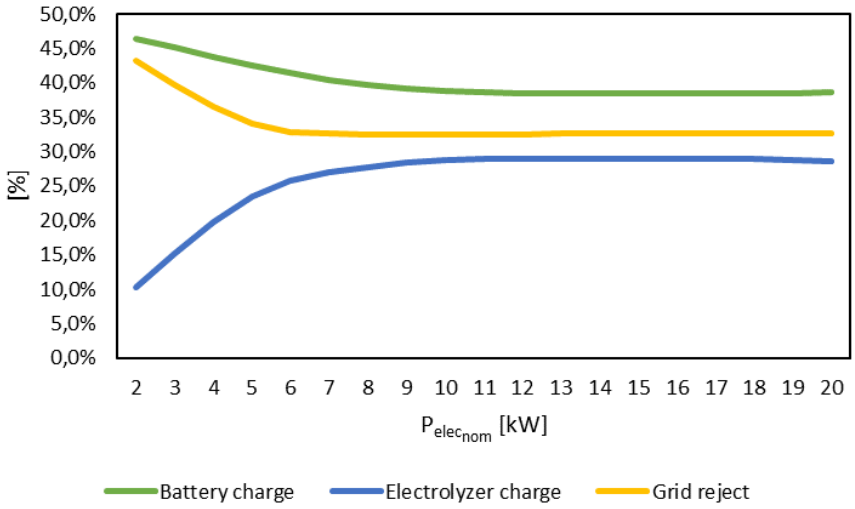

Figure 46. Charging percentages, electrolyzer power variation

In this case the trends are much more variable with respect to the ones presented in Figure 20 since the size of the electrolyzer determines how much of the panels excess can feed it. The relevant aspect is

that after the size of 10 kW we have no more rise in the share of energy that goes to the electrolyzer since it is not possible to produce hydrogen if the tank is already filled.

Going more in detail it is present also a reduction in this percentage when the electrolyzer power rises more and more, this can be explained by the fact that the minimum allowed working percentage of the electrolyzer will rise too and so if there is some small power left that can be used to drive it will not be exploited by the model causing a lower percentage at the end.

The last part left to be analyzed is the one relative to the discharging percentages, their trend is shown in Figure 47.

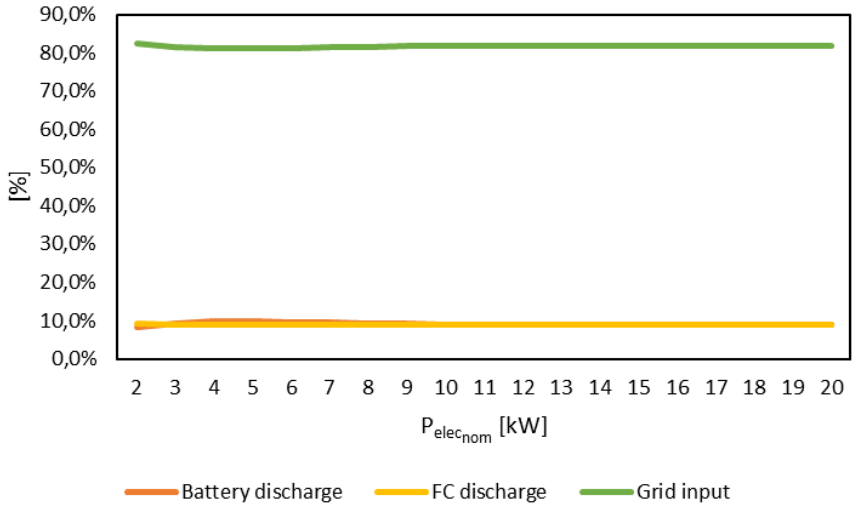

Figure 47. Discharging percentages, electrolyzer power variation

The graph of Figure 47 underlines that the discharging percentages are almost independent form the size of the electrolyzer. To be more precise, the battery discharge percentage shows a small rise for small sizes of the electrolyzer, up to 5 kW, and then it reduces again until becomes stable above 10 kW. This variation is coupled with a respective variation in the grid input required.

This trend can be explained considering that the battery power is firstly used to drive the electrolyzer in the function $LOH\ fixed$, presented in Section 3.5.2, and so if the electrolyzer becomes bigger the battery power is more used to drive the electrolyzer than to cover the load.

5.2.3 Hydrogen storage volume

The last element of the $P2P$ system is the hydrogen storage; in this case its size is made vary starting from 0,5 m^3 to a maximum of 10 m^3. This analysis considers almost only sizes way bigger that the real one since the storage volume of the case study is really small and so was considered not so relevant to analyze sizes lower than it.

In Figure 48 are presented the different working conditions of the electrolyzer with a varying hydrogen tank size.

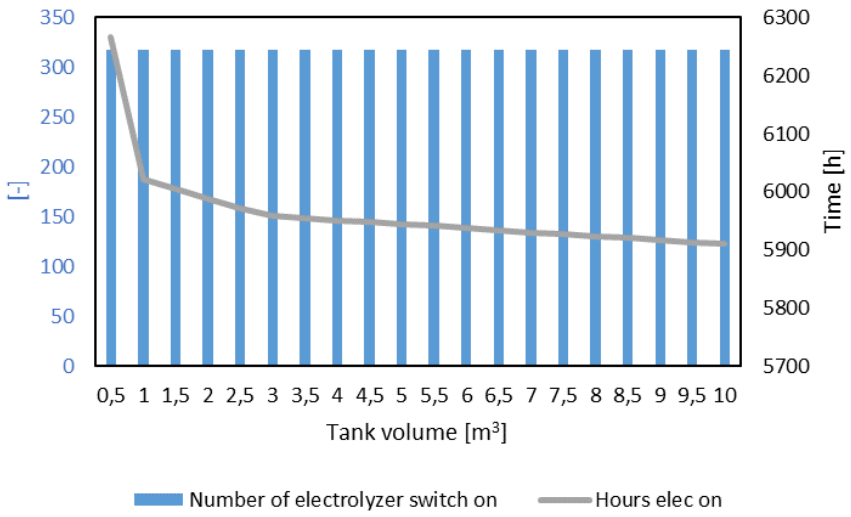

Figure 48. Electrolyzer working conditions, hydrogen tank volume variation

The graph of Figure 48 underlines how small is the impact of the storage volume on the operations of the electrolyzer, indeed the number of switches on is totally independent from it and also the total number of hours varies only of a little if compared to the variations presented in Figures 40 and 44.

The reduction of the electrolyzer operating hours is caused by the fact that having a bigger storage allows to store more hydrogen and so the electrolyzer can remain switched off for longer periods, reducing in this way the *hours elec on*.

The plot regarding the type of operation of the fuel cells, representing the hours in which they work in blending or methane conditions is not even reported in this case since the operation of the cells is totally independent from the size of the storage, at list in the analyzed range. If the storage is too small, the fuel cells will be forced to operate for some hours with methane.

In Figure 49 are reported the charging percentages variations with respect to the size of the hydrogen storage tank.

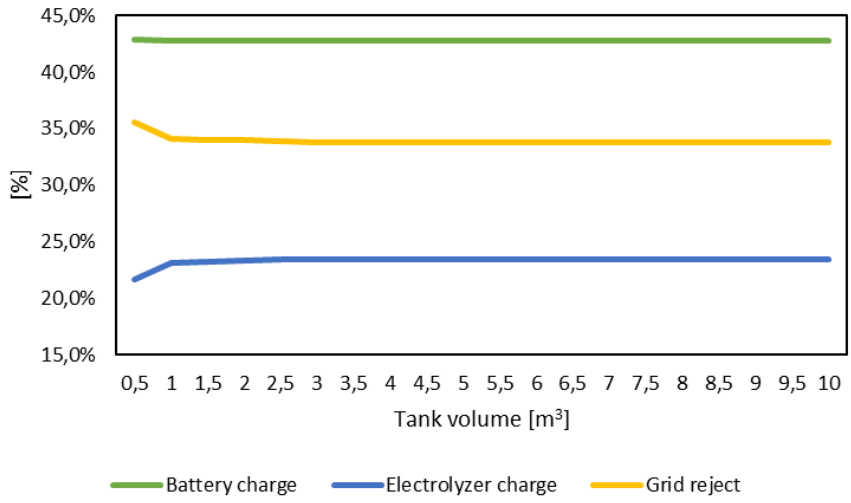

Figure 49. Charging percentages, hydrogen tank volume variation

Also in the plot of Figure 49 is evident that the tank size plays a not so relevant role in the characterization of the charging shares, indeed the trends are almost flat even if we can see a small rise in the $electrolyzer\ charge_{\%}$ from the smallest value up to 2,5 m^3.

This variation can be justified considering that a bigger tank allows a better exploitation of the extra power by the electrolyzer, indeed, it can be largely stored in form of hydrogen. This trend reaches a saturation determined by the nominal power of the electrolyzer. This variation is coupled with a reduction of the energy rejected to grid.

The discharging percentages are not influenced at all by the variation of the hydrogen tank volume. This is justified by the fact that the electrolyzer is able to directly satisfy the requirement of the fuel cells, otherwise the tank size will play a role.

5.2.4 Hydrogen elements simultaneous variation

The analysis performed in this section is done with the aim of determining the impact of a coherent variation in the sizes of the active elements of the $P2P$ system. The choice of performing the variation for the electrolyzer and fuel cell only is determined by the small impact of the hydrogen storage on the system performances, as presented in Section 5.2.3.

The driving element of the variation is the fuel cell size, on the basis of this chosen size, the electrolyzer nominal power is determined considering the necessity of having enough power to make the cell work constantly in the blending conditions selected.

Following this reasoning and considering that the selected blending percentage is 60 % and the efficiencies of the electrolyzer and fuel cell are the ones presented in Chapter 4, the nominal power of the electrolyzer has to be 1,1 times the one of the fuel cells in blending conditions. This choice of keeping constant the hydrogen tank size is performed with the purpose of determining if there is a fuel cell size too big for such a storage. This last element is relevant since the model always considers necessaire the passage of the hydrogen through the tank, the direct feed from the electrolyzer to the fuel cell is not considered.

In Figure 50 is shown the impact of this variation on the electrolyzer working conditions.

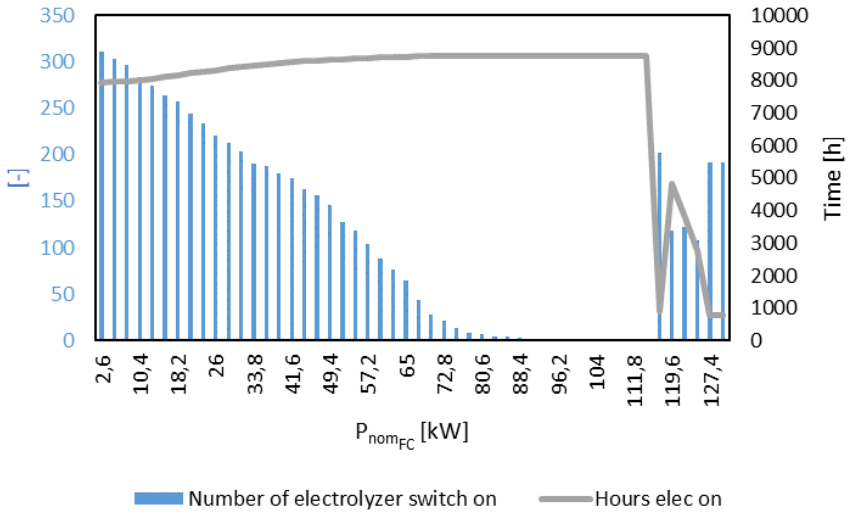

Figure 50. Electrolyzer working conditions, hydrogen elements variation

The plot in Figure 50 shows that with an increasing size of the active elements the electrolyzer is used more constantly until the fuel cell size of 117 kW where the behaviour starts to vary a lot. These two behaviours are both explained by the constant size of the hydrogen storage since when the tank becomes undersized the electrolyzer should work more.

However, the last points of the graph are characterized by a more random trend since the hydrogen storage becomes too small and the quantity inside it is no longer able to satisfy the requirement from the fuel cells, as a consequence in some iterations it will be possible to work the electrolyzer, if the storage is empty enough, while in many others the fuel cells will be forced to use methane only as showed by the graph of Figure 51.

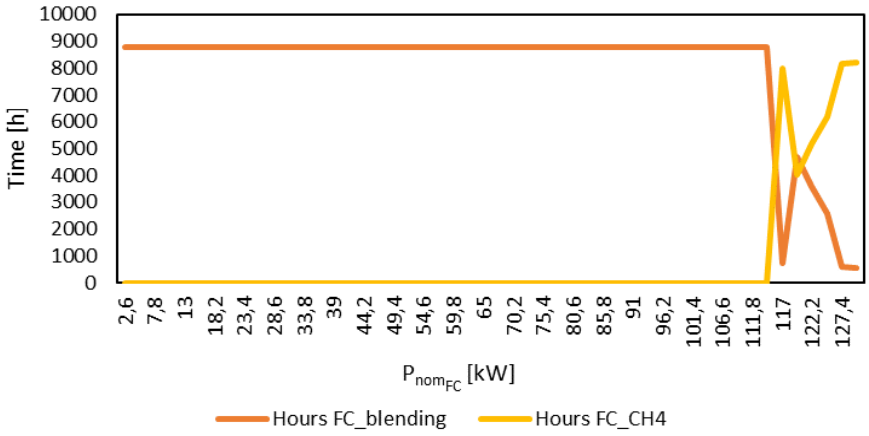

Figure 51. Fuel cells functioning, hydrogen elements variation

The plot in Figure 51 underlines that the fuel cells are constantly working in blending conditions, as defined by the size choose but after the reaching of the fuel cell size of 117 kW the behaviour is no longer constant. After this value, the trends are no longer even comparable with the previous ones since the model is not able to represent the direct feeding from the electrolyzer to the fuel cells.

Indeed, the hydrogen management in the model requires that the electrolyzer always charges the tank and the fuel cells can take hydrogen only from the latter; in a single iteration the electrolyzer can produce hydrogen only until the tank is filled. This model feature causes the more unpredictable behaviour when the hydrogen tank is too small.

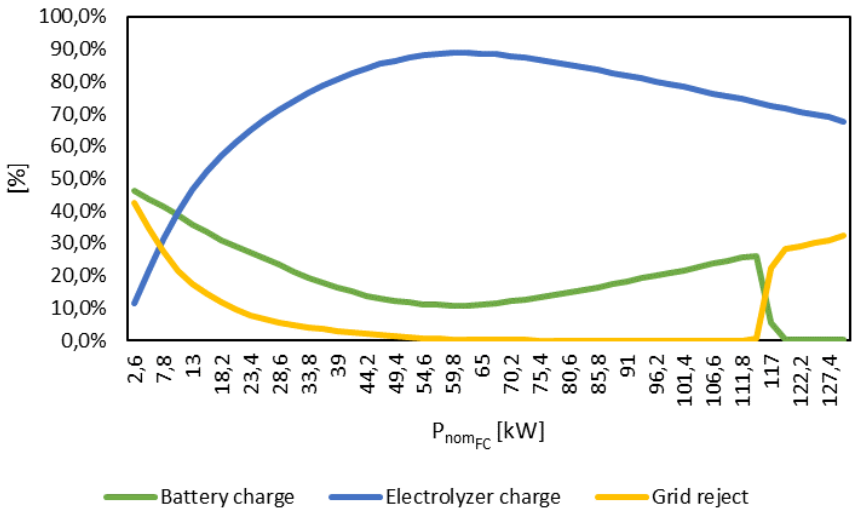

Figure 52. Charging percentages, hydrogen elements variation

Looking at the plots in Figure 52, it is evident that a larger electrolyzer determines that more energy is sent to it, even if this percentage reaches a maximum for a size of the electrolyzer equal to $52{,}8\ kW$, with a $\sim 88\ \%$ of the charging power used by the electrolyzer, and after it the percentage starts to decrease with a correspondent rise in the battery charge percentage.

This trend is justified by the fact that if the electrolyzer becomes too big, the available extra power form the *PV* panels in many iterations will not be enough to drive the electrolyzer, not even at the minimum allowed load. The battery instead is able to receive any amount of power if empty enough, as a consequence the percentage will rise. After the critical size of $117\ kW$ of the fuel cells, the trend is no longer reasonable to be analyzed.

In Figure 53 are presented the discharging percentages determined by this coupled variation.

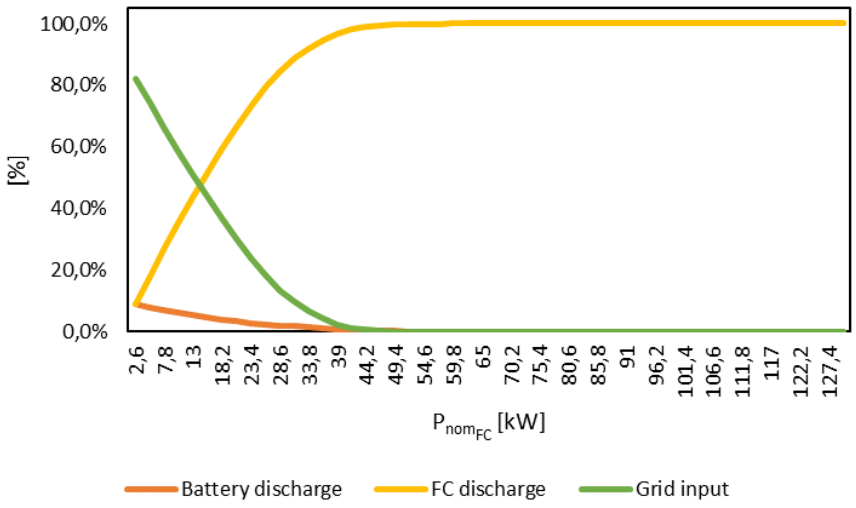

Figure 53. Discharging percentages, hydrogen elements variation

The trends followed by the discharging percentages are mainly influenced by the fuel cells size, indeed they are similar to the ones showed in Figure 43 even if the curve of the fuel cell rises more due to the higher installed powers analyzed in this sensitivity analysis. The fuel cell starts to be able to cover the entire demand if the installed power is higher or equal to $54{,}6\ kW$, more in details if the fuel cell nominal power is $44{,}2\ kW$, the covered load is already 99 % of the total.

The discharging trends are not affected by the problem in the hydrogen management since the fuel cells are able to work in methane conditions and from a power point of view, if the size is big enough, there is no difference at all between the blended or not operations.

The following sensitivity analysis will be performed making a coupled variation of two of the Power-to-Power elements, in order to determine if the trends presented in the single element variations are specific of the selected working point or can be extended to a more generic case.

5.2.5 Fuel cell installed power and electrolyzer nominal powerl

The sensitivity analysis in this section considers a simultaneous variation of both the nominal power of the fuel cells, in a smaller range then before, from $2{,}6\ kW$ to $13\ kW$ performing steps of $2{,}6\ kW$, and of the electrolyzer nominal power, also in this case considered in a smaller range, from $4\ kW$ to $14\ kW$ with steps of $2\ kW$.

Using this simultaneous variation, it is possible to verify if the trends determined in Sections 5.2.1 and 5.2.2 are exclusive of the specific conditions or if instead can be more generally considered. In Figure 54 it is possible to see how this coupled variation affects the electrolyzer work.

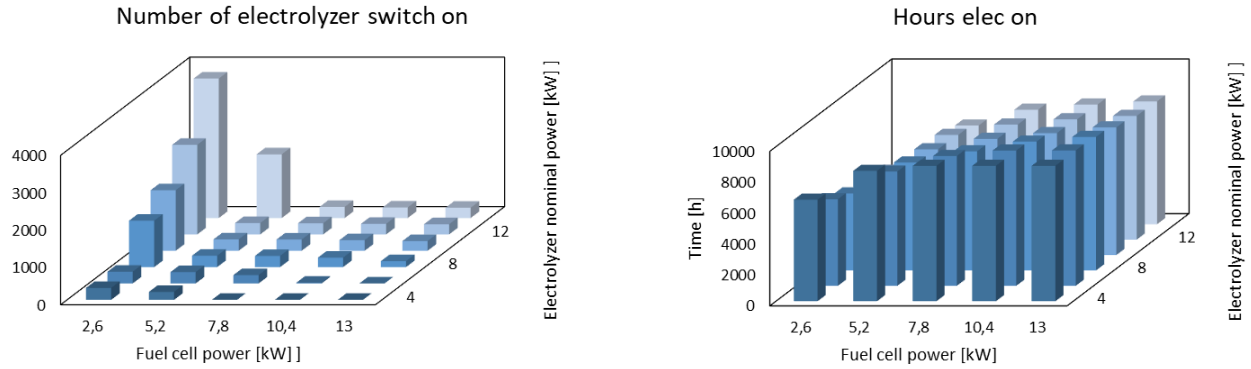

Figure 54. Electrolyzer working conditions, fuel cell power and electrolyzer power variation

Looking at the columns of the left graph it is evident that if the fuel cells are oversized with respect to the electrolyzer, front-right part of the graph, it is switched on less times. Looking instead at the right graph we can also say that it works globally more, it remains more on, producing more hydrogen for the cells in the same considered part of the graph.

The opposite part of the graphs, the left-back one, shows instead the cases in which the electrolyzer is oversized with respect to the fuel cells, in this case the electrolyzer works less and so is switched on and off more times. There is a difference of ~ 3700 switches of ~ 5000 working hours between the case with smallest electrolyzer and bigger fuel cells and the opposite case.

It is interesting to analyze that an electrolyzer of 4 kW works for the entire year if the fuel cell power is equal or higher to 7,8 kW while if its nominal power is 6 kW only fuel cells with powers equal or higher than 13 kW are able to meet this goal. This means that the electrolyzer power should be much smaller than the fuel cells one if we want to have it working in a constant way, obviously this means that the fuel cells will work for a longer time in methane condition, as can be seen in the graphs of Figure 55.

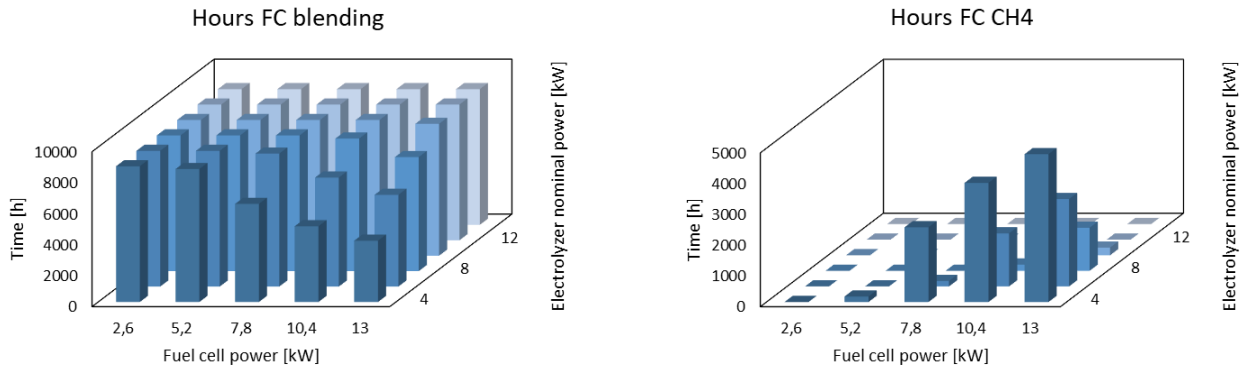

Figure 55. Fuel cell functioning, fuel cell power and electrolyzer power variation

The graph in Figure 55 shows us that, if the electrolyzer is undersized, there is no possibility for the cells to work constantly at the desired working point, this graph is obtained assuming a blending percentage if 60 % but if we rise it the results will be even worse, with the fuel cells forced to work with methane only for longer time. The comparison between the graphs of Figures 54 and 55 provide us the necessity of considering a trade-off between the electrolyzer constant operations and the fuel cells desired working condition. The graphs underline that good compromises can be found excluding the extreme areas, in that points the working hours are above 8000 h/y, the number of switch on lower than 300, considering that a switch on/off can happen every 15 min, and the fuel cells are able to work at the desired blending for more than 8500 h/y.

In Figure 56 is shown the trend of the $Grid\ reject_{\%}$ as representative of the charging percentages.

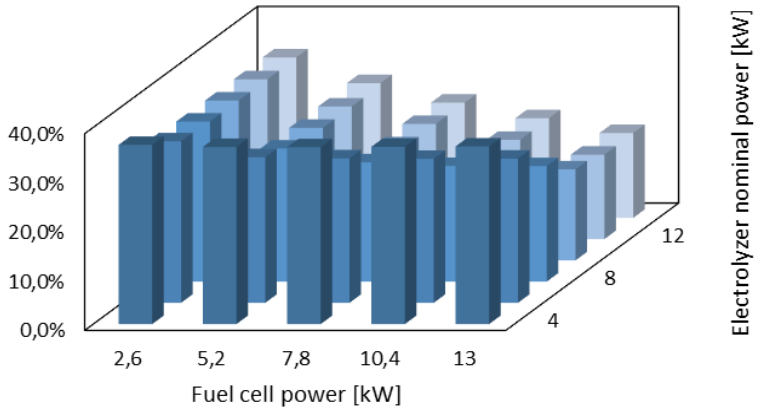

Figure 56. Grid reject percentage, fuel cell power and electrolyzer power variation

Looking at the different horizontal rows of Figure 56, where the electrolyzer power is fixed, there is evidence that the trend underlined in Figure 42 is valid only for a small electrolyzer, if instead the power of the electrolyzer rises more and more, the effect of fuel cell power becomes relevant. This trend can be explained by the fact that in this case the presence of more fuel cells allows a higher consumption of hydrogen and so the electrolyzer can be worked more reducing the percentage of energy rejected to the grid. Indeed, the fuel cell nominal power variation generates a reduction of 0,3 % if the electrolyzer size is equal to 4 kW while if the electrolyzer nominal power rises at 12 kW the produced variation is of 15,3 %.

Looking instead at the oblique rows we can see that the impact of the fuel cell power determines at which level the curve starts to flatter, if this power is higher also the one of the electrolyzer determining the flat value of this percentage rises. At the same time also the percentual value at which it flatters is lower since there will be a higher consumption of hydrogen allowing a better exploitation of the available energy from the electrolyzer.

For what concerns the discharging percentages instead the choice has been to report both the $Fuel\ cell_{\%}$ and the $Grid\ input_{\%}$ in order to provide a deeper analysis of the load coverage operation.

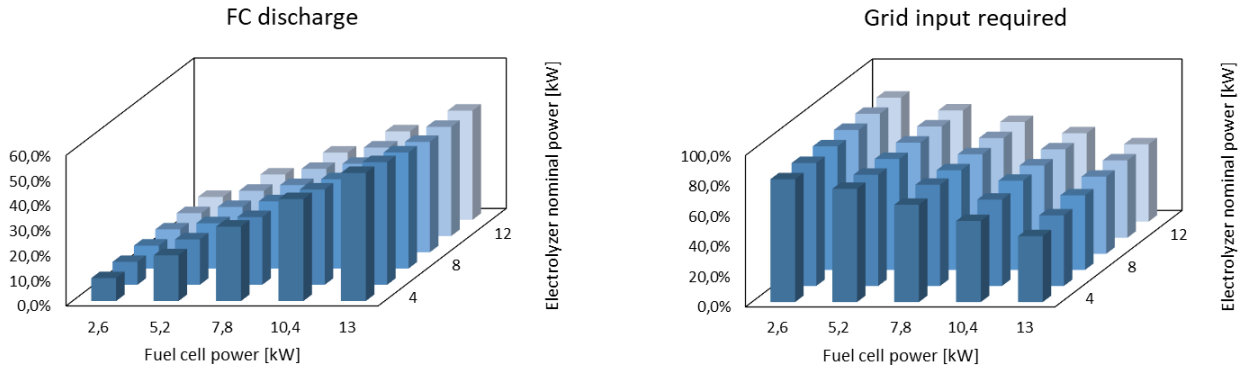

Figure 57. Fuel cell coverage, left, and grid input required percentage, right, fuel cell and electrolyzer power variation.

The left graph of Figure 57 shows that the presence of undersized electrolyzer determines a higher load coverage from the fuel cells since they will work more in full methane producing more power with respect to the blending operations, except from this, the trends are the same showed in Figures 43 and 47.

The consequences of this additional effect can be seen in the right graph in which there are, looking at the oblique lines, some not monotone trends caused by the switch in the fuel cells operations, from methane to blending, determining so a lower impact of the fuel cells. This trend is visible in the oblique lines.

5.2.6 Fuel cells installed power and hydrogen tank volume

In this case the variation of the fuel cells is the same as the one of Section 5.2.5 while for the hydrogen tank the variation starts from the real case of 0,7 m^3 and reaches 4,9 m^3 with steps of 0,7 m^3.

For what concerns the electrolyzer operations they appear as independent from the simultaneous variations, the trends of Figures 40 and 44 are almost unchanged for both the $number\ of\ electrolyzer\ switch\ on$ and for the $hours\ elec\ on$.

In Figure 58 are reported the variations of the fuel cell working conditions.

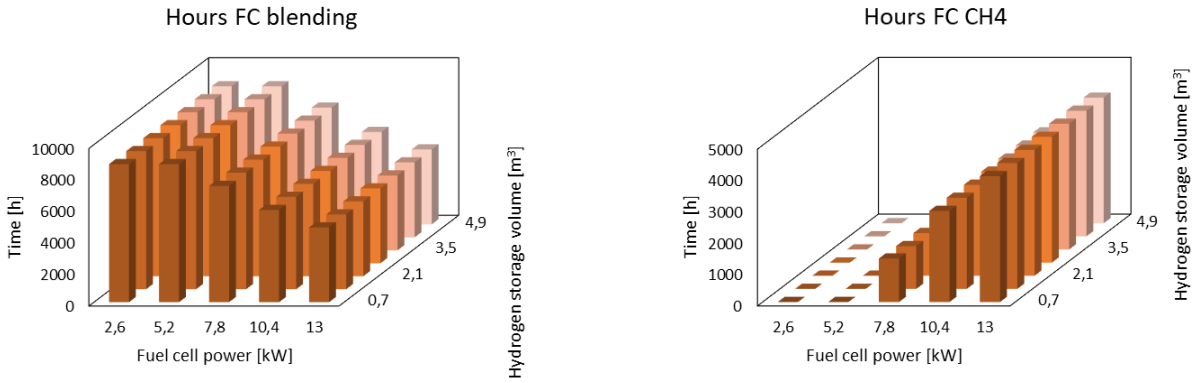

Figure 58. Electrolyzer working conditions, fuel cell power and hydrogen tank volume variation.

The trends over the horizontal lines, at constant hydrogen volume tank, are unchanged with respect to the one showed in Figure 41. Looking instead at the oblique trends, there are small variations absent in the case of single variation of the hydrogen volume tank.

This trend determines a small rise of the hours in blending operation when the hydrogen storage rises if the fuel cell power is big enough. This can be explained considering that a bigger storage allows to have more hydrogen available when we have energy excesses allowing the correct blending operations for longer times.

Considering the $Grid\ reject_{\%}$ there are no significant variations with respect to the trends showed in Figures 42 and 49; the same can be said for the $FC\ discharge_{\%}$ and the $Grid\ input_{\%}$ that present trends unchanged.

5.2.7 Electrolyzer nominal power and hydrogen tank volume

To perform this simultaneous variation, the choice has been to use the variation of electrolyzer nominal power showed in Section 5.2.5 and the one of the hydrogen tank presented in Section 5.2.6.

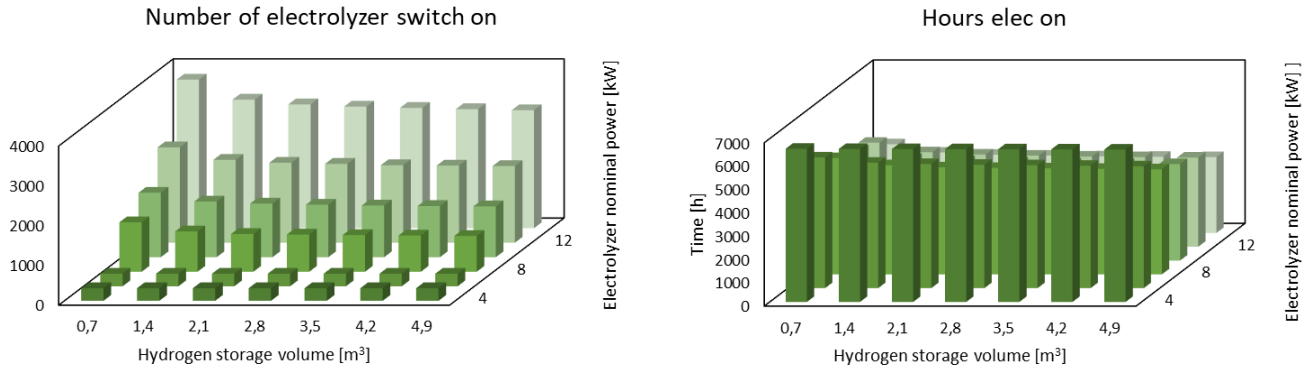

Figure 59. Electrolyzer working conditions, hydrogen tank volume and electrolyzer power variation

Looking at the graphs of Figure 59 can be seen that the variation of the analyzed key performance indicators is the same of Figure 44 if we consider the variations at constant hydrogen storage volume while we have a variation in the $number\ of\ electrolyzer\ switch\ on$ if we consider the different trends at constant electrolyzer nominal power.

Indeed, in Figure 48 is presented a constant trend that in the graph is present only for the electrolyzer nominal power equal to 4 kW and 6 kW, for bigger sizes instead it is evident a decreasing trend. This can be explained considering that a bigger hydrogen storage can be charged more and so a bigger electrolyzer can work more constantly, indeed the variation of the hydrogen tank volume determines a variation of ~ 800 switches and 600 working hours of the electrolyzer if it is the bigger analyzed.

The operations of the fuel cells are totally not affected by this variation, the fuel cell size, set at 2,6 kW as in the real case, determines a null impact of these variations.

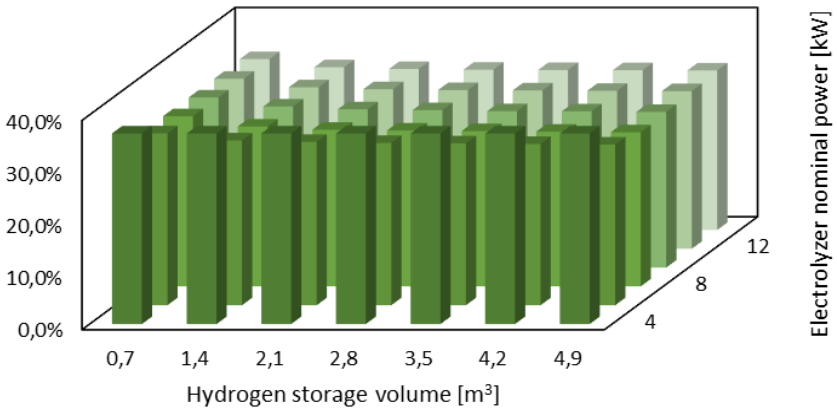

Figure 60. Grid reject percentage, hydrogen tank volume and electrolyzer power variation

Looking at Figure 60, it is possible to see that the curve at constant electrolyzer nominal power flatters at a lower level of the hydrogen tank if the electrolyzer power is higher, this can be explained considering that if the electrolyzer is bigger can be harder to have it work at the minimum power and so the grid reject percentage will rise more.

In Figure 61 are then showed the two discharging percentages relative to the fuel cell contribute and to the required input from the grid.

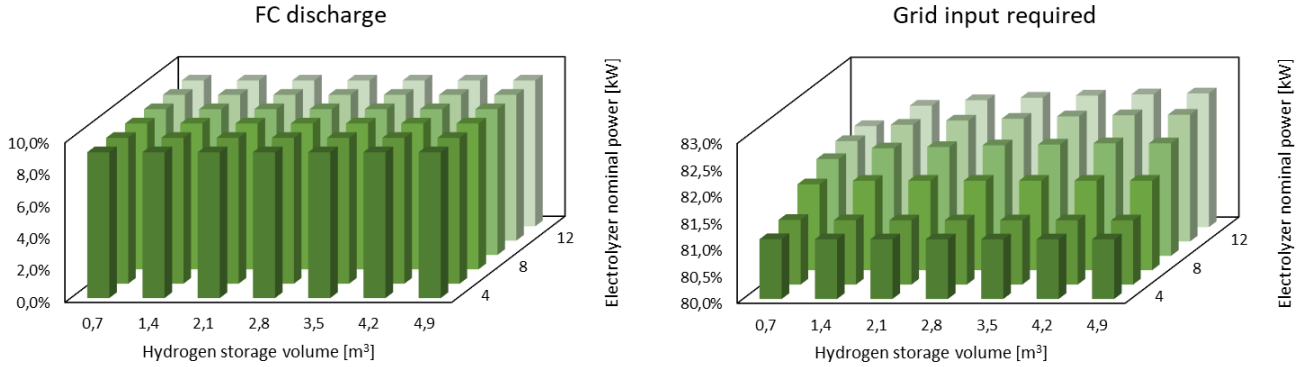

Figure 61. Fuel cell coverage percentage, left, and grid input required percentage, right, hydrogen tank volume and electrolyzer power variation.

The analysis of Figure 61 shows that even if the fuel cell percentage remains unchanged there are some small variations in the grid input requirement, more in details it rises more if both the electrolyzer nominal power and the hydrogen tank rises.

This can be explained considering that the bigger is the electrolyzer higher will be the power required to let it work also at the minimum working point to ensure the required LOH imposed by the function $LOH\ fixed$ presented in Chapter 3.5.2. This function prioritizes the energy stored in the battery to drive the electrolyzer, generating a lower amount of energy available to cover the load from the battery itself.

A peculiar behaviour can be seen looking at the oblique rows referred to a hydrogen storage of $0{,}7\ m^3$ in which it is evident that the biggest size of the electrolyzer generates a lower rise with respect to the previous ones, $0{,}1$ % with respect to 1 % if the hydrogen tank volume is $4{,}9\ m^3$, probably because at that size the electrolyzer will work less being oversized with respect to the storage, determining a lower rise in the consumption of the battery energy.

5.2.8 Total variation

In order to perform a deeper analysis of the interconnections between the three elements of the $P2P$ system, have been performed a series of sensitivity analysis in which all the three elements are made vary in the ranges used for the coupled variations and presented in Sections 5.2.5 and 5.2.6.

		Number of electrolyzer switch on	hours elec on	Battery charge	Electrolyzer charge	Grid reject charge	Battery discharge	FC discharge	Grid input required
	Target	**1**	**8322**	**43%**	**50%**	**14%**	**9%**	**45%**	**50%**
Parameter	m3								
Storage volume	0,7	4	9	5	0	0	4	3	3
Storage volume	1,4	6	10	5	6	3	3	3	2
Storage volume	2,1	6	10	5	7	3	3	3	2
Storage volume	2,8	6	10	5	7	3	3	3	2
Storage volume	3,5	6	10	5	7	3	3	3	2
Storage volume	4,2	6	10	5	7	3	3	3	2
Storage volume	4,9	6	10	5	7	3	3	3	2
	kW								
Nominal power electrolyzer	4	21	28	35	0	0	7	7	7
Nominal power electrolyzer	6	13	21	0	0	0	7	7	7
Nominal power electrolyzer	8	6	14	0	0	0	7	7	1
Nominal power electrolyzer	10	0	6	0	0	0	1	0	0
Nominal power electrolyzer	12	0	0	0	18	0	0	0	0
Nominal power electrolyzer	14	0	0	0	23	18	0	0	0
	kW								
P_FC_installed	2,6	0	0	7	0	0	22	0	0
P_FC_installed	5,2	0	7	7	5	0	0	0	0
P_FC_installed	7,8	7	14	7	12	6	0	0	0
P_FC_installed	10,4	13	21	7	12	6	0	0	0
P_FC_installed	13	20	27	7	12	6	0	21	15

Table 5. Simultaneous variation of the P2P elements results

In this case considering the presence of many simulations, the results are showed in Table 5 as the number of times in which a simulation characterized by the parameter on the left reaches a value, in the key performance indicator showed in the column, that is higher or lower than the target specified below the key performance indicator itself.

Looking at the $number\ of\ electrolyzer\ switch\ on$ for example, it is evident that the storage volume plays a much lower role with respect to the nominal power of electrolyzer or fuel cells while aiming to reach a maximum number of switch on equal to 1. This result can be reached only with a small electrolyzer or with significant big fuel cells able to consume enough hydrogen. An additional relevant information is that the presence of electrolyzers bigger than $10\ kW$ or fuel cells smaller than $7{,}8\ kW$ does not allow at all to reach the working conditions for a single switch on off the electrolyzer.

The column of $hours\ elec\ on$ shows the same trend already underlined by the first column, the target is set to the combinations able to reach a number of working hours for the electrolyzer higher than 8322 that represents the $95\ \%$ of the total hours in a year.

The targets for the percentages have been set looking at the results of the simulations and taking the higher results accounted in less than $25\ \%$ of the total simulations. For the $Grid\ reject_{\%}$ and the $Grid\ input_{\%}$ the target is to obtain values lower than the target set while for the other percentages the goal is to reach values above the target.

Looking at the results obtained it appears evident that the less impacting element is the hydrogen storage unless it is significantly undersized, on the other hand the electrolyzer size and the fuel cell sizes plays relevant roles.

To reach low levels of both $Grid\ reject_{\%}$ and $Grid\ input_{\%}$ it is required to have big fuel cell power, especially to obtain low values in the $Grid\ input_{\%}$. The effect of the electrolyzer size is instead opposite since to have really low $Grid\ input_{\%}$ is required a smaller electrolyzer while for a low $Grid\ reject_{\%}$ is required a big electrolyzer.

This last difference is justified by the already underlined impact of a big electrolyzer that produces lower energy left in the battery since it uses the battery power, on the other hand the presence of a bigger electrolyzer allows the better exploitation of the extra power produced by the panels.

5.3 Decision parameters variation

The sensitivity analysis performed in this section are relative to the parameters that can be freely set independently from the size of the real elements of the $P2P$ system, considered equal to the ones of the base case scenario presented in Table 1.

The modified parameters are: the blending percentage of the fuel cells, the level of hydrogen in the tank ensured by the function $LOH\ fixed$, the working point of the fuel cells at which they are forced to operate by $Cell\ on\ min$, named $load\ guaranteed\ FC$, and the minimum working point of the electrolyzer.

These parameters are made vary in some ranges defined by the nature of the problem analyzed, for example, for the blending percentage the range varies from 0 to 100 % since the fuel cells are supposed to be able to operate in the whole range. The value of $LOH\ fixed$ instead varies from slightly above the minimum allowed percentage in the storage, of 5 %, form 10 % to the full charge at 100 %; the $load\ guaranteed\ FC$ covers instead a shorter range since the fuel cells are not supposed to be able to work correctly below 40 % of the nominal power. The parameter $Load\ min\ elec$ is made vary from the minimum load accepted of 20 %, accordingly to [19], to a hypothetic condition where the electrolyzer can only work at its nominal power.

5.3.1 Blending

The analysis of the blending percentage effect on the system performances is a key element since one of the project aims is to determine how will the fuel cell work in such conditions.

In Figure 62 is analyzed the impact of the blending percentage selected on the electrolyzer working operations.

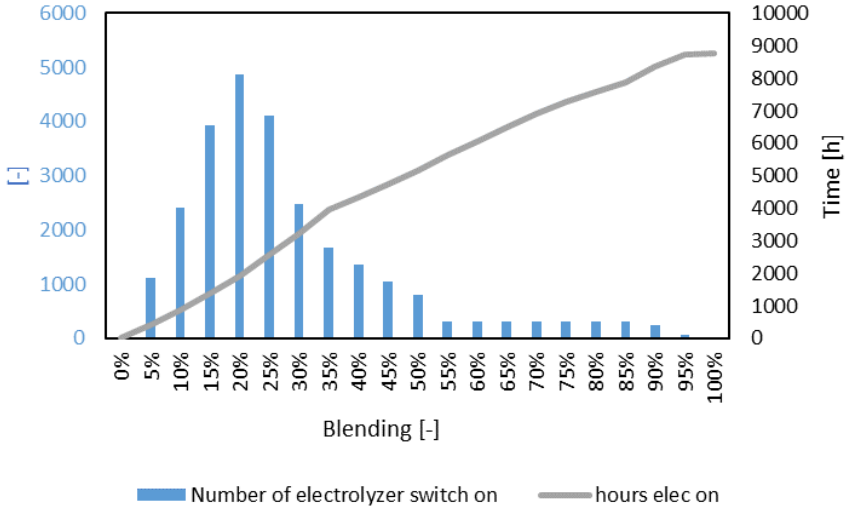

Figure 62. Electrolyzer working conditions, blending

Looking at the columns presented in Figure 62 it is possible to verify that above the blending percentage of 55 % the electrolyzer is switched on always ~ 315 times until it is reached a percentage higher than 90 % where the number of switches on decreases below 50. This trend is coupled with an

increasing number of hours in which the electrolyzer is operated, as can be seen from the grey curve, in the range from 55 % to 90 % of blending the electrolyzer operating hours rise from $\sim 5500\ h$ to $\sim 7500\ h$; above the value of 90 % the electrolyzer is used almost during the whole year, for more than $8700\ h$.

This last aspect is explained considering that, having a higher blending percentage, is required more hydrogen and so the electrolyzer is used more. For what concerns the number of switches on instead, this trend means that even if the working hours rise there are some moments in the year in which the electrolyzer is not worked at all, unless the required quantity of hydrogen is high.

Looking instead at the left part of the graph, there is an initial increasing and after the value of 20 % the number of switches on decreases, meanwhile the number of working hours is continuously rising. The initial rising trend can be explained considering that, if the required quantity of hydrogen is low, the electrolyzer can remain switched off for more iterations, than, with a rising request of hydrogen it is used more times.

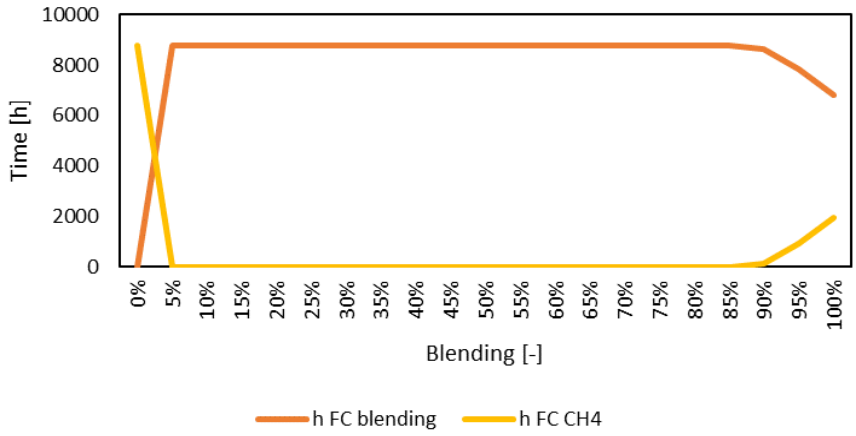

Figure 63. Fuel cell functioning, blending

The plot in Figure 63 determines if the electrolyzer is able to make the fuel cell work at the required blending percentage over the whole year. The first point of the graph, with the absence of blending, determines of course that the fuel cells are constantly working in methane conditions.

The electrolyzer is able to satisfy the hydrogen request from the fuel cells only below a working percentage of 90 %, indeed below this threshold the fuel cells are always operated in blending conditions; above this value instead, the electrolyzer is no longer able to provide enough hydrogen and the fuel cells are forced to operate in methane conditions for some hours of the year. If the selected working condition is in full hydrogen, blending at 100 %, the fuel cells will use methane from almost $2000\ h$ in a year.

In Figure 64 are presented the variations in the charging percentages determined by the blending variation.

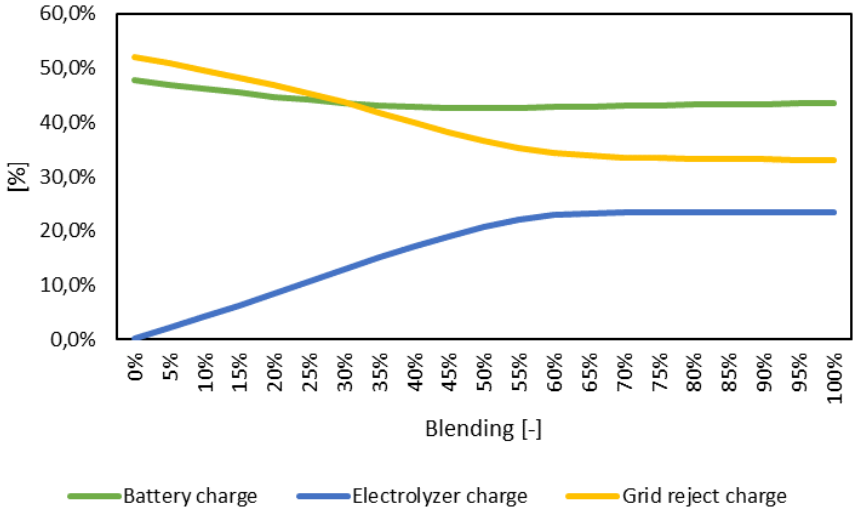

Figure 64. Charging percentages, blending

The main effect of the blending percentage is on the electrolyzer charging percentage since this element is used more if the hydrogen demand rises. Looking at the blue line in the graph, above 55 % of blending the curve starts to flatter and after 70 % the electrolyzer charging percentage remains constantly at 23,5 %. This trend determines that even if the electrolyzer is worked more, the amount of power from the PV panels that it can accept cannot rise above a certain percentage since in the hours in which it is available it is already exploited.

Coupled with this variation, there is an initial decrease in the battery charging percentage from the 47 %, associated with the blending percentage of 5 %, to 42,7 % when the blending lies in the range from 45 % to 60 %. After this decrease there is a small rise up to 43,5 %. The first decreasing trend is determined by the higher use of the electrolyzer removing energy from the battery, then the second trend instead is determined by a larger use of the battery to drive the electrolyzer while calling the function $LOH\ fixed$ causing the battery to be emptier, so able to accept more energy from the PV panels.

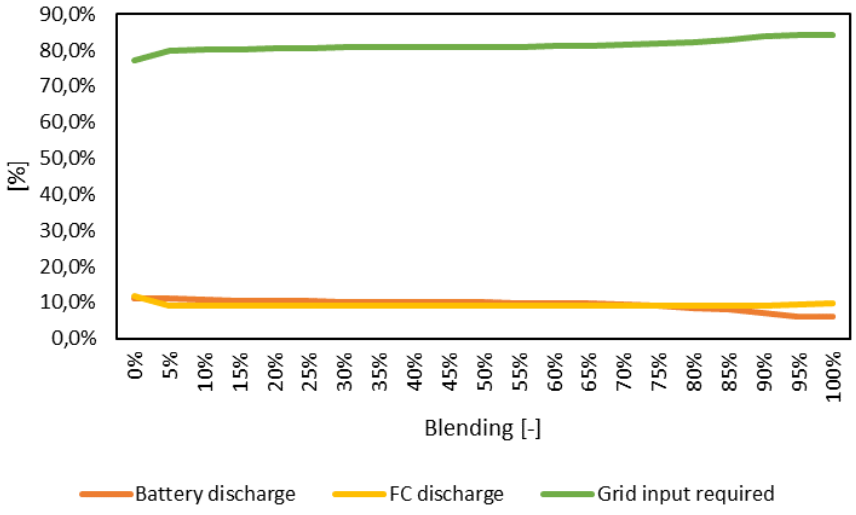

Figure 65. Discharging percentages, blending

The trend relative to the fuel cell percentual contribute to the satisfaction of the load is totally determined by the hours in which the fuel cells operate in blending or methane, indeed this percentage is constantly equal to 9,1 % when the fuel cells are totally in blending, from 5 % to 90 % of hydrogen in input. The $FC\ discharge_{\%}$ rises if the fuel cells work with methane since the nominal power of the fuel cells will be higher.

Considering the $Battery\ discharge_{\%}$, can be seen a decreasing trend for higher percentages of blending since the battery energy will mainly be used to drive the electrolyzer; these trends of the battery and of the fuel cell determine a rising trend in the percentage of energy needed from the grid.

5.3.2 LOH target

In Figure 66 is presented the effect of the parameter $LOH\ target$ on the electrolyzer operations.

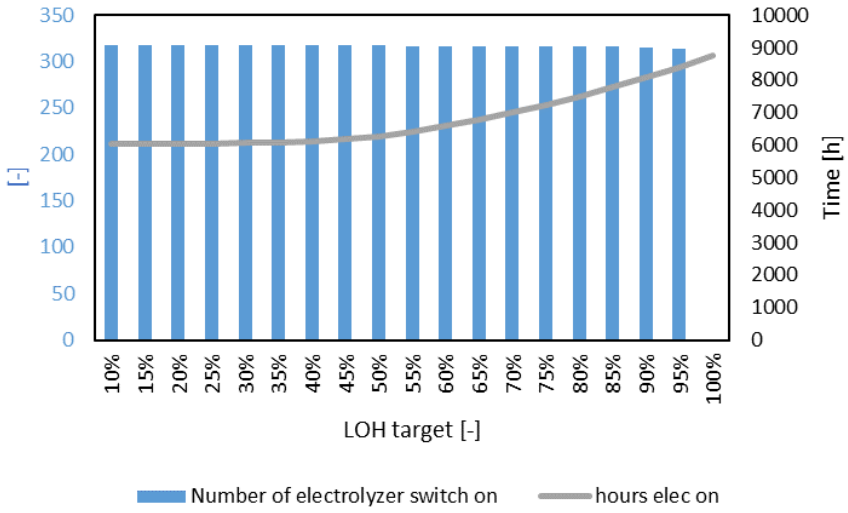

Figure 66. Electrolyzer working conditions, LOH target

Looking at the columns showed in Figure 66, the impact of the parameter $LOH\ target$ appears not so relevant since the electrolyzer is switched on 317 times if the value of this parameter is between 10 % to 50 % and decreases only to 314 times if the value of $LOH\ target$ is 95 %. Even considering the number of hours in which the electrolyzer effectively works, the value is kept almost constant around 6100 h in the first range while it rises a lot, reaching the full operations when $LOH\ target$ is equal to 100 %.

This last point is coupled with a single switch on of the electrolyzer, this means that the electrolyzer should be always on to guarantee a fully charged hydrogen tank; if instead it is acceptable to not have always charged the storage, there are some iterations in which the electrolyzer will never be switched on.

Considering that the required blending percentage is at 60 % and the chosen discharging logic, the fourth, considers the possibility of working the electrolyzer also during the discharging phase, the parameter $LOH\ target$ has no impact at all on the fuel cell functioning, they will always work at the correct blending.

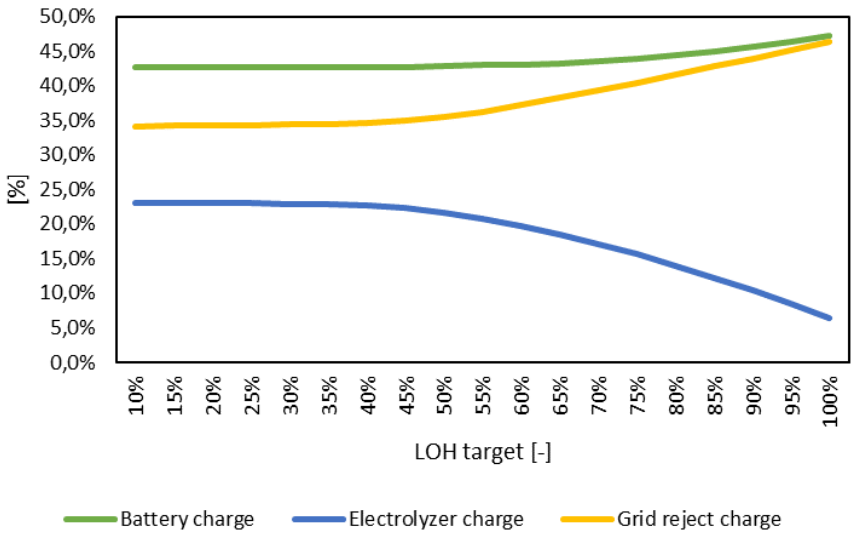

Figure 67. Charging percentages, LOH target

Looking at the blue line in Figure 67 it is evident that a rising $LOH\ target$ determines a lowering percentage of the PV panels energy accepted by the electrolyzer, starting from a value of 23,1 % when the level of the $LOH\ target$ is equal to 10 % to the lower reached percentage of 6,4 % at the right end of the graph. This trend is explained considering that, if the electrolyzer is forced to guarantee a higher level in the hydrogen tank, the tank will be less empty for the following iterations and so, considering that with the actual sizes the fuel cells, at 60 % of blending, consumes less than what the electrolyzer produces at full power, the storage will be less filled thanks to the panel's energy.

This trend is coupled with a symmetric trend of the percentage of energy rejected to the grid but also with a higher percentage accepted by the battery since it will be exploited more to drive the electrolyzer, as a consequence it will be able to accept more energy.

The discharging percentages are almost not influenced at all, the only visible trend is a small reduction in the $Battery\ discharge_{\%}$ since, as said, it will be emptier to drive the electrolyzer. This reduction will be compensated by a rising input form the grid, the fuel cells contribute is constantly fixed at 9,1 % since their operation does not vary.

5.3.3 Load guaranteed FC

The fuel cell guaranteed working percentage will affect the electrolyzer operations, as underlined by the graphs in Figure 68, since it will produce a higher or lower consumption of hydrogen.

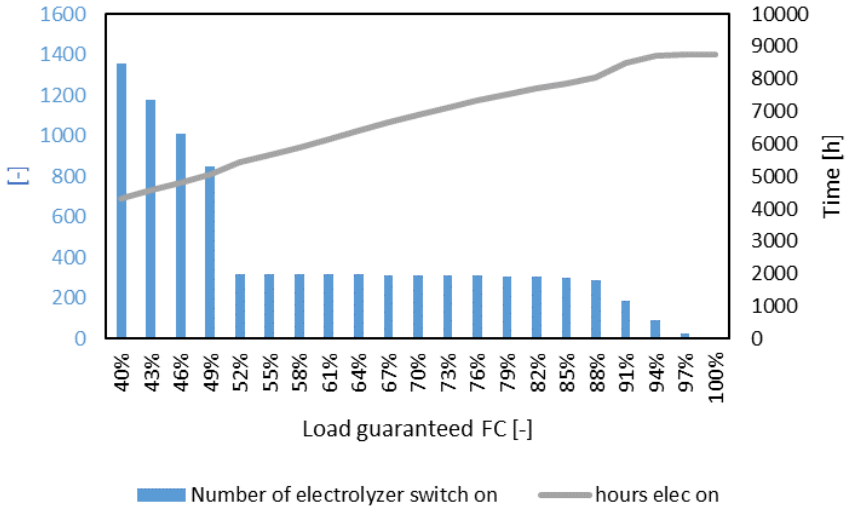

Figure 68. Electrolyzer working conditions, load guaranteed FC

Analyzing the bars in Figure 68, it is evident that if the guaranteed working percentage is lower than 50 %, the electrolyzer will be switched on a lot, around 1000 times, while above this threshold, this number remains almost constant up to 90 %, to be more precise at 52 % the number of switches is equal to 321 while at 88 % it reaches 290. This trend is coupled with a constant rise in the number of hours in which the electrolyzer is effectively on, from ~ 5400 h to more than 8000 h when the 88 % of guaranteed load is reached.

These trends are justified by the higher request of hydrogen from the fuel cells, if the working point is higher the amount of hydrogen requested will be higher even during the iterations in which there is excess of power production from the photovoltaic panels.

The higher demand of hydrogen determines the impossibility for the fuel cells to constantly work in blending conditions, as showed in Figure 69.

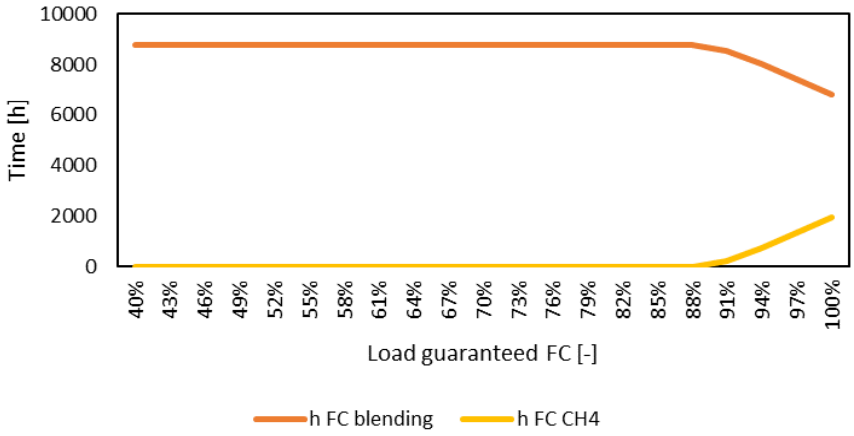

Figure 69. Fuel cell functioning, load guaranteed FC

The demand of hydrogen will be too high if the guaranteed load of the fuel cells is higher or equal to 88 %, even if at this value only for 5,5 h in a whole year the fuel cells are forced to use methane only. This type of working condition is forced for more time if the guaranteed load rises more, up to 1930 h when the fuel cells are constantly worked at their nominal power.

This also determines a rise in the $FC\ discharging_{\%}$ since in full methane the fuel cells are producing more power. Dealing with the discharging percentages, the battery one will show a decreasing caused by the higher use of the electrolyzer that causes the higher drain of the battery charge from it.

For what concerns the charging percentages, the trends are the same of Figure 64 since are determined by a larger use of the electrolyzer caused by the higher demand of hydrogen. Indeed, there is increasing trend in the electrolyzer charging percentage coupled with a decrease in the $Grid\ reject_{\%}$.

5.3.4 Load min electrolyzer

Theoretically this value is fixed by the kind of electrolyzer installed, in this case it has been supposed to force the electrolyzer to work at minimum conditions even above this minimum threshold. This has been done in order to verify if there could be some positive gains making the electrolyzer work constantly at higher loads.

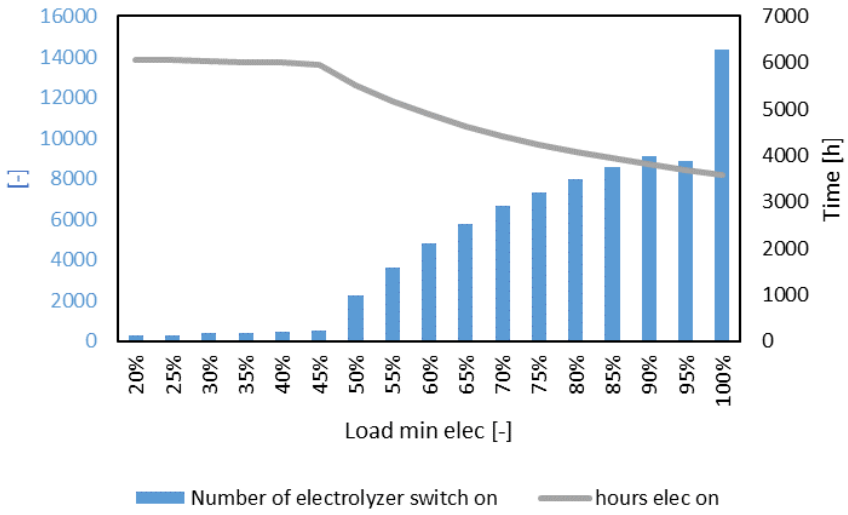

Figure 70. Electrolyzer working condition, load min electrolyzer

The plots in Figure 70 shows opposite trends with respect to the ones of Figures 62 66 and 68 since in this case the higher is the parameter $load\ min\ elec$ the worst will be the performances of the electrolyzer considering that the target is to have it working as constantly as possible.

If the minimum allowed working percentage of the electrolyzer is lower than 45 %, the electrolyzer works for about 6000 h with a number of switches on that varies from 316 to 542 times with a rising trend. Indeed, if the electrolyzer can be worked at a lower percentage, it can be worked even if the hydrogen storage is not totally empty.

Above the percentage of 50 % the electrolyzer working conditions becomes even worst, reaching ~ 9000 switches on at 95 % and 14000 if the electrolyzer can only work at its nominal conditions.

The fuel cell operations are not affected at all by the variation of this parameter since the size of the storage allows them to constantly work in blending conditions even if the electrolyzer can be operated only at full power.

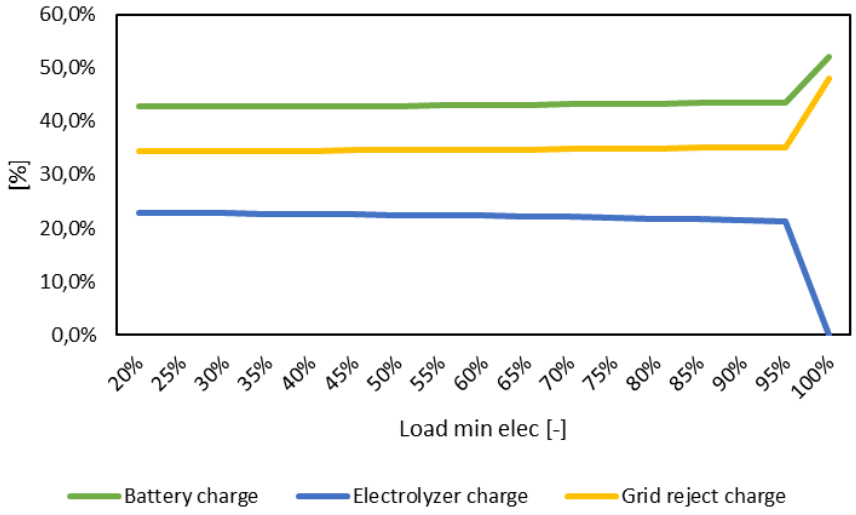

Figure 71. Charging percentages, load min electrolyzer

Looking at Figure 71, the electrolyzer charging percentage is negatively affected by a rise of the electrolyzer minimum allowed load, indeed this percentage passes from 22,9 % to 21,3 % with a decreasing trend. This can be explained considering that if the minimum percentage is higher the electrolyzer will be able to accept only the excesses if they are above a higher threshold, as a consequence there will be some iterations in which the excess from the *PV* is too low.

The amount of power not accepted by the electrolyzer is partly sent to the battery, but party has to be rejected to grid since it will be not possible to safely charge the battery. The discharging percentages are almost not affected by this parameter, only if there is more power available in the battery, this element will contribute more to the load satisfaction.

5.3.5 Blending and LOH target

In the following sections, the sensitivity analysis has been performed making vary a couple of parameters together, as it has been done in Sections 5.2.5, 5.2.6 and 5.2.7. For a computational issue, the ranges of the parameters have been varied, also reducing the number of points taken in the range.

For what concerns the blending percentage, the range has been set starting from zero to 90 % considering 7 points inside, each one distant 15 % from the other; the points above 90 % have been neglected considering that they have already shown the impossibility for the electrolyzer to satisfy the demand of hydrogen.

The range in which the parameter $LOH\ target$ can vary has been enhanced making it start from 5% but the number of points inside has been reduced to 5. In this way it is possible to also explore the effect of the absence of any fixed level of the hydrogen in the tank.

In Figure 72 it is possible to visualize the effect of the coupled variation of these parameters on the electrolyzer working.

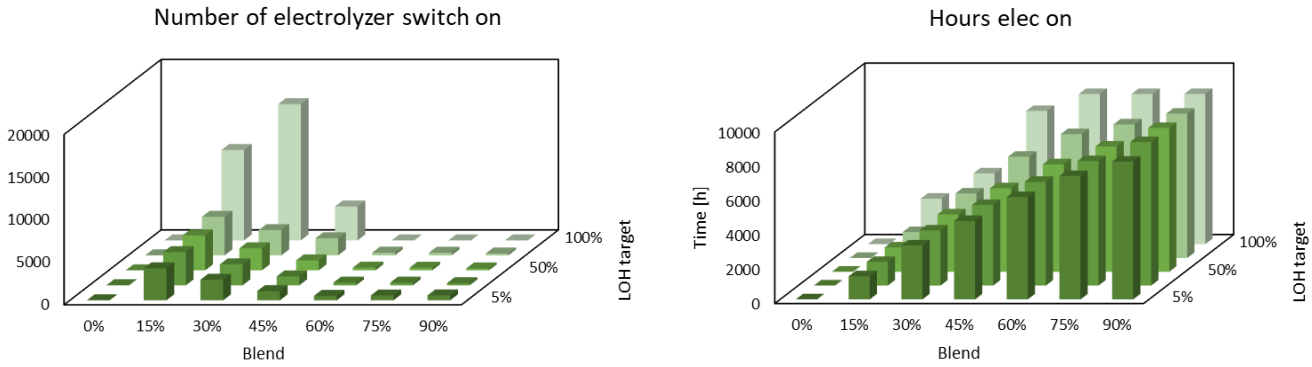

Figure 72. Electrolyzer working conditions, blending and LOH target

Looking at the left graph of Figure 72, it is possible to identify that the blending percentage plays a more relevant role in the number of switches on of the electrolyzer, indeed, the horizontal lines shows trends similar to the one of Figure 62, except for the cases in which the $LOH\ target$ is equal to 5 % or to 100 %.

More in details, if the system is let free to work the electrolyzer only when needed or possible, i.e., when the $LOH\ target$ is equal to the minimum allowed percentage in the storage of 5 %, the number of switches on will be higher than in the other cases, reaching around 550 switches, for mid blending, over the ~ 300 of the cases in which the fixed value is not so low. If instead the requirement is to have an always full hydrogen tank, for blending percentages above 60 % the electrolyzer will never be switched off.

The number of hours when the electrolyzer is on rises with the rise of the blending percentage, this trend is enhanced if the chosen level of hydrogen in the tank is higher; however, remains predominant the effect of the blending percentage.

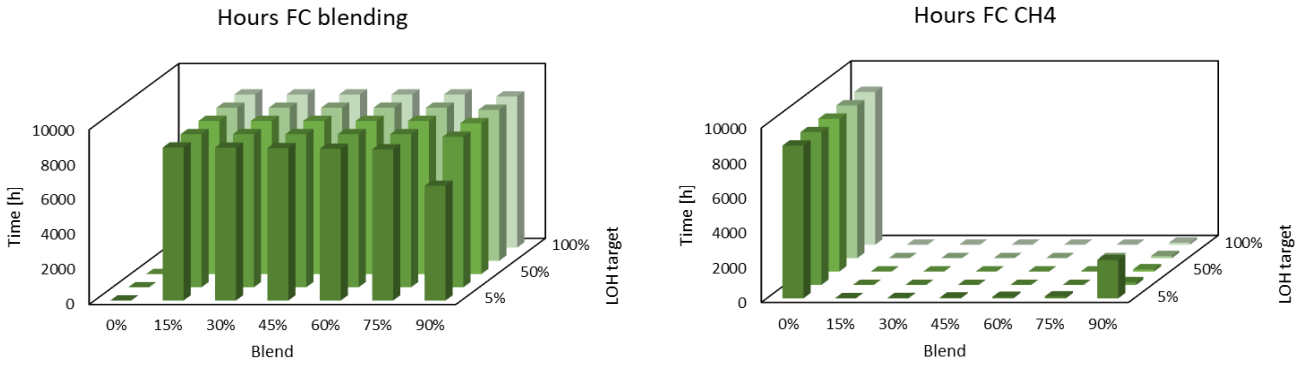

Figure 73. Fuel cell functioning, blending and LOH target

The more relevant aspect underlined by the plots in Figure 73 is related to the curve relative to the value of 5 % of the parameter $LOH\ target$, indeed, if the system is not forced to store any additional quantity of hydrogen, the fuel cells are always forced to work in methane condition for at least some hours in the year; more in detail if the blending is at 15 %, the fuel cells will work 6 h in methane. This number of hours rises if the blending percentage rise, at 75 % is equal to 111 h while if it reached the value of 90 % of blending, that makes the electrolyzer undersized with respect to the fuel cells as shown in Section 5.3.1, the hours in methane grow up to ~ 2200.

Considering the discharging percentages, and more in detail the $Grid\ reject_{\%}$, it is possible to verify that the coupled variation of the two parameters simply determines an enhancement of the curves showed in Figures 64 and 67, whit a rising percentage if the $LOH\ target$ rises and a decreasing one if instead the blending grows. These trends have been already analyzed in sections 5.3.1 and 5.3.2.

In Figure 74 is reported the required grid input to satisfy the load.

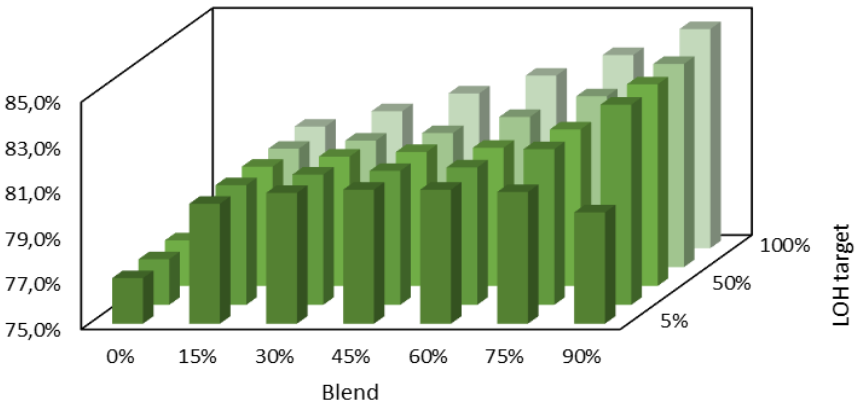

Figure 74. Grid input required, blending and LOH target

The plot of Figure 74 presents the same trends presented in Sections 5.3.1 and 5.3.2 for what concerns this percentage with the exception represented by the first value of $LOH\ target$. Indeed, the trend with a rising required level of hydrogen should be an increasing one but the first column is much higher in all the oblique rows.

This trend is justified considering that in these cases the fuel cells are working for some hours in methane producing more than in blending, as a consequence the requirement from the grid is reduced a bit.

5.3.6 Blending and load guaranteed FC

The variation of the $load\ guaranteed\ FC$ is performed in the same range used in Section 5.3.3 but whit only five points inside, every 15 %; the range and the points of the blending percentage are the same of Section 5.3.5.

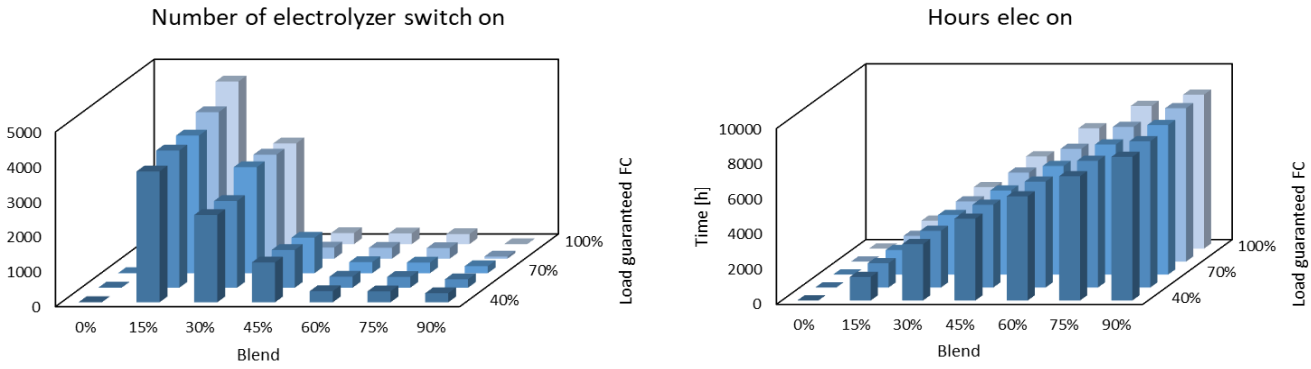

Figure 75. Electrolyzer working conditions, blending and load guaranteed FC

Looking at the left plot of Figure 75, considering the oblique curves, it is possible to verify that the trend showed in Figure 68 is representative only of the cases with an enough high blending percentage, above 45 % while instead below this value the followed trend is totally different.

Considering the left part of the graph it is possible to identify a rising number of switches on if the $Load\ guaranteed\ FC$ rises; the trend of the operating hours is instead constantly a growing one for all the blending percentages.

Analyzing the growing trend at low blending percentages, it can be justified considering that the electrolyzer will be used more if the fuel cells are required to work constantly at higher percentages. The electrolyzer is switched on more times because probably at this blending percentage and low fixed load the electrolyzer can remain off for more following iterations, with a raised demand of hydrogen instead this will no longer be possible.

At higher blending percentages is instead positive if the electrolyzer is worked more, since in that case it is kept on for more consecutive iterations.

Considering the fuel cells functioning, the dominating trend is determined by the blending percentage, only at 90 % they are forced to work in methane conditions as in Section 5.3.1, the rise of the working percentage determines a growth in the number of hours in which effectively the system is operated using methane only.

The trends in the charging percentages are always the same showed in Sections 5.3.1 and 5.3.3 with, also in this case, the predominant effect of the blending over the $load\ guaranteed\ FC$, with the latter determining very small variations in the $Grid\ input_{\%}$.

The same behaviour can be seen in the discharging percentages that exactly follows the trends determined by the single variations of the two parameters.

5.3.7 Blending and load min electrolyzer

The parameter $load\ min\ elec$ is varied in the same range used in section 5.3.4, from 20 % to 100 % but are used only five values in this range.

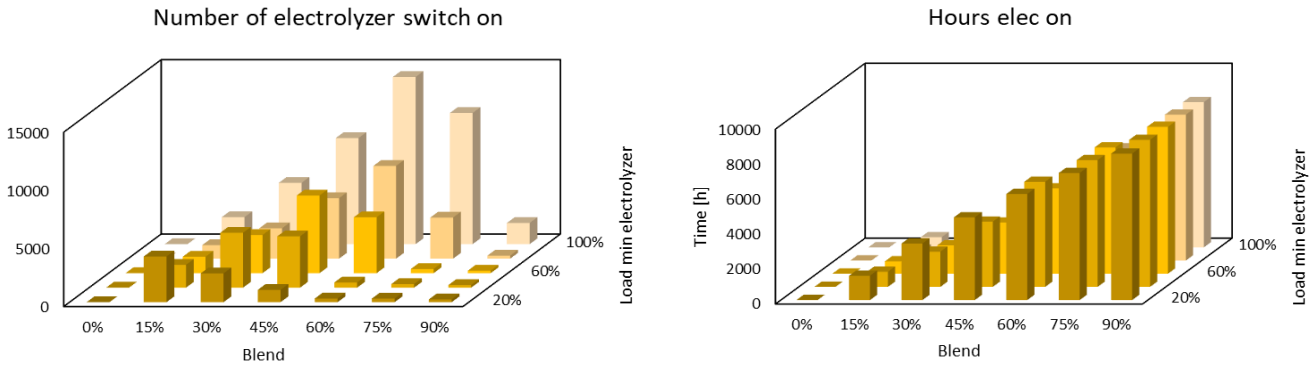

Figure 76. Electrolyzer working conditions, blending and load min electrolyzer

Analyzing the plots of Figure 76, it is evident that the selected minimum allowed load of the electrolyzer strongly affects the impact of the blending percentage over the number of switches on; for what concerns the number of worked hours instead the trend is a rising one with respect both to the raised blending and minimum electrolyzer load percentage.

Going more in detail about the trend of the number of switches on, it can be possible to identify that the maximum of the number of switches is shifted toward higher blending percentages if the minimum load rises, at the same time the absolute value is also higher; indeed, if the $load\ min\ elec$ is at 20 % the maximum of the switches are ~ 4000 at 15 % of blending while if $load\ min\ elec$ is 100 %, the higher switches becomes more than 14000 and are reached when the blending is at 60 %.

This trend is determined by the higher demand of the hydrogen when the blending is higher, but, if this is coupled with the rise in the minimum load of the electrolyzer, it determines the impossibility to work in some conditions and so, if the demand is higher, the electrolyzer will be used in less constant way.

These parameters do not show any additional effect on the fuel cell operating conditions, excepting for the fact that if the blending is at 90 %, the higher load of the electrolyzer firstly determines a increase of the number of hour in which the system is forced to work with methane only, than the number decreases again thanks to the higher production.

The charging percentages presents the same trends showed in the single parameter variation, also in this case the dominating parameter remains the blending percentage of the fuel cell. The same can be seen in the discharging percentages.

5.3.8 LOH target and load min electrolyzer

In the performed sensitivity analysis, the $LOH\ target$ is considered with seven points in the same range used in Section 5.3.5, from 5 % to 100 %.

In Figure 77 it is presented the effect of the simultaneous variation of the two parameters on the electrolyzer performances.

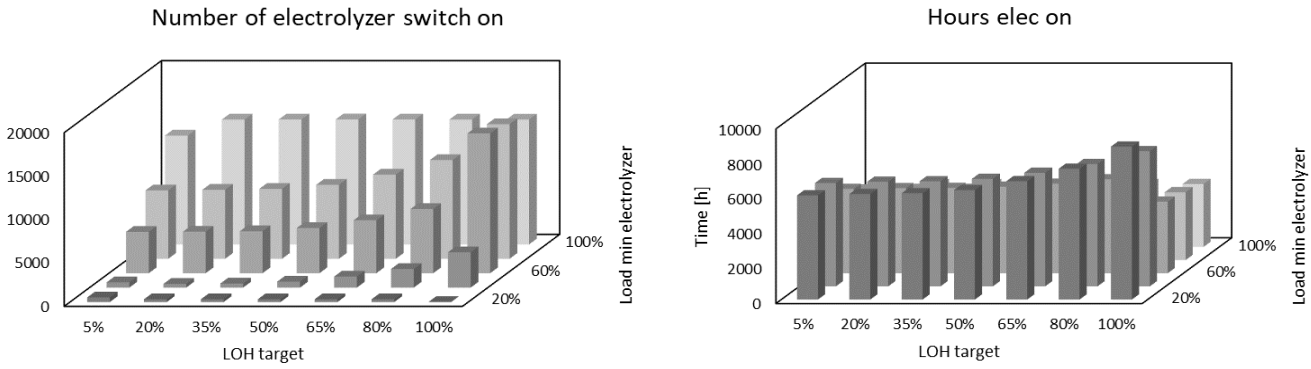

Figure 77. Electrolyzer working conditions, LOH target and load min electrolyzer

The trend presented in Figure 66 is characteristic of the variation of $LOH\ target$ only if the value of the minimum load of the electrolyzer is exactly equal to 20 % otherwise the trend is exactly the opposite with a rising number of switches on if the target rises; looking at the number of hours in which the electrolyzer is on is instead the same.

The rising trend of the number of switches on with the rising level of $LOH\ target$ is justified by the fact that the electrolyzer is worked more but it is harder to use it due to the higher minimum percentage allowed, as a consequence the electrolyzer is switched on more times.

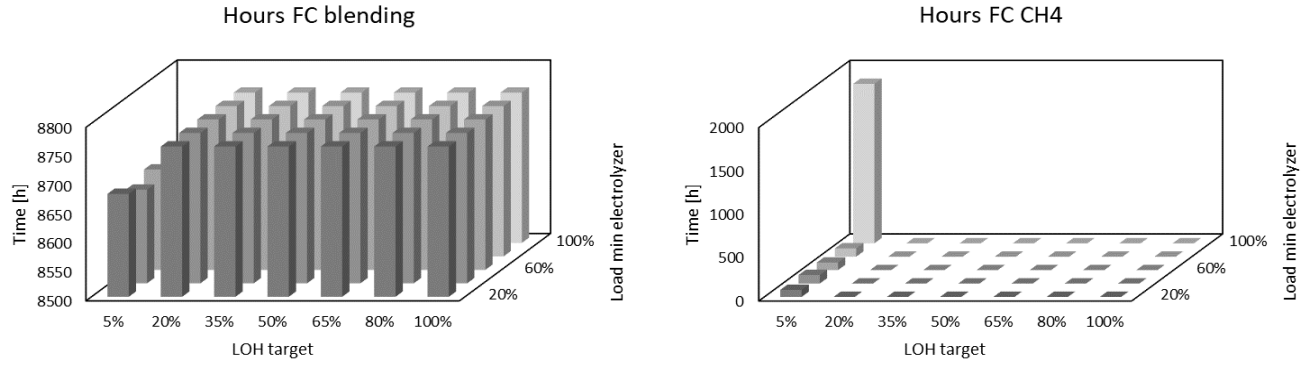

Figure 78. Fuel cell functioning, LOH target and load min electrolyzer

Looking at Figure 78, the more interesting aspect is relative to the trend driven by the $load\ min\ elec$ variation when the $LOH\ fixed$ is absent due to the choice of target equal to 5 %. In this case there is a rising trend in the hours in which the fuel cells are forced to work in methane mode, caused by the more difficult work of the electrolyzer if the minimum allowed percentage rises.

If the minimum load of the electrolyzer varies from 20 % to 80 %, the number of hours in methane mode of the fuel cells is always around 90 h while if the electrolyzer is always at its maximum itis not able to produce correctly for almost a quarter of the yearly time, causing $\sim 2000\ h$ of methane work for the fuel cells. This trend underlines that the function $LOH\ fixed$ has a positive effect on the operations of the fuel cells if it is required to make them work in blending conditions.

In Figure 79 is presented the $Grid\ reject_{\%}$ as representative of all the discharging percentages.

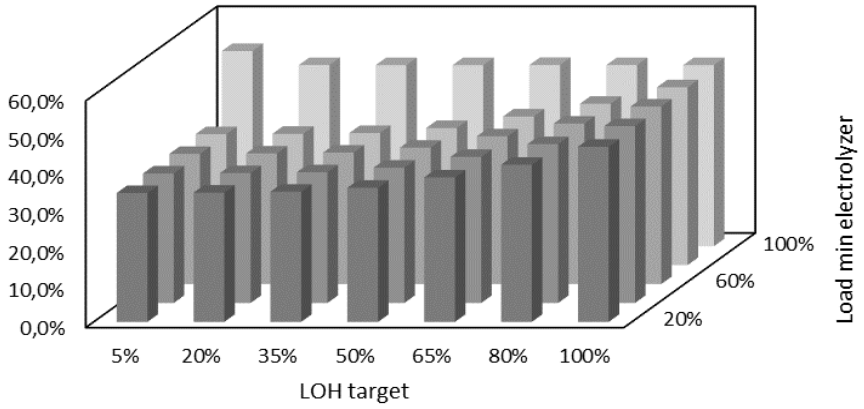

Figure 79. Grid reject percentage, LOH target and load min electrolyzer

The trend presented in Section 5.3.4 is representative of the effect on the discharging percentages of the minimum allowed load of the electrolyzer since at each value of the parameter $LOH\ target$ it is possible to always see a rising trend of this percentage.

Looking instead at the trends at constant $load\ min\ elec$ it is possible to verify the rising trend presented in Section 5.3.2 is visible for the first four horizontal rows while in the fifth one, correspondent to the case with the electrolyzer always at full power, the trend is a decreasing one. This can be explained considering that the electrolyzer is helped by the larger use due to the higher $LOH\ target$, in this way it can better exploit the extra power produced by the PV panels.

The impact on the discharging percentages is determined by the coupled effect of the trends reported in Sections 5.3.2 and 5.3.4.

5.3.9 LOH target and load guaranteed FC

The parameters $LOH\ target$ and $load\ guaranteed\ FC$ are made vary in the same ways presented in Section 5.3.8 and 5.3.3.

The analysis of the effect on the electrolyzer working conditions does not provide any additional information since the effect of the $LOH\ target$ is impactful only if the value is set equal to the value of LOH_{min} or LOH_{max}. In the first case this determines a lower use of the electrolyzer while in the latter condition the electrolyzer is not able to totally satisfy the hydrogen demand. These trends can be visualized in Figure 80.

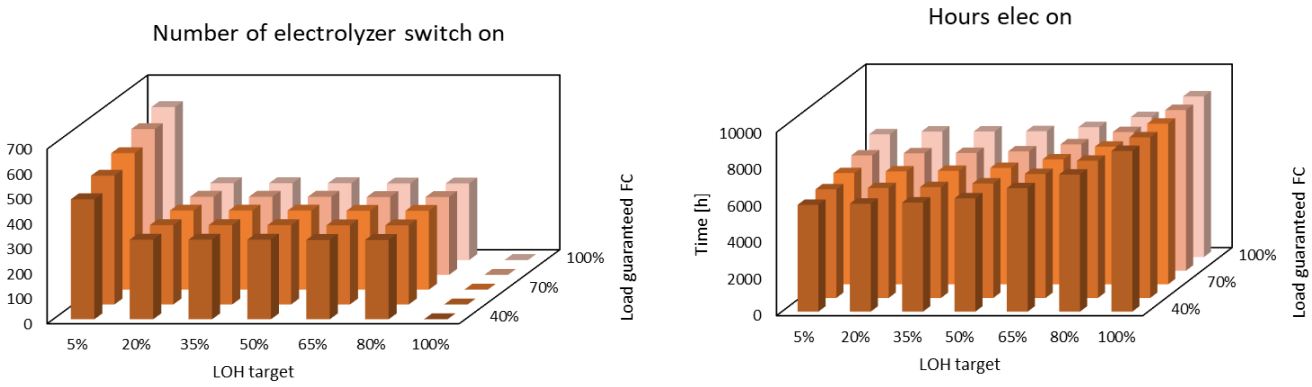

Figure 80. Electrolyzer working conditions, LOH target and load guaranteed FC

The effect on the fuel cells working conditions shows instead that there is an interconnection between these two parameters. Indeed, if the value of $LOH\ target$ is high enough, above 30 %, the guaranteed working point has no impact, with the fuel cells always able to work in blending conditions. If the system is instead free from the function $LOH\ fixed$, the fuel cells will never be able to work without methane for some hours of the year, this number of hours rises if the $load\ guaranteed\ FC$ is higher, i.e., 55 h when the fuel cells are at 40 % and 163 h if the cells are always at full power.

Analyzing the charging percentages there is no additional effect that can be seen with respect to the ones of the single variations of the two parameters in Sections 5.3.2 and 5.3.3.

In Figure 81 is showed the $Grid\ input_{\%}$ as representative of the discharging percentages.

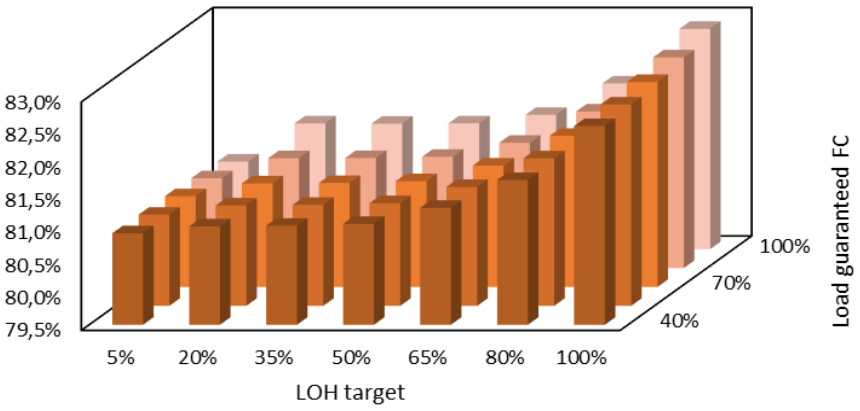

Figure 81. Grid input required, LOH target and load guaranteed FC

Looking at Figure 81, it is possible to identify that the rising trend in this percentage presented in Section 5.3.3 is not representative of the case with $LOH\ target$ equal to 5 % since in that case the percentage remains constant with the variation of the working point of the fuel cells. It is also evident that the more relevant parameter of the two analyzed in this Section is the $LOH\ target$, even if the variations are really small.

5.3.10 Load min electrolyzer and load guaranteed FC

The last coupled sensitivity analysis is performed taking seven values of the parameter $load\ min\ elec$ in the already exploited range, the values of the $load\ guaranteed\ FC$ remains the same.

In Figure 82 it is possible to look at the effect of these parameters on the electrolyzer working conditions.

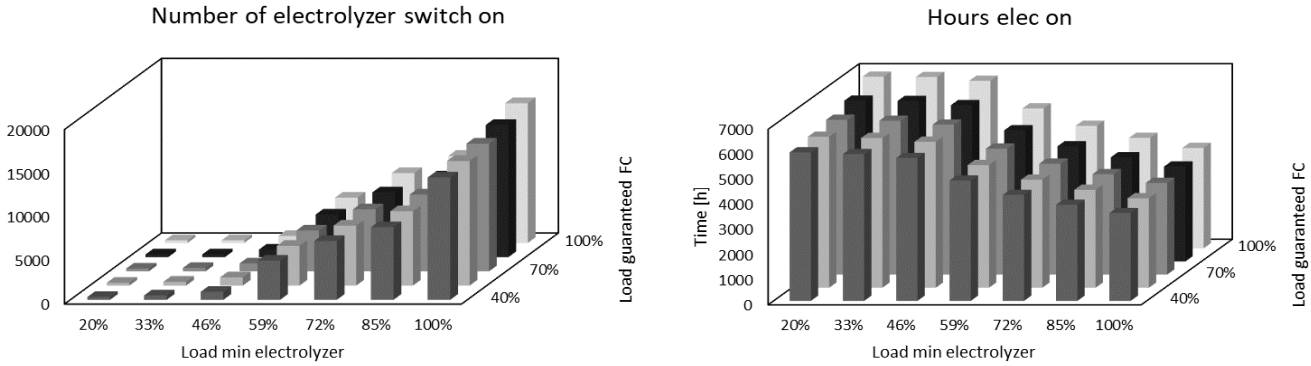

Figure 82. Electrolyzer working conditions, load min electrolyzer and load guaranteed FC

The plots in Figure 82 shows a constant trend when the $load\ guaranteed\ FC$ is fixed, in these cases the electrolyzer is always switched on more times and used less hours if the minimum load of the electrolyzer rises.

There are presented instead two different trends at variable guaranteed working point of the fuel cells, if the $load\ min\ elec$ is lower than $50\ \%$ the electrolyzer will be switched on less times if the cells are forced to be used more while if the electrolyzer parameter rises above this threshold, the trend becomes the opposite. Looking instead at the number of hours with the working electrolyzer, the trend is always the same, it is used more with the rising selected working point of the electrolyzer.

The difference in the trends of the switches on can be justified considering that the electrolyzer is harder to be used if its minimum allowed load is lower, as a consequence the higher demand of hydrogen generated by a higher $load\ guaranteed\ FC$ determines worst performances for the electrolyzer that is switched on more times. Indeed, there is a rise of 2000 switches between the $40\ \%$ and $100\ \%$ of selected guaranteed working point if the electrolyzer is always on while the difference is of less than 1000 switches when the electrolyzer minimum working point is at $59\ \%$.

This sensitivity analysis shows no additional information with respect to the ones presented in Section 5.3.3 and 5.3.4 on the effect of these parameters on the fuel cell operation.

The same can be underlined for the charging percentages where the only information that can be taken is that the $load\ min\ elec$ is more impacting than the other parameter since the variation in the percentages determined by its variation is bigger than the other. This aspect is underlined also by the analysis of the discharging percentages where the trends are the same of the ones presented in the analysis of the single variation of the two parameters.

5.3.11 Total variation

The last sensitivity analysis performed, as it has been done in Section 5.2.8, considers the simultaneous variation of the four decision parameters. In this case it is not possible to use the same ranges used in the coupled variation of the parameters since the computational time required to perform such a number of variations would be too high, as a consequence the choice has been to take five points in the ranges for each parameter.

		Number of electrolyzer switch on	hours elec on	Battery charge	Electrolyzer charge	Grid reject charge	Battery discharge	FC discharge	Grid input required
	Target	1	8322	55%	23%	33%	11%	11%	77%
Parameter									
Blend	0	45	0	0	0	0	0	125	45
Blend	0,25	0	0	0	0	0	5	0	0
Blend	0,5	3	3	0	0	0	5	0	0
Blend	0,75	9	9	8	13	0	5	0	0
Blend	1	90	114	20	25	22	5	0	0
LOH target	0,05	5	14	0	10	2	20	25	5
LOH target	0,25	20	25	7	10	5	0	25	5
LOH target	0,5	30	25	7	7	5	0	25	5
LOH target	0,75	30	25	7	6	5	0	25	5
LOH target	1	62	37	7	5	5	0	25	25
Load min elec	0,2	31	32	0	38	22	0	25	5
Load min elec	0,4	26	27	0	0	0	0	25	5
Load min elec	0,6	24	24	0	0	0	0	25	5
Load min elec	0,8	23	23	0	0	0	0	25	5
Load min elec	1	43	20	28	0	0	20	25	25
Load FC guaranteed	0,4	25	21	4	7	4	4	25	9
Load FC guaranteed	0,55	25	23	4	7	4	4	25	9
Load FC guaranteed	0,7	32	27	4	7	4	4	25	9
Load FC guaranteed	0,85	32	27	8	8	5	4	25	9
Load FC guaranteed	1	33	28	8	9	5	4	25	9

Table 6. Decision parameters simultaneous variation results

In Table 6 are reported the analyzed key performance indicators in the columns with a target behind them, the number in the cells determines the number of times in which a simulation, characterized by the parameter on the row, reaches a value higher or lower than the target.

For what concerns the $number\ of\ electrolyzer\ switch\ on$ has been reported the number of simulations able to keep the electrolyzer always on during the year. Looking at the distribution of the bars in the column, it is possible to determine that the less impacting parameter is the $load\ guaranteed\ FC$ while the most impacting two are the $LOH\ target$ and the blending percentage. This is determined by the fact that the electrolyzer is used more if the last two parameters are higher, as a consequence it is switched on less times. The same trend can be seen looking at the $hours\ elec\ on$, additionally the analysis of this key performance indicator provides us the information that the low switches when the $blend$ is at zero, is determined by the fact that the electrolyzer remains switched off.

Considering the $Battery\ charge_{\%}$, the set value is at $55\ \%$, determined looking at the higher percentages obtained considering the results in all the performed simulations, this is the reasoning followed to determine the values of all the target for the percentual indicators.

Looking at the results, the simulations showing percentages higher than the target, are the ones characterized by high levels of blending or of minimum allowed load of the electrolyzer since in both cases the battery is exploited more to drive the electrolyzer and can be charged more by the extra power from the photovoltaic panels. The other two parameters have a much smaller impact on the battery charging percentage.

For the electrolyzer charge with the excess power, the target has been set at $23\ \%$ and also in this case it is reached if the blending percentage selected is high, determining a higher hydrogen demand, or if the $load\ min\ elec$ is low since in this case the electrolyzer will more easily exploit the PV panels production.

The $Grid\ reject_{\%}$ is analyzed determining the number of simulations reaching a value lower than 33 %, trying to determine the optimal conditions where the power from the panels is better exploited, this condition is reached with the values of the parameters equal to the optimal conditions for the $Electrolyzer\ charging_{\%}$, this is justified considering that the higher demand of hydrogen and the simpler use of the electrolyzer determines a better use of the available power.

Looking at the battery discharging percentage, the impacting parameters are the ones related to the electrolyzer working since only if the $LOH\ target$ is equal to 5 % and the $load\ min\ elec$ at its maximum can be reached the highest percentages. It is also required to have a blending percentage different from zero since the electrolyzer has to be used.

The requirement of having the absence of the function $LOH\ fixed$ is determined by the worst exploitation of the hydrogen section of the storage in this condition, determining higher contribute of the battery.

The analysis of the fuel cells contribution to the load satisfaction underlines that the relevant contribution is determined by the blending percentage, this is justified by the higher nominal power of the fuel cells when they are working with methane only.

The same impact is visible in the $Grid\ input_{\%}$ where the parameter that allows to reach percentages lower than the target set at 77 % is the blending percentage set at null value. Looking at the other parameters, the guaranteed working point of the fuel cells has no impact while the other two parameters should be higher to allow the easier reach of lower percentages of the input from the grid.

5.3.12 Control logics

The obtained results are strongly affected by the initial choice of the charging and discharging logic selected, to have a deeper analysis of the impact of this element on the results, have been performed a sensitivity analysis on the key performance indicators exploring the eight combinations of the control logics.

In Figure 83 is shown the impact of the control logic variation on the electrolyzer performances.

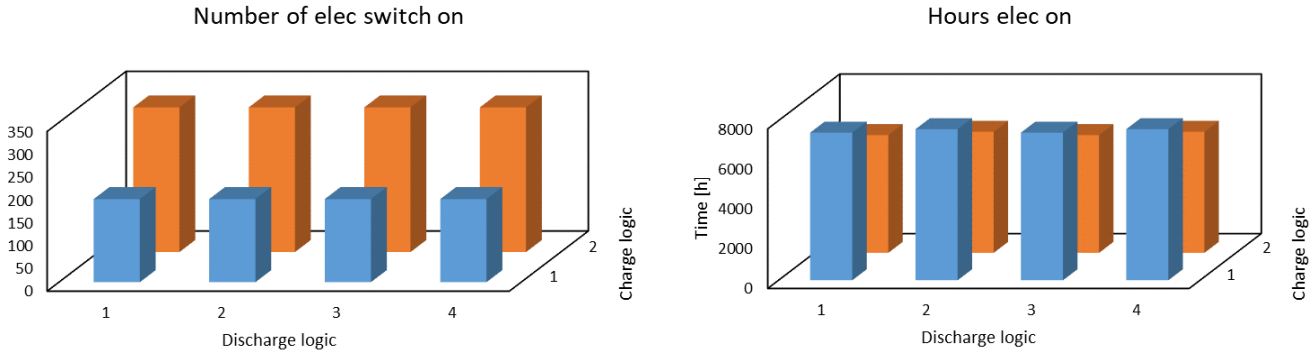

Figure 83. Electrolyzer working conditions, control logics

Analyzing the number of switches on of the electrolyzer, it is possible to verify that only the choice of the charging logic is impacting this parameter, indeed, the electrolyzer is switched on less times if the

control logic prefers to use the battery over the electrolyzer; the discharging logic has no impact over this parameter instead.

The first trend is justified considering that the electrolyzer will remain more time on if the system prioritizes the battery as storage, as underlined by the right graph of Figure 83, since the main use will be forced by the function $LOH\ fixed$ and so it will work more constantly but at a lower load; if the system prioritizes the electrolyzer it will operate at higher power when there is availability from the panels, determining more time off in other iterations of the model. The electrolyzer will be used for longer times if the discharging logic prioritizes the fuel cells, i.e., in second and fourth discharging logics, since there will be higher demand of hydrogen. The charging choice of the charging logic determines a higher, or lower, use of the electrolyzer of $\sim 1500\ h$ while the choice of the discharging logic only around $150\ h$; as a consequence, it is possible to determine that the choice of the charging logic is more important in this case.

It is important to underline that there is no shown difference between first and third discharging logics, and also between second and fourth one, due to the presence of the function $LOH\ fixed$ that makes no need for the working of the electrolyzer during the discharging logic.

Considering the selected blending percentage and other decision parameters, the choice of the control logics has no impact on the fuel cells working conditions, it will be always possible for them to work in blending conditions.

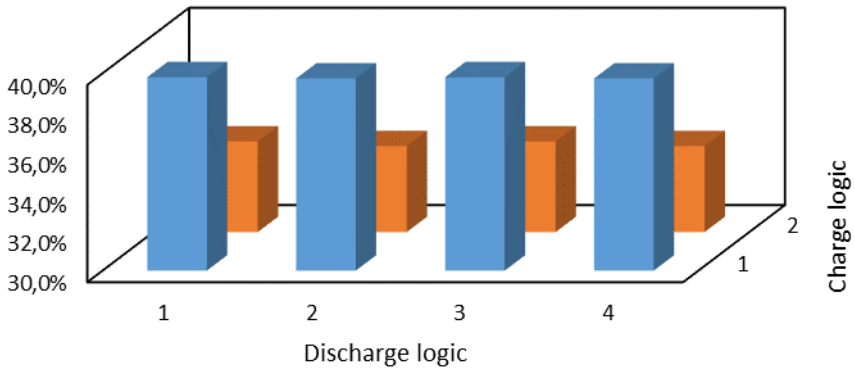

Figure 84. Grid reject percentage, control logics

In Figure 84 is shown trend of the percentual energy available rejected to the grid, it is possible to identify that the larger impact is determined by the choice of the charging logic. Indeed, if the system firstly charges the hydrogen system, there a higher exploitation of the available energy, this trend is justified considering that the electrolyzer cannot work under a given load, if the system prioritizes the battery there will be some iterations in which the left power for the electrolyzer will not be enough to drive the electrolyzer. This problem is instead absent if the battery is the second element since it will accept any small percentage of power.

The percentual difference between first and second charging logic is around 5 % while there is a reduction of $\sim 0{,}1$ % if the choice is to use the second, or fourth, discharging logic over the first, or third, one. This second effect is caused by the higher use of the hydrogen that emphasizes the use of the electrolyzer.

The impact on the discharging percentages is much smaller as can be seen on Figure 85.

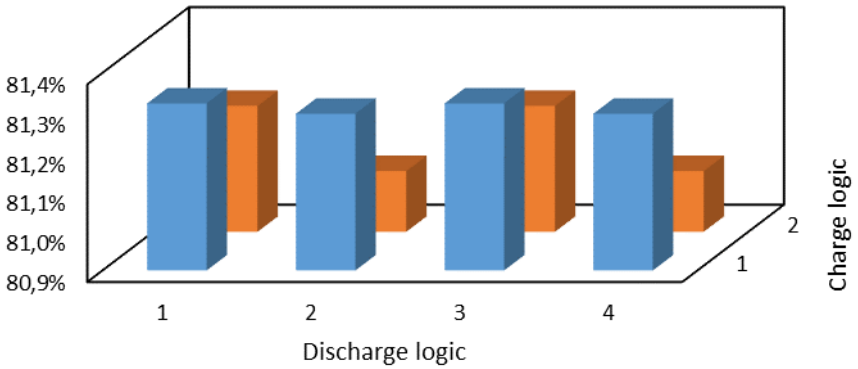

Figure 85. Grid input required, control logics

Analyzing the plot of Figure 85 it is important to underline that the difference between the results of the simulations performed is really small, at most it is of 0,2 %. In this case the relevant trend is that the difference in the choice of the discharging logic is more relevant if the chosen charging logic is the second one.

The storage system is able to better satisfy the demand if the choice is to adopt the second charging logic and the second, or fourth, discharging logic.

6. Conclusions

Summarizing the obtained results, it is important to underline that, using the base case scenario, the system will be able to cover at most ~ 23 % of the yearly electrical load. This result can be obtained only if the fuel cells are used with full methane in input since in this condition they are characterized by a higher nominal power since they are not worked in derating conditions.

The chosen sizes of the $P2P$ elements appear to be not well proportionate in the base case since the electrolyzer is highly oversized with respect to the necessity of the small fuel cell system (1.84:1). As shown in Section 5.2.4, the optimal size of the electrolyzer should be 1.1 times the nominal power of the fuel cells in blending; with this proportionality it is possible to ensure that the fuel cells are constantly working with the correct blending if it is kept equal to 60 %. The sensitivity analysis performed on the simultaneous variation of fuel cell and electrolyzer sizes have determined that this proposed EL-FC sizing ratio is sufficient to make the fuel cells able to work always with the correct hydrogen input. It is important to mention that the electrolyzer should be bigger if the blending percentage is higher while if the latter is lower also the first can be smaller.

In Figure 86 is shown the different blending percentage that is possible to guarantee in a continuous work of the fuel cells for different sizing ratios between electrolyzer and fuel cells. In this graph the sizing ratio is expressed as the nominal power of the electrolyzer needed to ensure that a fuel cell of 1 kW can constantly work at the selected blending ratio for the entire year.

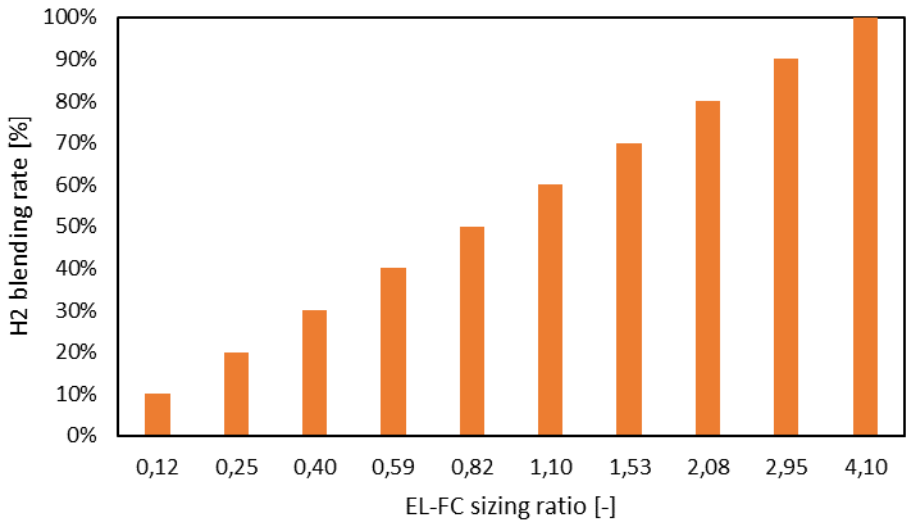

Figure 86. Sizing ratio required for a specific blending percentage

Looking at the graph in Figure 86, the EL-FC sizing ratio selected for the Tulips project appears to be sufficient only if the selected H_2 blending ratio is below 80 %. However, this analysis considers the required sizing ratio for a continuous work at the selected blending level for the entire year, but this condition is not required for the Tulips project where the blending level is supposed to be varied during the year, as a consequence the chosen sizing ratio can be considered oversized. The blending percentages above 70 % can be analyzed during the summer period where it is possible to exploit better the PV power excess.

Performing some sensitivity analyses on the sizes of the hydrogen storage elements, as presented in Section 5.2.4, it is possible to determine that the fuel cell nominal power required to have a storage system

able to totally satisfy the load is equal to $54{,}6\ kW$, considering the fuel cells working only in blending conditions at the fixed percentage of 60%.

From the different sensitivity analysis performed it is possible to determine that the less impacting element is the hydrogen storage volume, even if it shows some small impacts on the different key performance indicators. It is important to underline that the chosen size of $0{,}7\ m^3$, considering the storage pressure of $16\ bar$, is able to correctly work for fuel cells sizes much bigger than the selected one, indeed only if the nominal power of the fuel cells rises above $114\ kW$ the storage becomes too small.

To better analyze the impact of the hydrogen storage size, in Figure 87 is reported the maximum allowed fuel cell size that makes the system correctly working with a given hydrogen storage size; if the fuel cell power rises above the reported value, the system starts to have strange behaviours as shown in Figure 51. These results are obtained considering the sizing ratio between electrolyzer and fuel cells of 1.1: 1 and a constant blending fixed at 60 %.

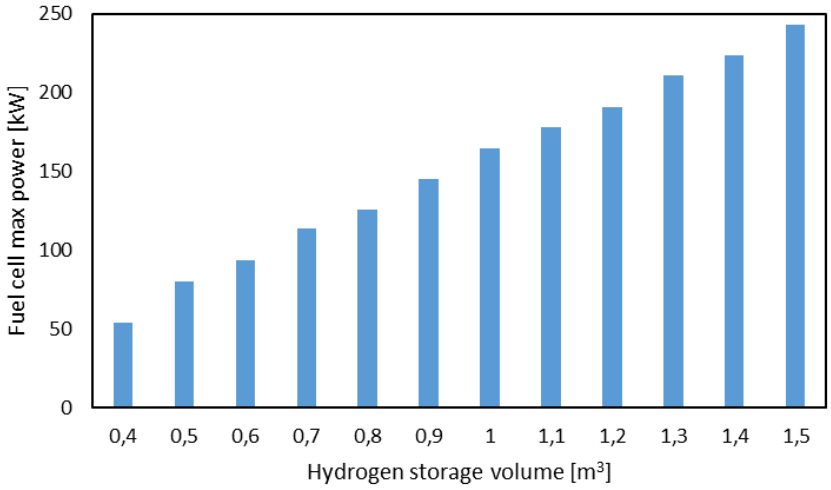

Figure 87. Fuel cell and hydrogen storage coupling

The electrolyzer size is the more impacting parameter while considering the charging percentages and the electrolyzer working related key performance indicators. For the percentages it could be required to have smaller or bigger accordingly to the target that should be reached, as shown in Table 5, while for the performances of the electrolyzer itself, it is better to have it not oversized with respect to the fuel cells. At the same times the fuel cells size plays an important role for the electrolyzer working since, if they are big enough, the hydrogen demand will be higher and the electrolyzer will work in a more constant way.

The largest impact of the fuel cells size is on the discharging percentages since, with a bigger fuel cells system, the grid input can be reduced more. The electrolyzer plays a less important role since the fuel cells are allowed to work also with methane only in input.

Considering the model decision parameters, whose sensitivity analysis results are presented in Table 6, their variation is able to determine big variations in the analyzed key performance indicators, indeed the correct choice of them can make vary the required input from the grid of ~ 15 %.

The less impacting decision parameter is the forced working point of the fuel cells while the blending percentage is determinant for all the key performance indicators analyzed. Indeed, having a null

blending percentage rises the output of the fuel cells while if the cells are working with hydrogen only the electrolyzer is asked to constantly work to supply the demand.

The other decision parameters play a lower role even if they have a specific effect on the different key performance indicators. From the performed analysis it is suggested to have a blending percentage in the range from 55 % to 90 % in order to have at the same time the electrolyzer worked enough and the fuel cells that operates with the wanted blending.

For what concerns the forced level of hydrogen in the tank, it is better to have it in the range from 20 % to 40 % since behind the lower threshold the electrolyzer will work under worse conditions while above the higher value it is too forced to work in the periods without the energy excess from the renewables and this latter power will not be exploited correctly.

The best conditions are reached when the electrolyzer is let free to work in the largest range possible, the only parameter that receive a positive impact if the electrolyzer is able to work only at higher loads is the battery that will be exploited more.

Even if the guaranteed working point of the fuel cells is the less impacting element, it is better to have it in the range from 60 % to 85 % since in this range the amount of power rejected to the grid is the lower possible and the fuel cells are able to work correctly at the selected blending of 60 %. If the blending percentage rises or lowers it is better to have the guaranteed load with the same variation.

The choice of the control logics determines small variations, however, it is better to select the charging logic that prioritizes the electrolyzer over the battery, to better exploit the extra power from the panels, and the discharging logic that prefers the fuel cells as first element to supply the demand. The correct choice allows to reduce the percentage of energy rejected to the grid of ~ 5 % and the required input from the grid of $0,2$ %.

7. Acknowledgments

I would like to kindly thanks Ing. Gandiglio, Ing. Marocco and Ing. Audisio, for the support that they have provided me during the development of this master thesis. Then I would thank Prof. Santarelli for the possibility of performing such an interesting analysis and all the people working in SAGAT for the support during the months in which I worked with them.

I have to thank my family for their help during these years and for the constant support they showed me, I hope that they can be proud of me and of the results I have obtained.

Another special thank should be given to my mates that have made these five years the best of my life, I will never be able to return them back all what they gave me, I hope them the best for their life.

A last thank to all my friends and to the people that have shared with me part of their time since it is the best way to become better people.

8. References

[1] https://www.iea.org/reports/renewables-2021/executive-summary

[2] "Challenges in load balance due to renewable energy sources penetration: The possible role of energy storage technologies relative to the Italian case", L. Barelli, U. Desideri, A. Ottaviano, Energy, 2015

[3] "Application of energy storage in integrated energy systems — A solution to fluctuation and uncertainty of renewable energy", Wei Wang, Baoqiang Yuan, Qie Sun, Ronald Wennersten, Journal of Energy Storage, 2022

[4] "Overview of current development in electrical energy storage technologies and the application potential in power system operation", Xing Luo, Jihong Wang, Mark Dooner, Jonathan Clarke, Applied Energy, 2014

[5] "Energy storage technologies and real-life applications – A state of the art review", Mathew Aneke, Meihong Wang, Applied Energy, 2016

[6] "The application of power-to-gas, pumped hydro storage and compressed air energy storage in an electricity system at different wind power penetration levels" Harmen Sytze de Boer, Lukas Grond, Henk Moll, Ren_e Benders, Energy, 2014

[7] "A stochastic self-scheduling program for compressed air energy storage (CAES) of renewable energy sources (RESs) based on a demand response mechanism" Afshin Najafi Ghalelou, Alireza Pashaei Fakhri, Sayyad Nojavan, Majid Majidi, Hojat Hatami, Energy Conversion and Management, 2016

[8] "The role of compressed air energy storage (CAES) in future sustainable energy systems" Henrik Lund, Georges Salgi, Energy Conversion and Management, 2009

[9] "Feasibility study and economic analysis of pumped hydro storage and battery storage for a renewable energy powered island", Tao Ma, Hongxing Yang, Lin Lu, Energy Conversion and Management, 2013

[10] "Technical feasibility study on a standalone hybrid solar-wind system with pumped hydro storage for a remote island in Hong Kong", Tao Ma, Hongxing Yang, Lin Lu, Jinqing Peng, Renewable Energy, 2014

[11] "An improved min-max power dispatching method for integration of variable renewable energy", Wei Wang, Bo Sun, Hailong Li, Qie Sun, Ronald Wennersten, Applied Energy, 2020

[12] "A developed control strategy for mitigating wind power generation transients using superconducting magnetic energy storage with reactive power support", Mohamed M. Aly, Mamdouh Abdel-Akher, Sayed M. Said, Tomonobu Senjyu, Electrical Power and Energy Systems, 2016

[13] Escamilla A et al., "Assessment of power-to-power renewable energy storage based on the smart integration of hydrogen and micro gas turbine technologies", International Journal of Hydrogen Energy, https://doi.org/10.1016/j.ijhydene 2022.03.238

[14] "Hydrogen Economy outlook", Kobad Bhavnagri, BloombergNEF, 2020

[15] "Hydrogen storage methods: Review and current status" Muhammad R. Usman, Renewable and Sustainable Energy Reviews, 2022

[16] "A study of the techno-economic feasibility of H2-based energy storage systems in remote areas" P. Marocco, D. Ferrero, M. Gandiglio, M.M. Ortiz, K. Sundseth, A. Lanzini, M. Santarelli, Energy Conversion and Management, 2020

[17] "Economic analysis of standalone hybrid energy systems for application in Tehran, Iran" Farivar Fazelpour, Nima Soltani, Marc A. Rosen, International journal of hydrogen energy, 2016

[18] "Coupled effects of charge–discharge cycles and rates on the mechanical behavior of electrodes in lithium–ion batteries" Yingping Ji, Xiaoping Chen, Tao Wang, Hongbo Ji, Yu Zhang, Quan Yuan, Ling Li, Journal of energy storage, 2020

[19] "Techno-economic analysis of hydrogen production from PV plants" Liponi A., Baccioli A., Ferrari L., Desideri U., E3S web of conferences, 2022

[20] "Efficiency analysis of 50 kWe SOFC systems fueled with biogas from waste water" Hendrik Langnick Markus Rautanen Marta Gandiglio Massimo Santarelli Tuomas Hakala Marco Acri Jari Kiviaho, Journal of Power Sources Advances, 2020

[21] "A study of the techno-economic feasibility of H2-based energy storage systems in remote areas" P. Marocco, D. Ferrero, M. Gandiglio, M.M. Ortiz, K. Sundseth, A. Lanzini, M. Santarelli, Energy Conversion and Management, 2020

[22] "Large-scale compressed hydrogen storage as part of renewable electricity storage systems" Ahmed M. Elberry, Jagruti Thakur, Annukka Santasalo-Aarnio, Martti Larmi, Internationa journal of Hydrogen energy, 2021

[23] https://cordis.europa.eu/programme/id/H2020_LC-GD-5-1-2020

[24] "Aeroporto di Torino-Caselle regolamento di scalo", SAGAT, 2020

[25] "Sizing of a hybrid P2P system for the TULIPS project", Marocco P., Gandiglio M., Santarelli M., Politecnico di Torino, 2021

[26] "Studio di fattibilità, relazione generale", Syspro Engineering, 2021